ENHANCED VISCOUS FLOW DRAG REDUCTION USING ACOUSTIC EXCITATION

NASA Research Grant NAG-1-654

Final Report to
NASA Langley Research Center
Hampton, Virginia
23665 - 5225

ATTENTION :

Mr. John B. Anders, Jr. MAIL STOP 163

Submitted by:

Dr. R.T. Nagel
Mechanical & Aerospace Engineering
North Carolina State University
Campus Box 7910
Raleigh, North Carolina 27695-7910

(919) 737-2365

TABLE OF CONTENTS

LIST OF TABLES

LIST OF FIGURES

Page

Page

NOMENCLATURE

a	curve fitting parameter
B	logarithmic law constant
b	curve fitting parameter
CCF	cross correlation function
c	chord length
c_D	total drag coefficient
c_f	local skin friction coefficient
DP	fluctuating pressure
dB	decibel
du_{max}	maximum velocity defect at wake's axis of symmetry
du_w	velocity defect caused by LEBU's wake
e	flow parameter
f	frequency
H	shape parameter
h	height above floor
k	logarithmic law constant
L	LEBU configuration
LA	acoustically excited LEBU configuration
L5	LEBU configuration number 5
L5A	acoustically excited LEBU number 5
P	nondimensional pressure
PL	plain flow configuration
Re	Reynolds Number
r^2	correlation coefficient

r_c	ratio of measured peak values of cross-correlation functions
r_T	ratio of measured relative turbulence intensities
r_θ	ratio of measured momentum thicknesses
SPL	sound pressure level
s	distance from upstream probe to LEBU's trailing edge
T	relative turbulence intensity
t	time delay
U_c	convection velocity
U_o	free stream velocity
u	axial velocity
u_{LE}	velocity of a LEBU manipulated boundary layer
u_{PL}	velocity for a plain flow
u_t	wall friction velocity
V_a	hot film sensor voltage output
V_r	reference voltage
v	longitundinal velocity component
w	spanwise velocity component
w_1	wake function
x	axial distance measured from the leading edge of the test section
y	longitundinal distance measured from the test section floor
y^+	wall units
y	longitundinal distance from wake's axis of symmetry
z	spanwise distance measured from the centerline of the plate test surface

β	wake semi-width
δ	boundary layer thickness
ε	constant
θ	momentum thickness $= \int_0^\infty \frac{u}{U_o}(1 - \frac{u}{U_o})dy$
κ	average roughness height
λ	flow parameter
ν	kinematic viscosity
ξ	probe separation distance
Π	wake parameter
π	pi
ρ	density
$-\rho\overline{u'v'}$	Reynolds stress
$\overline{\ }$	signifies average
$'$	signifies fluctuating quantity

1. INTRODUCTION

1.1. STATEMENT OF THE PROBLEM

The flow of fluid about a solid body can be separated into two regimes: a thin layer of fluid adjacent to the body surface where friction is the dominant phenomenon, and the region outside the thin layer where the fluid can be treated as inviscid. The thin layer adjacent to the body surface is called the velocity boundary layer. The thickness of the boundary layer, δ, increases along the body in a downstream direction. Inside the boundary layer the flow is retarded because of friction with the solid surface and it forms a velocity profile that varies smoothly from zero at the wall to the undisturbed free stream velocity U_o. The reduction of skin friction drag between a solid surface and a moving fluid can greatly improve the performance of many vehicles or fluid machinery.

Boundary layer development over a flat plate can be separated into three regions. A laminar region starts from the flat plate leading edge and forms a Blassius velocity profile where the velocity fluctuations are negligible. Further downstream the flow undergoes transition to turbulent flow [1] where the velocity inside the boundary layer exhibits irregular velocity fluctuations. The value of the Reynolds number, Re_x, can provide an estimate of the laminar, transition and turbulent regions. The skin friction

coefficient for the laminar region of a boundary layer is smaller than that for the turbulent region. The most popular approach in wall friction drag reduction therefore has been to attempt to delay the transition from laminar to turbulent flow [2] and maintain the laminar skin friction coefficient for as long as possible. Most practical flows are, however, turbulent and at large Reynolds numbers all flows will eventually undergo transition to turbulence. The main object of the following investigation is to reduce the skin friction drag of a turbulent boundary layer by altering its structure [3].

Visual investigation of turbulent boundary layers have shown them to contain at least three distinct types of eddy structure (figure 1) :

i. Large eddies which dominate the outer region of the boundary layer and have an average length of approximately 1.6δ [4]

ii. Typical eddies having a typical length of 200 wall units, y^+, are encountered throughout the turbulent boundary layer [5].

iii. Well organized motions in the laminar sublayer can form low speed streaks [6].

The large scale eddies have an average axial length of about 1.6δ [4] and cause a peak velocity fluctuation of the order of $0.2U_o$ where U_o is the external velocity. The large scale structures are convected downstream with an

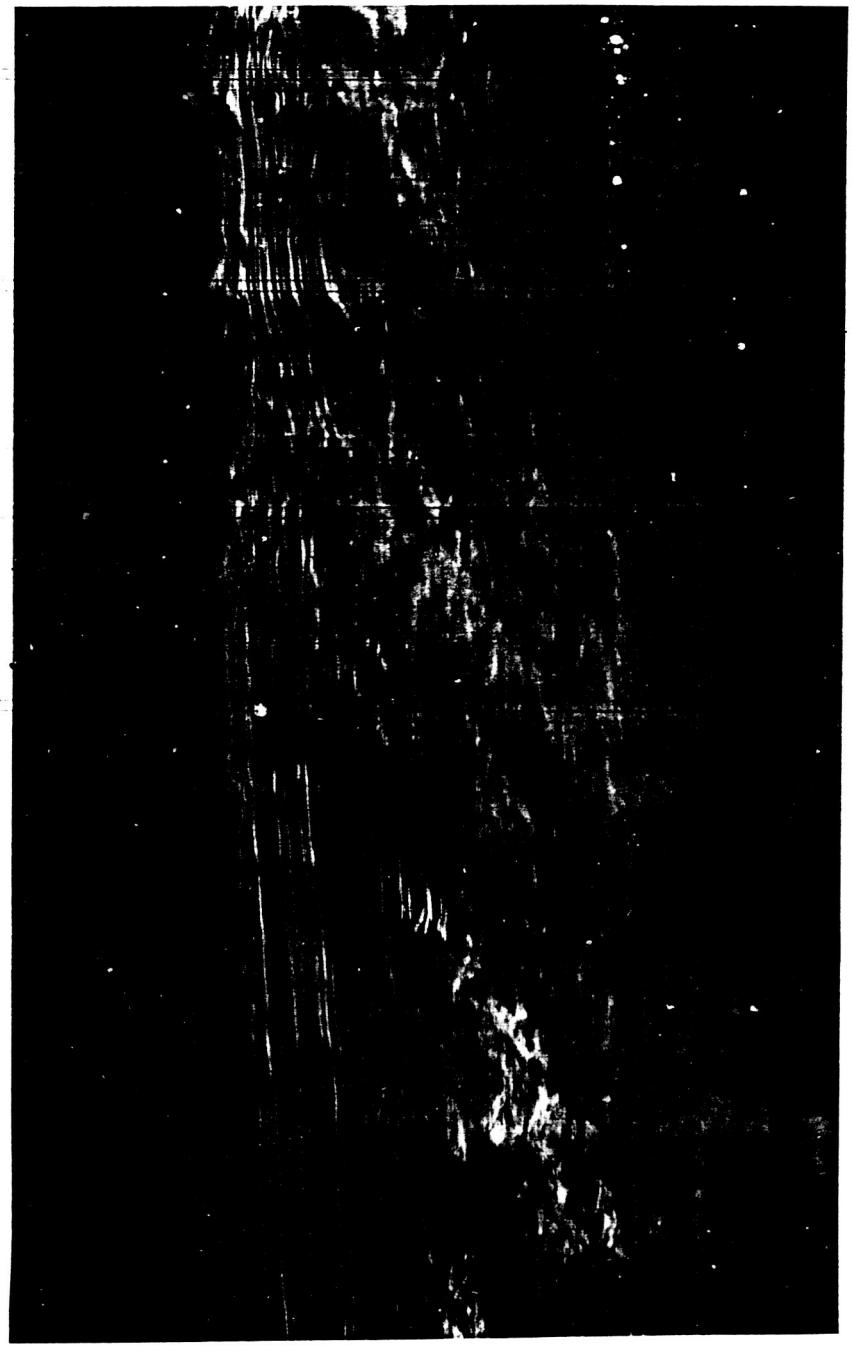

Figure 1. Typical flat plate boundary layer (flow visualization with smoke).

average velocity $U_c=0.93U_o$ [7], and appear semi-periodically with an average frequency of appearance $f=\frac{U_o}{2.5\delta}$ [8]. These large scale structures have a limited life span. They decay after traveling a distance of about 10δ and lose their coherence after about 4δ [9]. Large eddies are associated with the production of turbulent energy and the production of Reynolds stress $-\rho u'v'$, although the exact mechanism linking them to the sublayer skin friction producing phenomena is still unclear [4,6,9]. The reason for this is the lack of comprehensive experimental data in the laminar sublayer. Consequently, manipulation of the turbulent boundary layer structure could lead to reduced skin friction as described in the following sections.

1.2. HISTORICAL REVIEW

Early boundary layer manipulation [10] was performed by positioning mesh screens of height approximately equal to δ inside the boundary layer. This resulted in the destruction of the large eddies and a skin friction drag reduction of 50 percent extending a distance of 100δ to 150δ downstream of the mesh screens. The drag of the device itself was excessive. Pursuing the same goal of eliminating the large eddies, Hefner et al [11] mounted horizontal and vertical plates of various shapes and sizes inside the boundary layer. These plates or elements interacted with and modified the large eddies, interrupting the turbulence production. The

reduction of the wall skin friction was attributed partially to the alteration of the outer turbulence scale. An average of 24 percent drag reduction for a distance of 45 device heights was measured but no net drag reduction was observed. A study utilizing four parallel plate manipulators embedded inside the boundary layer was performed by Corke et al [12]. This method was effective in removing the large scale structures and a 30 percent skin friction drag reduction was documented at a distance of 70δ downstream. Flow visualization recorded the breaking up of the large eddies by the parallel plates which resulted in a thinner manipulated boundary layer. The streamwise turbulence intensity close to the wall of the manipulated boundary layer was found to be reduced. No net drag reduction was measured. In order to improve upon the net drag reduction Corke et al [13] mounted a pair of tandem flat plates within the boundary layer. They measured a 20 percent net drag reduction at some locations. The local skin friction drag coefficient did not relax to that of the undisturbed flow until a distance of 60δ. They also identified the possible mechanisms leading to such results as the suppression of the normal velocity component of the large eddies by the manipulators and the redistribution of the turbulent kinetic energy by the blade wake. Bertelrud et al [14] used thin transverse ribbons in tandem for various flow configurations. A 40 percent skin friction drag reduction was measured and this phenomenon

persisted for about 80 downstream of the manipulator. The net drag reduction was moderate.

These experiments adopted similar boundary layer manipulating schemes, but the specific dimensions of chord length, height and tandem spacing varied considerably. In a review paper Hefner et al [15] presented the parameters for an optimum plate manipulation of a turbulent boundary layer. They stated that the flat elements should be thin and mounted as tension members. They estimated that the element chord length should be approximately equal to the boundary layer thickness, δ, and the outer element should not exceed a height of 0.8δ above the wall surface. It was also noted that the number of horizontal elements should not exceed two and that the plates operate most effectively in the range of momentum thickness Reynolds number from 3,000 to 6,000. In recent investigations [16], 10 to 30 percent net drag reduction was achieved with optimized flat plate manipulators in tandem under zero, mildly adverse and favorable pressure gradient flows. Most of the net drag reduction occurred within 50 boundary layer thicknesses from the manipulator.

Airfoil shaped [17] large eddy break-up devices (LEBU's) were tested in a range of momentum thickness Reynolds numbers at the manipulator near 7,400. The results indicated that only symmetric airfoils in tandem were effective in manipulating the turbulence boundary layer and a 7 percent net drag reduction was recorded. Finally it should be

mentioned that the repeatability of net drag reduction experiments was not found satisfactory [15] and the microgeometry of the plate manipulators is critical with respect to their effectiveness [18].

1.3. OBJECTIVE OF STUDY

Large eddy break up devices (LEBU's) constitute a new, promising method of obtaining drag reduction in a turbulent boundary layer. The destruction of the large scale eddies and the associated reduction in momentum transfer to the wall can result in lower skin friction drag. One of the suggested mechanisms, based upon the work of Liss and Usol'tsev [13,19,20], leading to large eddy elimination is schematically represented in figure 2. Large eddies (discrete vortices) impinging upon a LEBU plate generate unsteady lift forces upon it due to the effective angle of attack variation. Because of the unsteady circulation around the device, vortices are shed from its trailing edge. The oncoming large eddies in the boundary layer interact with the shed vorticity and are partially canceled. The focus of this dissertation is to enhance the LEBU effectiveness by exciting its trailing edge with acoustic waves phase locked to the large scale structure and thus influence the momentum transfer to the wall.

An initial estimate of the required sound pressure level for an effective acoustic pulse was obtained by considering

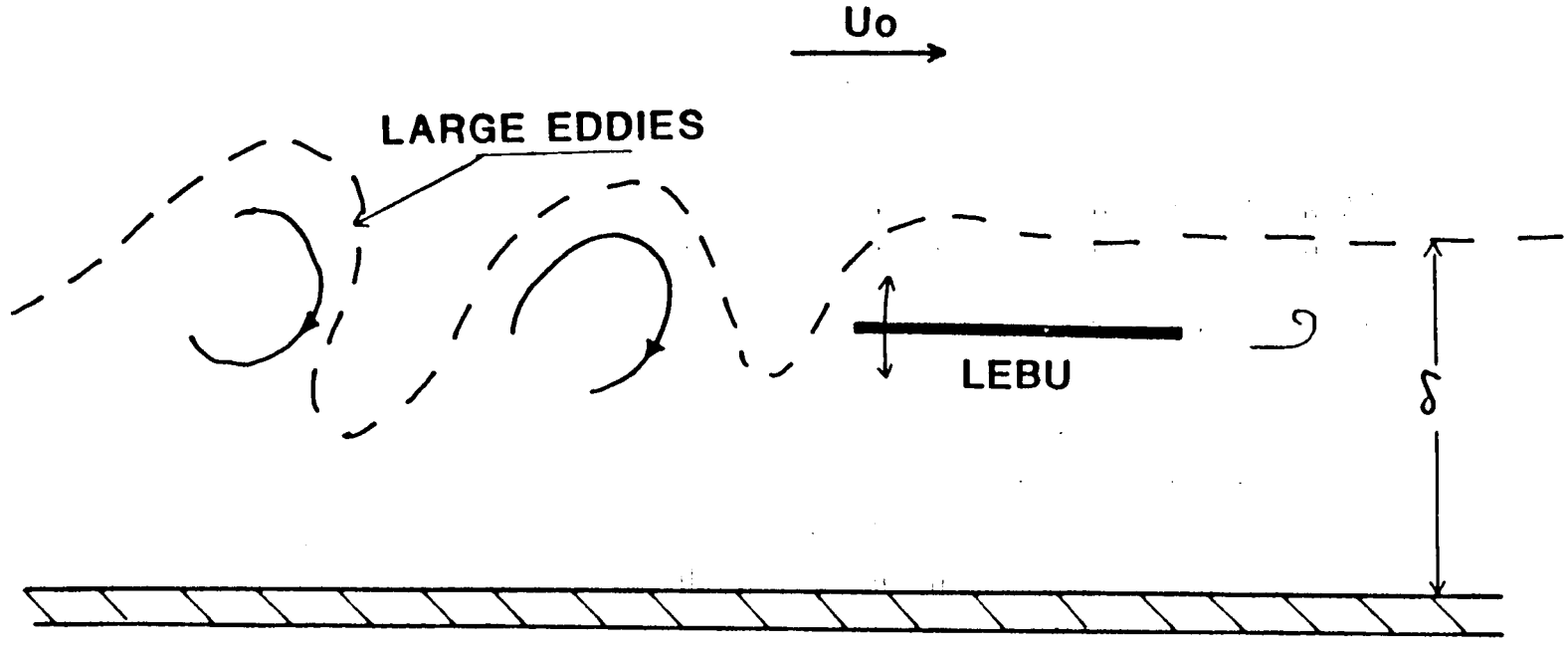

Figure 2. Large eddy brake-up process.

the magnitude of the pressure perturbations at the near wake of a thin plate in inviscid flow. A sound wave of approximately 100 dB (Appendix 1) pressure level, arriving at the LEBU trailing edge together with the large eddies was considered adequate to influence the already manipulated boundary layer.

Detailed skin friction measurements were obtained in the flow region downstream of a LEBU excited with acoustic waves. The data are compared with skin friction measurements of a simply manipulated flow, without acoustic excitation and with a plain flow configuration. The properties and the scales of motion in the flow regime downstream of the acoustically excited LEBU are studied. A parametric study based upon the characteristics of the acoustic input was pursued in addition to careful mapping of the drag reduction phenomenon within the acoustically manipulated boundary layer. This study of boundary layer manipulation has lead to improved skin friction drag reduction and further understanding of the turbulent boundary layers.

2. EXPERIMENTAL PROCEDURE

2.1. BASIC EXPERIMENTAL APPARATUS

The experimental study was conducted in the recently constructed NCSU Boundary Layer Wind Tunnel [21]. A general view of the wind tunnel is shown in figure 3. This facility features: a long test section (~7.0 m) to achieve high Reynolds numbers with low speeds, a velocity range of 4 to 33 m/s and extremely uniform mean flow with turbulence intensities of less than 0.25 percent. A single LEBU plate was carefully fabricated from stainless steel shimstock and mounted at a distance of 2.0 m from the leading edge of the test section, in the boundary layer (figure 4). A mounting system for the LEBU was designed and built. The mount has accurate control over the LEBU's height above the test surface, the LEBU's angle of attack and tension. The LEBU extends through openings in the wind tunnel side walls across the full span of the test section. Each side of the LEBU mount is independently adjustable to assure precise alignment and eliminate possible vibrations of the stretched plate.

The experimental arrangement to acoustically excite the LEBU trailing edge is shown in figure 5. A hot film probe is positioned upstream of the LEBU at the LEBU height. The signal from the sensor is obtained from an anemometer and fed into a specially designed processor whose electronic diagram is drawn in Appendix 3. The processor responds only to large

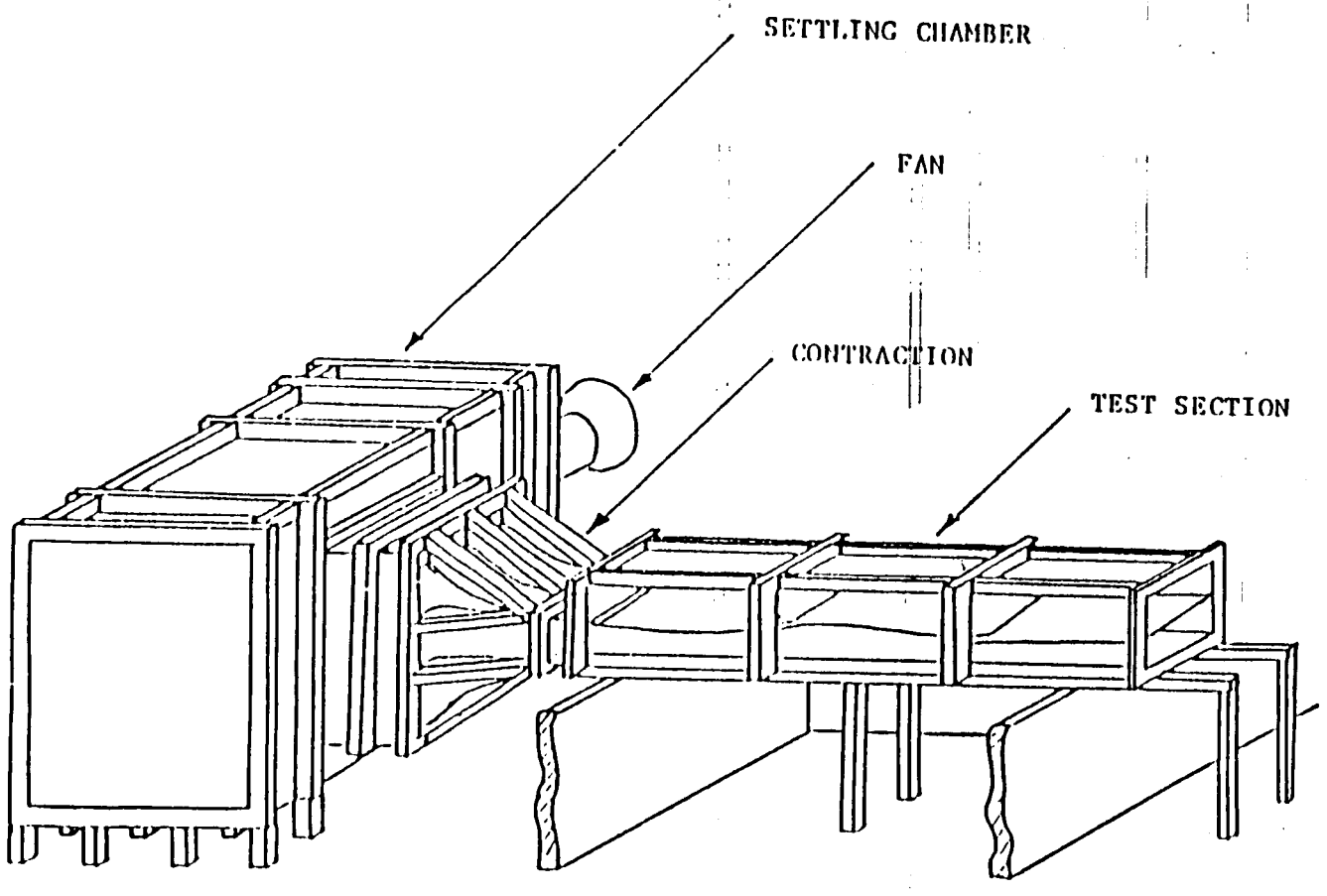

Figure 3. General view of the NCSU Boundary Layer Wind Tunnel.

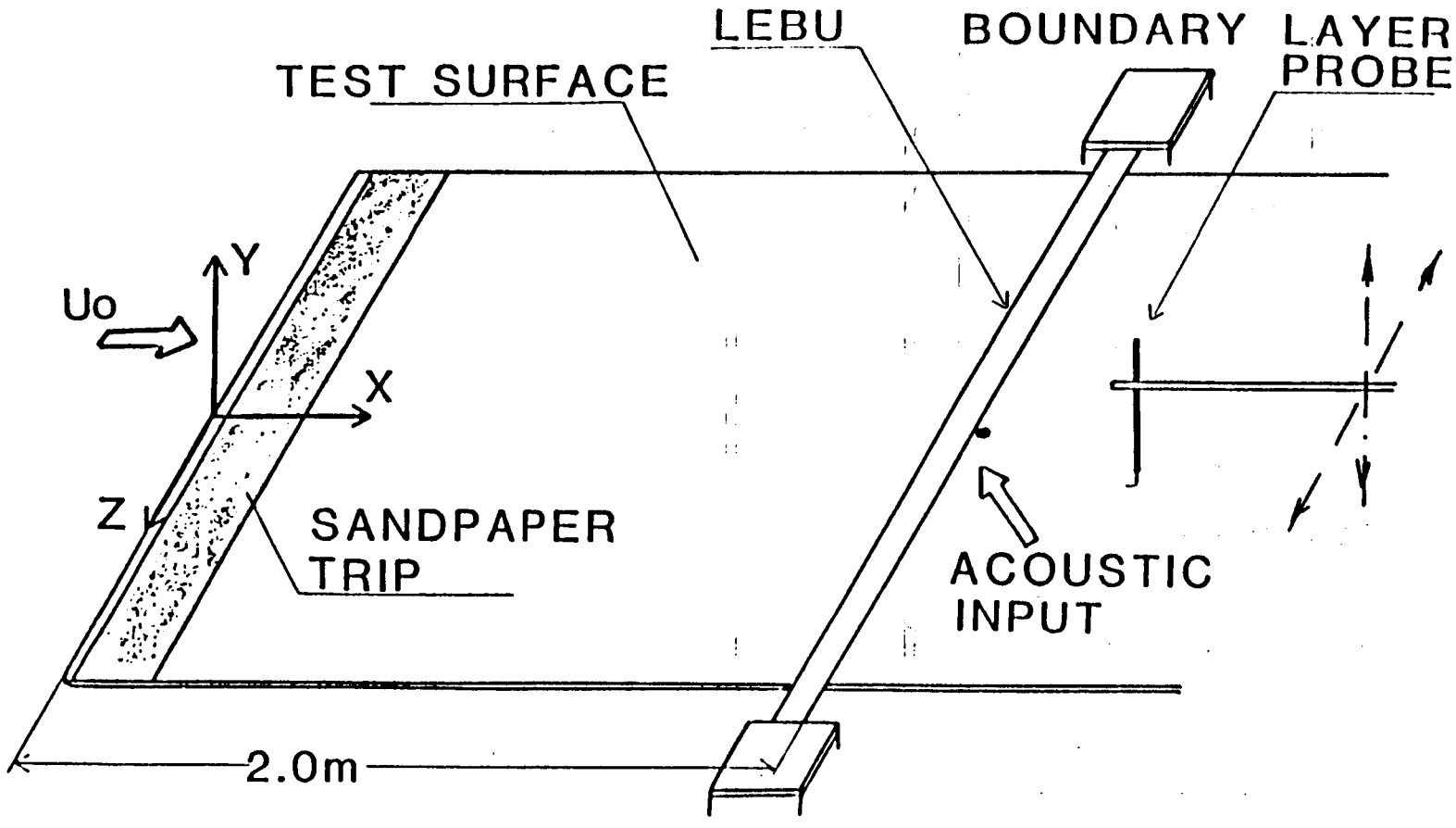

Figure 4. Wind tunnel test surface.

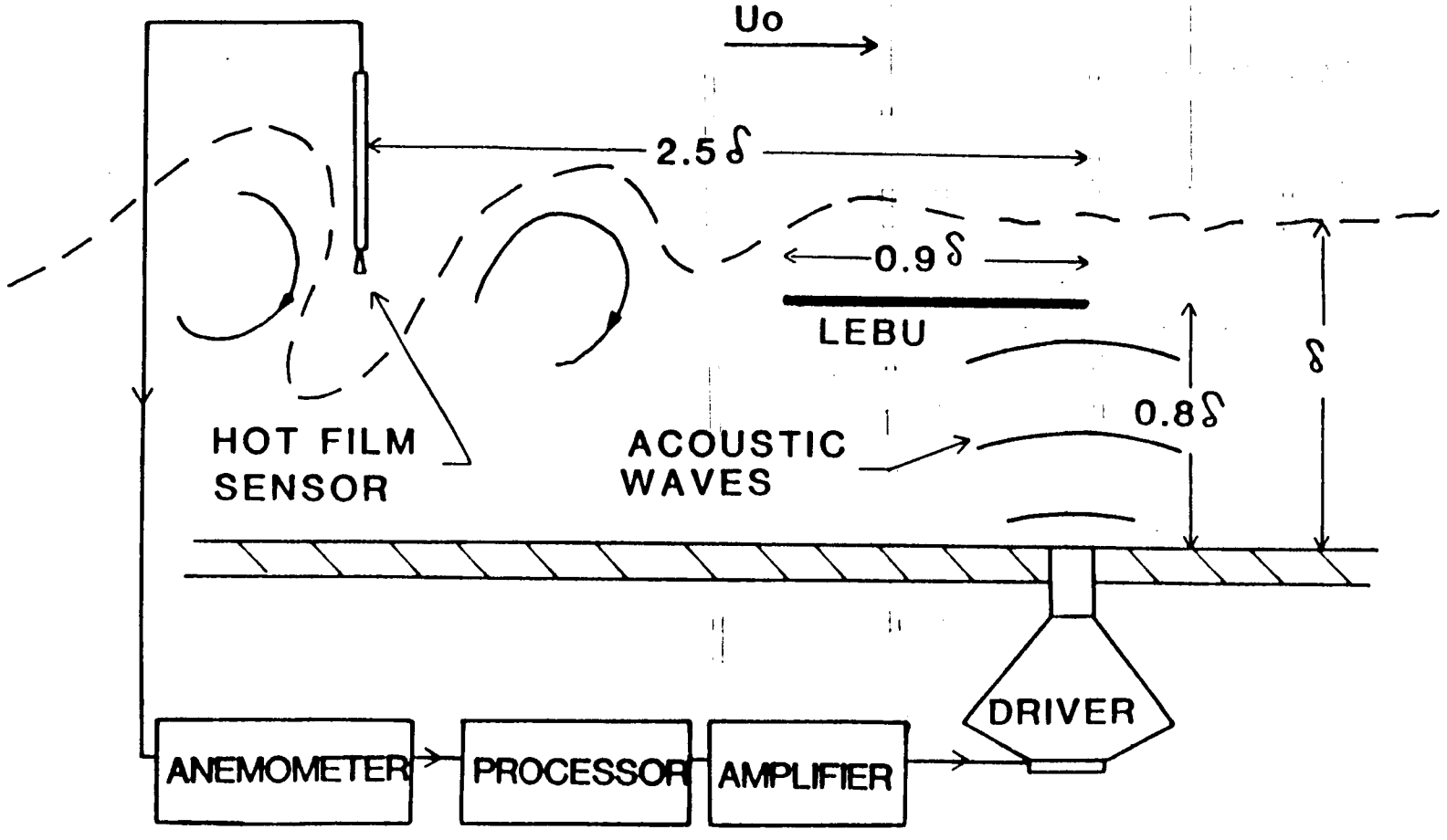

Figure 5. Schematic representation of the acoustic excitation mechanism.

excursions of the hot film signal. The threshold voltage level, V_r, to which the processor responds is adjustable. This adjustment allows selection of a lower limit of large scale eddies to which the processor will respond. Eddies with velocity fluctuations above this threshold level (reference voltage) are ignored while eddies with associated velocity excursions below the threshold level produce a response from the processor. The response is a signal with character and duration similar to the anemometer's large fluctuations as shown on the dual trace oscilloscope display of figure 6. The response of the processor must also be time delayed and amplified. The time delay, t, is set equal to the large eddy convection time [7] between the upstream hot film sensor and the LEBU trailing edge. The delayed processor response is then amplified to produce an acoustic input capable of influencing the LEBU wake.

The processor response is then used to drive acoustic waves from a location on the floor of the wind tunnel below the trailing edge of the LEBU. The acoustic waves can therefore be made to arrive at the LEBU trailing edge together with the incident large eddies. In this manner the vorticity shed from the LEBU, which apparently influences the eddy cancellation, can be modified. The pressure pulse device consists of an 8 inch woofer speaker which is seal mounted on the wide side of a conical channel. The speaker apparatus is housed in a lined box to restrain noise signals from entering

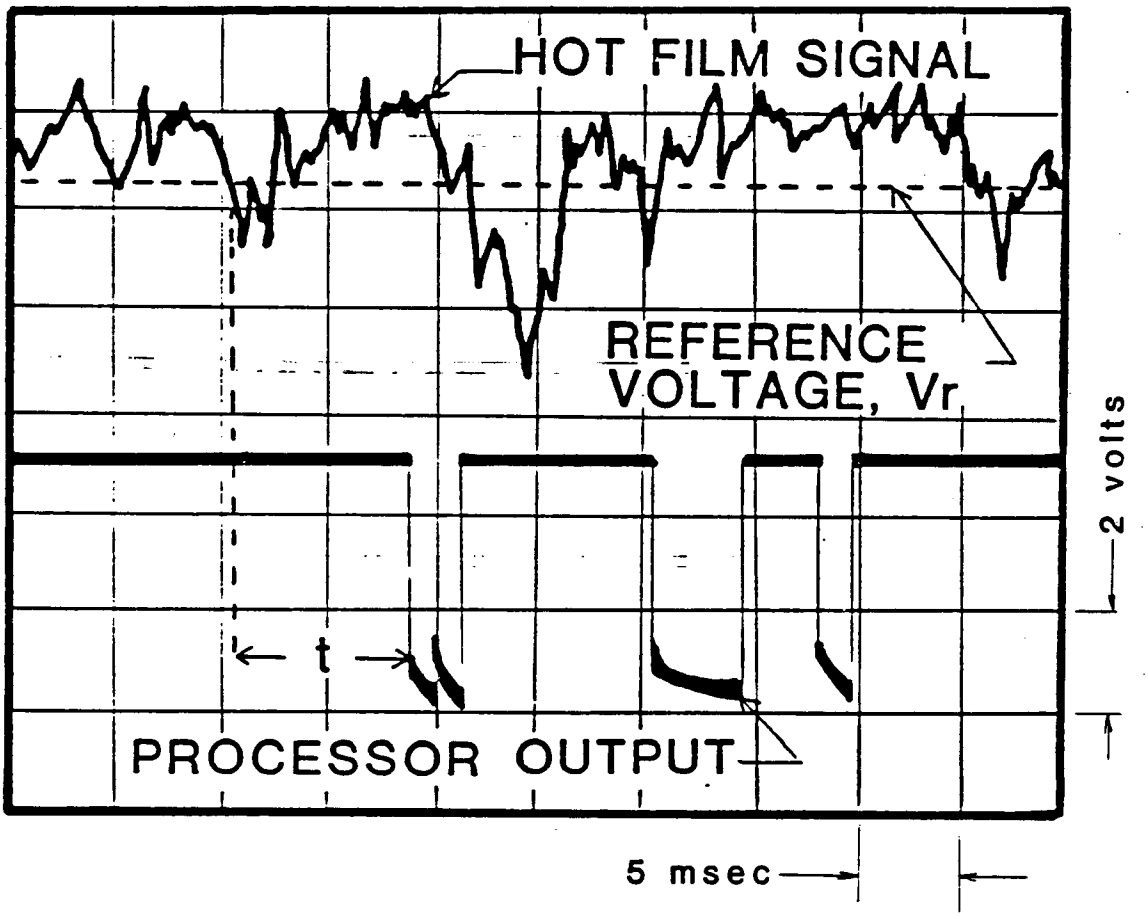

Figure 6. Time delayed processor response to incident flow.

the test surface by spurious paths.

2.2. OPERATING CONDITIONS

The wind tunnel is adjusted to produce a zero pressure gradient flow along its length. The variation of the free stream turbulence intensity in the test section is shown in figure 7. For the operating velocity range a 0.25 percent turbulence intensity was measured. The boundary layer is forced turbulent by a coarse sandpaper trip mounted 3 cm downstream of the test surface leading edge. The length of the boundary layer trip is 21 cm which quickly establishes a fully developed turbulent boundary layer with a complete range of length scales as can be seen from the photograph in figure 1. The wind tunnel unit Reynolds number, $\frac{U_o}{\nu}$, was set at $0.7 \times 10^6 m^{-1}$ The corresponding typical mean flow velocity was approximately 11.0 m/s and the Reynold's number based upon the momentum thickness, θ, at the LEBU location was about 3,100. The boundary layer thickness, δ, at LEBU location was estimated as 4.1 cm. This was determined using the definition of the boundary layer thickness as the height at which $\frac{\bar{u}}{U_o} = .995$, where $\bar{u}$ is the local velocity and U_o is the velocity of the external flow. The LEBU chord length was $\approx 0.90\delta$, its height above the test surface was $\approx 0.80\delta$ and its thickness was 0.005δ according to the recommendations of reference [15].

This LEBU configuration is an improved version of

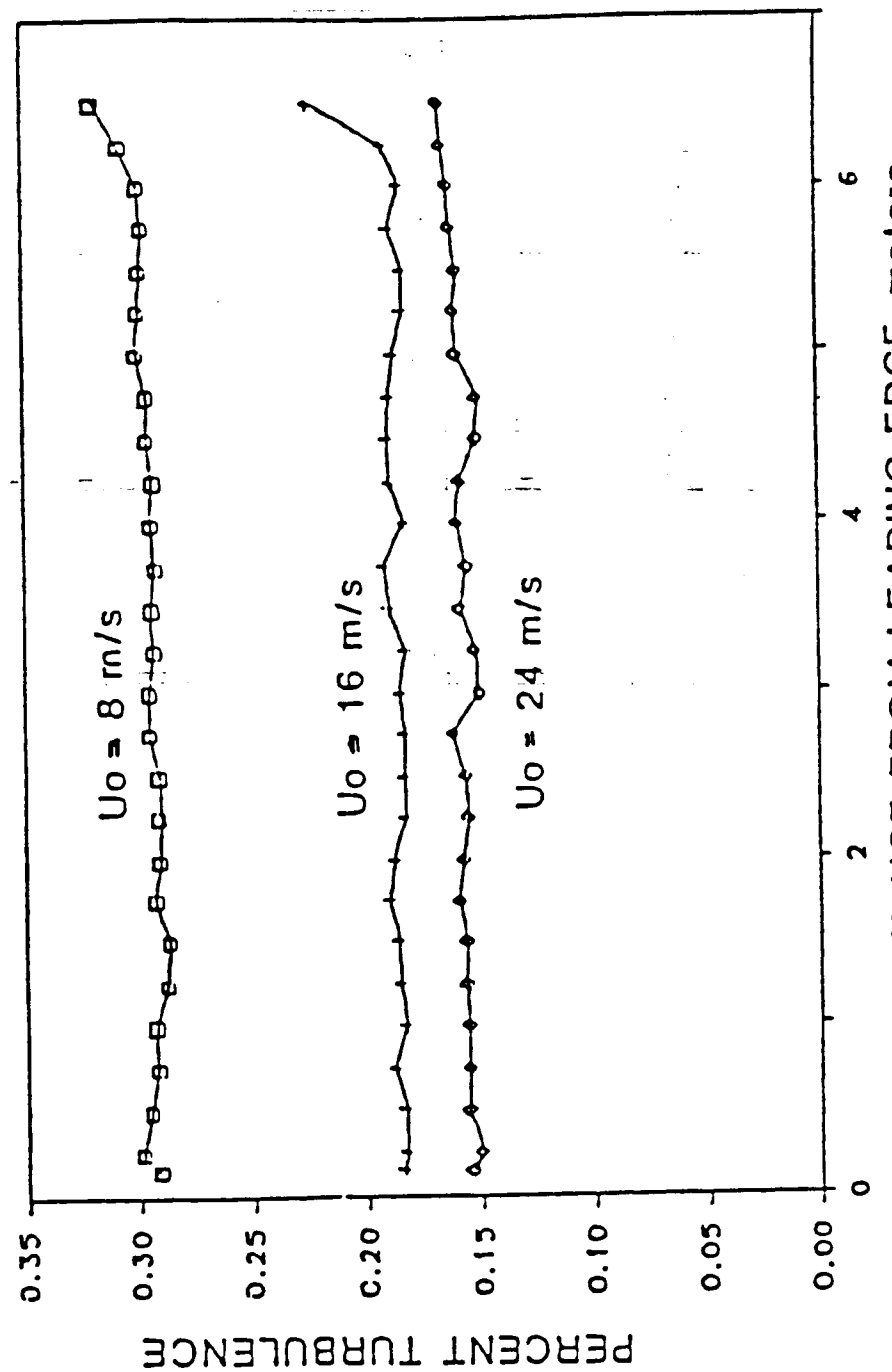

Figure 7. Axial distribution of turbulence intensity.

several manipulators that were tested. It is described in detail because a major portion of this study was spent upon it. This plate configuration was the fifth tested (LEBU #5) and was the most successful. The configurations previously tested also used a wind tunnel unit Reynolds number of $0.7 \times 10^6\ m^{-1}$, were located at a distance of 2.0 m from the test section leading edge and are described in section 3.6.

The upstream eddy detector hot film probe was positioned at the midspan of the test surface at a height of 0.85δ and at a distance, s, of 2.45δ upstream the LEBU trailing edge as shown in figure 5. This probe, used to detect the incident large eddies, was positioned as close as possible to the LEBU trailing edge because the large eddies lose their coherence after a distance of about 4δ [4]. The location of the large eddy detector probe must be, however, far enough upstream in order to prevent a feed back from the acoustic pulses. The axis of the probe was inclined at 45 degrees with respect to the test section vertical plane of symmetry (figure 4) in order to avoid probe interference with the downstream flow field. The processor delay time was set at $t = \frac{s}{0.93\,U_o}$; a typical value of t was 10 msec.

The pressure pulse mechanism was mounted under the test surface at midspan below the LEBU device trailing edge. The acoustic input was directed to the LEBU trailing edge through a circular opening (3/8 inch diameter) covered with fine screen flush mounted to the test surface.

A first approximation of the required sound pressure level of the acoustic waves was obtained by considering the boundary layer pressure perturbations near the trailing edge of a flat plate. According to detailed calculations (Appendix 1) a typical value of about 100 decibel (dB) pressure perturbation was predicted at the LEBU trailing edge. This is not the pressure fluctuation generated at the flat plate trailing edge when it encounters an oncoming average large eddy, but rather the typical pressure fluctuation in that location for a flat plate in inviscid free stream flow. It was assumed that sound pressure levels of this magnitude would be necessary to have some effect upon the trailing edge flow. A power amplifier was utilized to deliver the required power to the pulse mechanism.

The pressure pulse mechanism was bench tested with the wind tunnel operating at a unit Reynolds number of 0.7×10^6 m^{-1} using the output of the upstream hot film probe. The speaker mechanism was mounted outside of the wind tunnel under a wooden baffle plate with an acoustic wave port identical to that in the wind tunnel test section. The time averaged Root Mean Square (RMS) power spectra of the acoustic output at the LEBU's height was measured in a hard wall room under zero flow conditions. Figure 8 shows the RMS broadband spectra from 0 Hertz to 2,000 Hertz of the acoustic pulse emanating from the floor pressure port. The acoustic power is concentrated over a narrow region from 60 Hertz to 200 Hertz

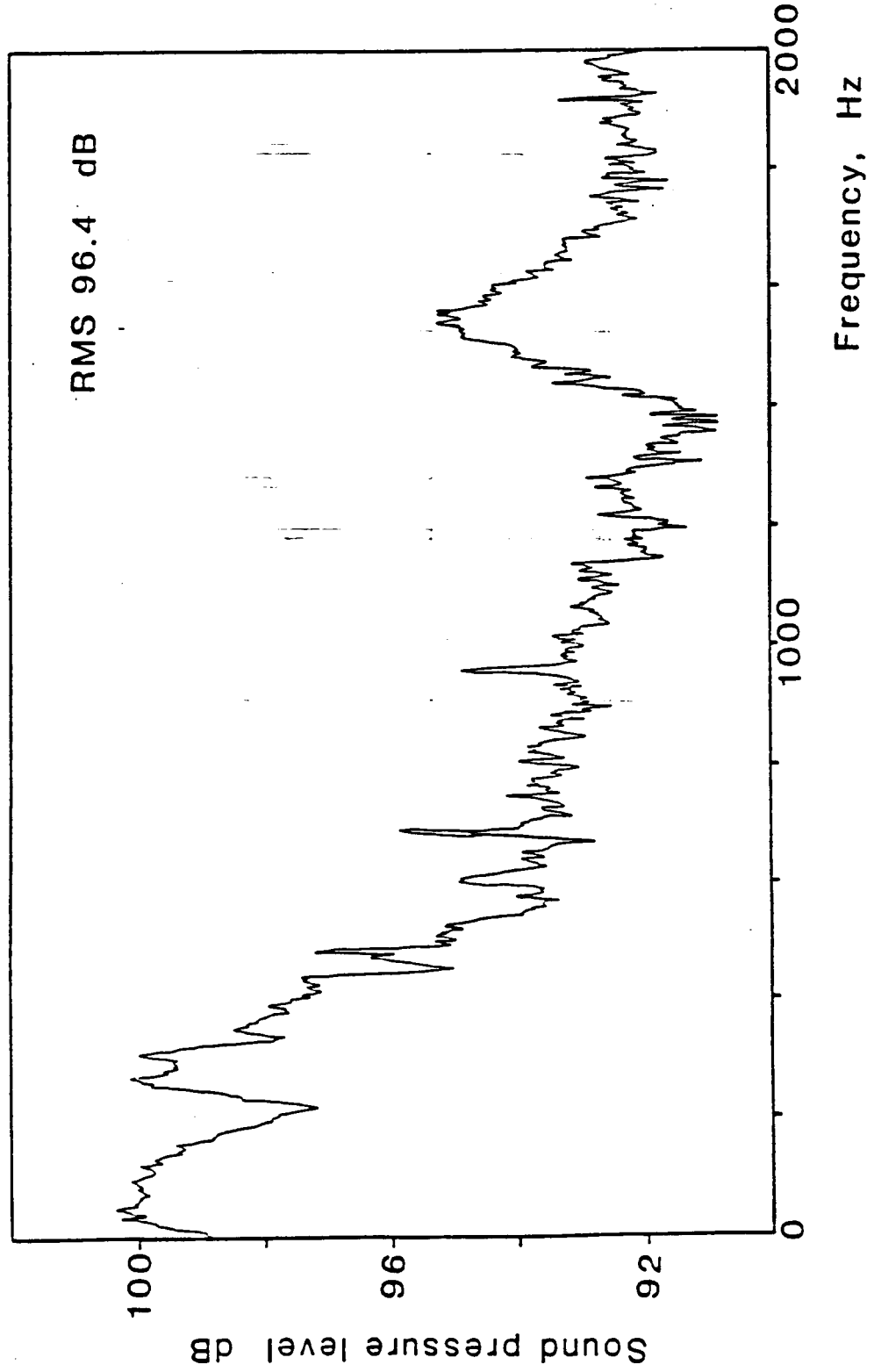

Figure 8. Narrow band acoustic signal of the pressure pulse at LEBU's height.

approximately at a level of 100 decibels. The sound pressure level at the LEBU's height integrated from 0 Hertz to 2,000 Hertz was 96.4 decibels. The large eddy passing frequency was expected to be approximately 110 Hertz, hence the bulk of the acoustic power occurred at the expected frequencies. The remaining part of the spectra consists of the harmonics of the acoustic pulses, the background noise, "ground dip" phenomenon and the harmonics of the wind tunnel fan blade passing tone. A 1/2 inch Bruel and Kjaer condenser microphone was utilized for these measurements.

2.3. DETERMINATION OF THE SKIN FRICTION COEFFICIENT, c_f

Measurements of the boundary layer profile downstream of the manipulator plate were obtained using a small boundary layer Pitot probe with an outside diameter of 0.5mm. A remotely controlled traversing mechanism was used to assist with the precision probe positioning. The traversing device provides probe movement over the Y-Z plane in the wind tunnel test section (figure 4) with a positioning accuracy of ± 0.1 mm. The pressures from the boundary layer probe were measured with a Validyne differential pressure transducer. The static pressure was obtained from static taps in the test surface. Approximately 200 samples were obtained and averaged at each point and the velocity profile was determined by 40 such points distributed over the thickness of the boundary layer. A Digital 16 bit resolution data acquition system in

conjunction with a Digital Computer were utilized in order to process the measured data and monitor the wind tunnel's operation. Variations in mean velocity of more than 1 percent and mean flow temperature of more than 2 percent automatically stopped the acquisition process, so that the exact conditions could be reset.

The momentum thickness, θ, is calculated from its definition (list of symbols) by numerically integrating the velocity profile over the boundary layer thickness. For zero pressure gradient two-dimensional flow the Von Karman Momentum Integral Equation reduces to:

$$\frac{c_f}{2} = \frac{d\theta}{dx} \qquad (2.1)$$

where, c_f is the local skin friction coefficient and x is the axial length. The momentum thickness, θ, is determined as described above for a plurality of positions downstream of the LEBU. The values can be least square fitted to a power curve of the form:

$$\theta = ax^b \qquad (2.2)$$

Hence, the skin friction coefficient can be estimated by :

$$c_f = 2abx^{b-1} \qquad (2.3)$$

An alternative calculation of the skin friction coefficient can be obtained by applying a central finite difference scheme upon equation 2.1

The previously described indirect method of measuring c_f, although time consuming, has certain advantages compared to other methods of wall shear stress measurement [22]. Skin

friction gauges have problems with the nessecary gaps and possible misalignement related to the floating element. Preston tubes, Stanton gauges and sublayer fences cause flow obstruction, and measurements are heavily dependent upon geometry and positioning. The method used in this study was the most economically sound and the most directly related to proven theory.

2.4. VERIFICATION OF THE BASIC FLOW CONFIGURATION

The momentum thickness, θ, of the turbulent boundary layer is of primary interest in the present investigation because it is used for determining the skin friction coefficient. Figure 9 shows measured and theoretically predicted values of θ for the plain flow case versus downstream distance x. The solid line represents values of momentum thickness predicted by Head's method [23]. The experimental values of θ were obtained by averaging 3 values across the span of the test surface. Head's method was applied for zero pressure gradient flow and initialized with a momentum thickness predicted empirically at the end of the sandpaper trip (Appendix 2.1). The initial shape parameter, H=1.375, was selected as the averaged measured value. The shape parameter H for a boundary layer is defined as the ratio of displacement to momentum thickness. Measured values of H at different axial locations are listed in table 1 along with the average. The initial or starting values in Head's

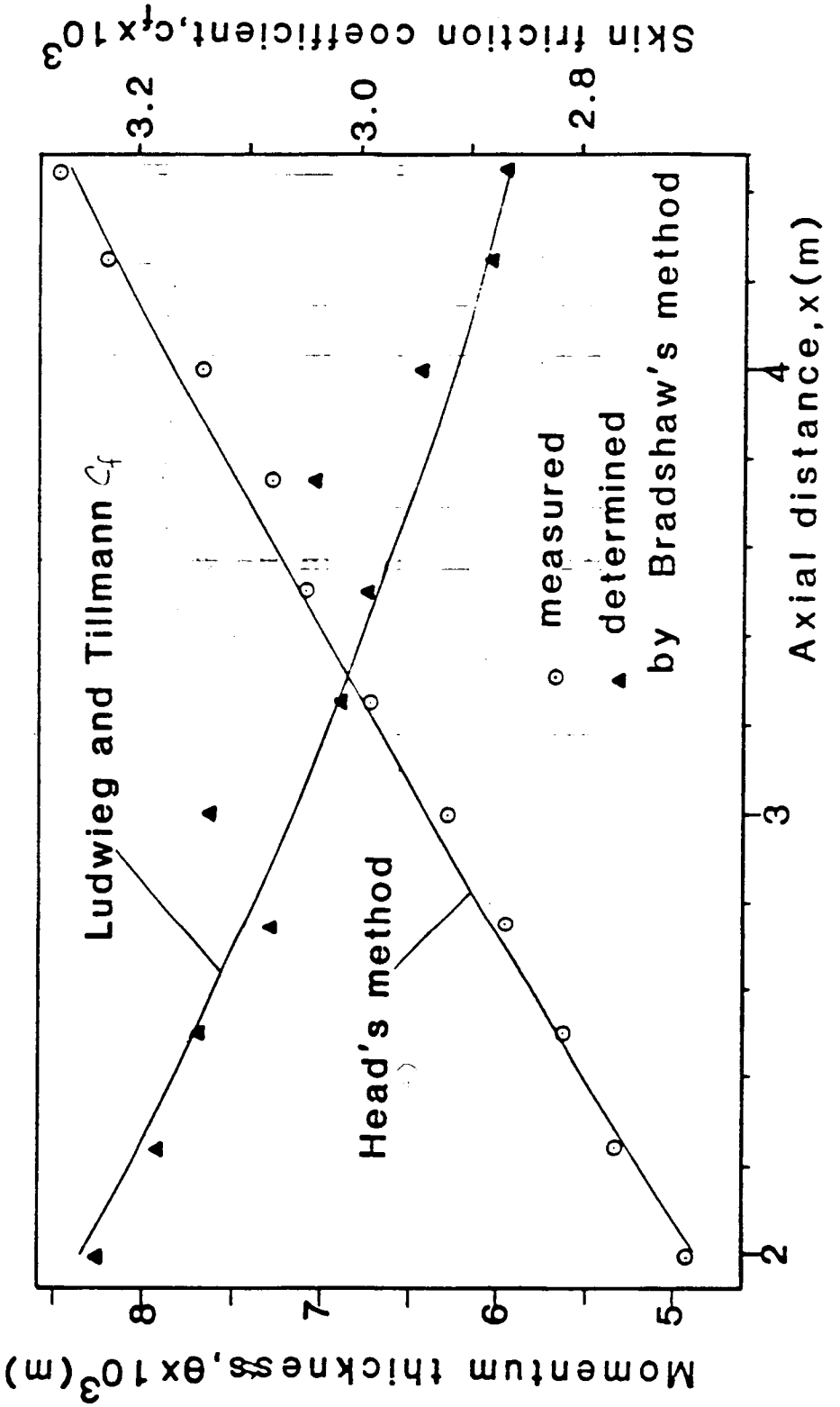

Figure 9. Predicted and measured momentum thickness, θ, and skin friction coefficient, c_f, for the plain flow.

Table 1. Measured shape parameter, H, versus axial distance, x ($\frac{U_o}{\nu}=0.7\times10^6$ m^{-1}).

x [m]	H
2.00	1.379
2.25	1.382
2.50	1.485
2.75	1.375
3.00	1.361
3.25	1.363
3.50	1.366
3.75	1.343
4.00	1.356
4.25	1.358
4.50	1.357

* average $\bar{H}=1.375$

method are relatively unimportant except for the first few points of the calculation. Agreement between the predicted and measured values of appeared satisfactory with a maximum deviation of 3 percent. The momentum thickness, θ, at 9 spanwise locations across the test section centerline at 2.0 m and 3.5 m from the test surface leading edge is shown on figure 10. The maximum deviation from the mean was 4 percent.

The local skin friction coefficient for a plain flow configuration was determined according to the procedure suggested by Bradshaw [24]. This method explained in Appendix 2.4 determines c_f from a measured boundary layer velocity profile. These measured results are compared with the axial skin friction coefficients predicted by the empirical formula of Ludwieg and Tillmann [1],

$$c = 0.246 Re_\theta^{-0.268} 10^{-0.678 H} \qquad (2.4)$$

in figure 9. The shape parameter H and momentum thickness Re in the above equation were predicted with Head's method. A maximum deviation of 2 percent was observed between the c_f predicted by Ludwieg and Tillmann's formula and the c_f determined by Bradshaw's method. Although Bradshaw's method predicted c_f very well for the plain flow, it was not used in other flow configurations because it is based upon the previous knowledge of the logarithmic law ; the form of the logarithmic law for a LEBU manipulated boundary layer has not been established yet.

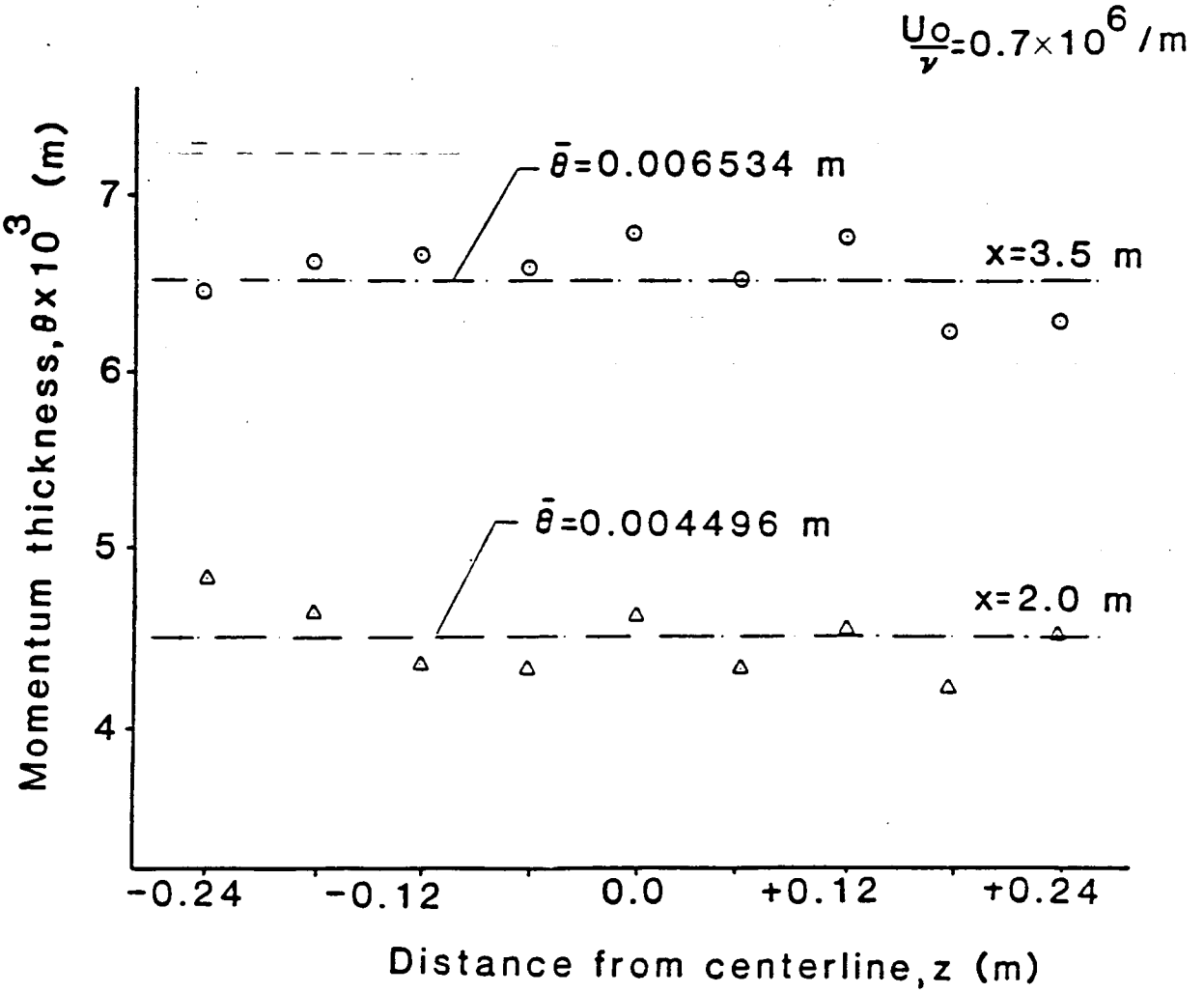

Figure 10. Spanwise variation of momentum thickness, θ, at two axial locations.

The measured velocity profile for the plain flow configuration was compared to a theoretically predicted profile using a modified Coles' boundary layer (Appendix 2.2). The velocity profile was calculated for an axial location 2.5 m from the test section leading edge. The free stream velocity was set at 11.35 m/s to satisfy the unit Reynolds number requirement of $0.7 \times 10^6 m^{-1}$ and the resulting theoretical and experimental profiles are shown in figure 11. The maximum deviation between predicted and measured velocity values was 2 percent.

Measurements of the fluctuating axial velocity component were obtained across the turbulent boundary layer at an axial location of 2.0 m with a hot film probe. These data are plotted in figure 12 and compared with classical measurements of Klebanoff [1]. The trend of the data agrees fairly well although the magnitude of the measured data is lower than Klebanoff's classic measurements. Such deviations should be expected since Klebanoff's data are for a Reynolds number of 10^7 whereas the measurements of figure 12 were obtained with a Reynolds number of 1.4×10^6. A method to scale the measured data to correct for the difference in Reynolds numbers was not available.

The boundary layer velocity profile for a LEBU configuration was predicted by superimposing the turbulent wake velocity distribution from a thin plate upon a plain flow profile. The detailed calculation procedure is described

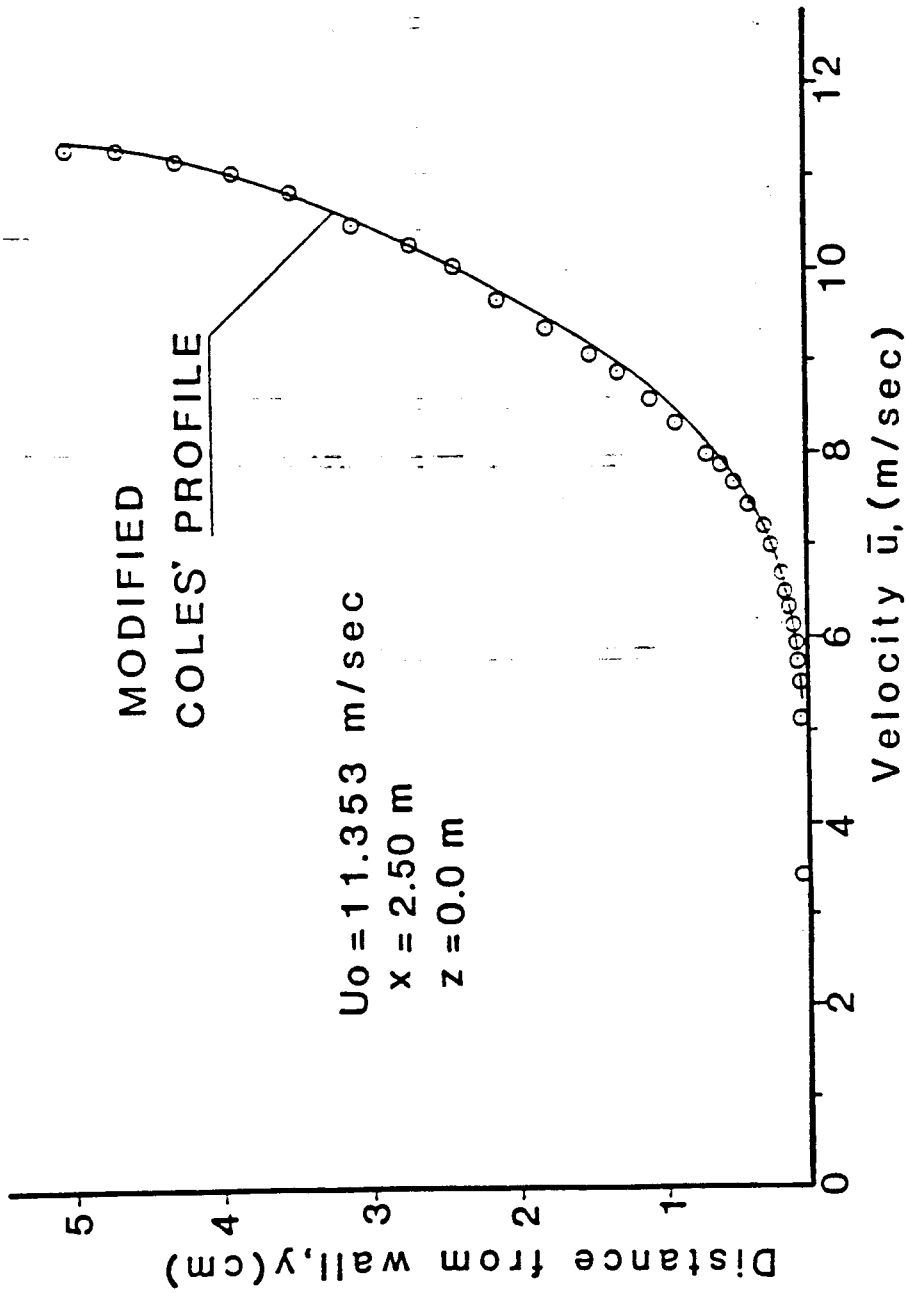

Figure 11. Predicted and measured mean velocity profile for the plain flow.

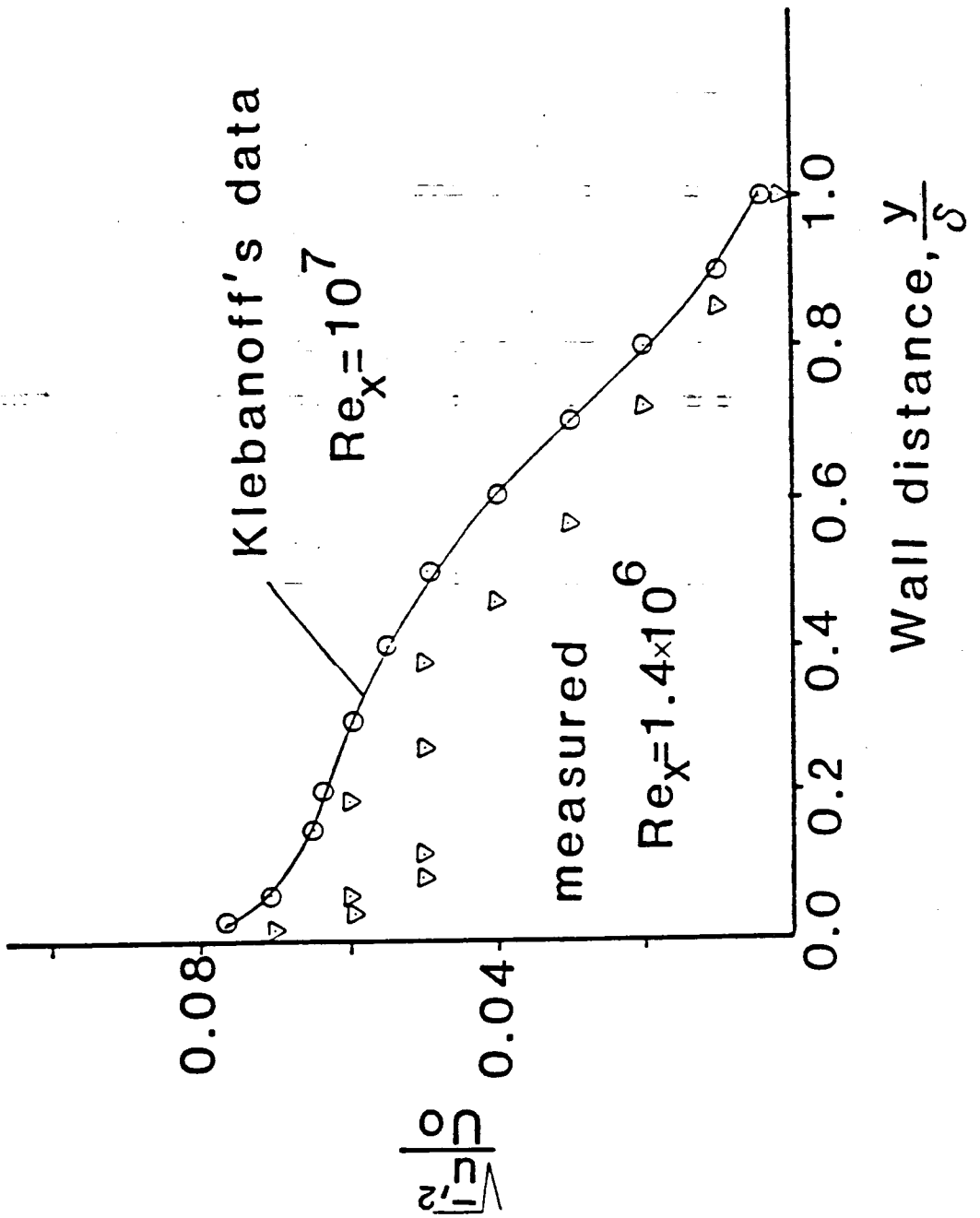

Figure 12. Measurements of the streamwise velocity, $\frac{u'}{U_o}$, across the boundary layer.

in Appendix 2.3 and the predicted and measured profiles are shown in figure 13. Their agreement was found satisfactory and a 4 percent maximum difference was measured.

The structure of the turbulent boundary layer was investigated by using flow visualization with the Smoke-Wire method of Raspet and Moore [25]. The smoke was produced by vaporizing oil from a fine stainless steel wire by impulsive resistive heating. The smoke wire was mounted vertically in the test section with the tunnel operating at low speed. Large scale eddies shaping the boundary layer intermitancy region and typical eddies throughout the layer can be observed in figure 1.

The mean free stream velocity was uniform in the spanwise direction within 0.2 percent [21] and momentum thickness across the test section span varied within 4 percent of the mean value. These small deviations combined with the satisfactory agreement found between predicted and measured flow characteristics allow the assumption of a two dimensional ergodic turbulent boundary layer with the large eddy break-up device removed. When the LEBU is installed the basic velocity profile downstream of the device is also as expected. The wake of the plate appears normal and the slight increase in the velocity profile, at approximately y=1.0 cm in figure 13, may be attributed to the viscous drag reduction capability of the LEBU which manifests itself as a reduction in momentum thickness.

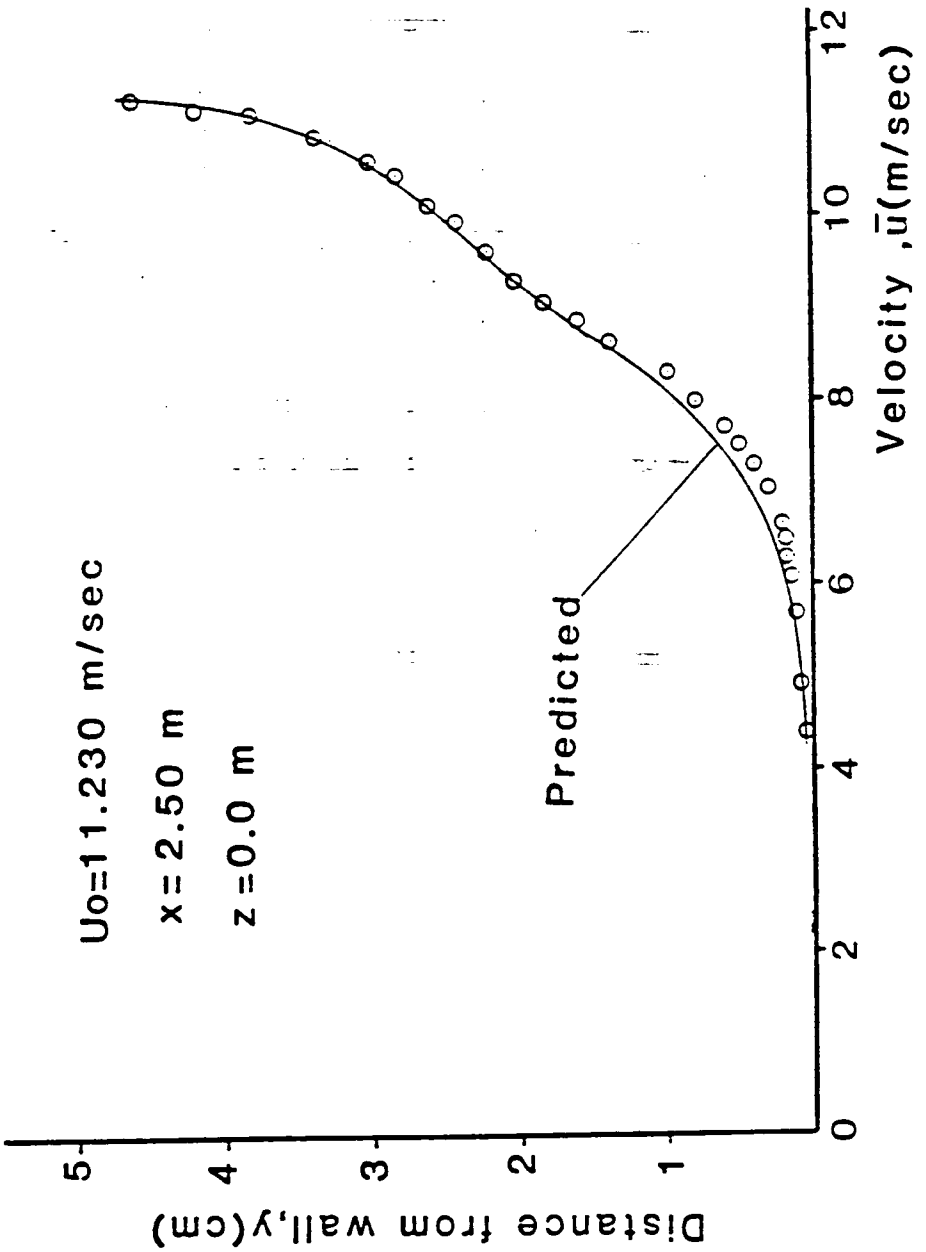

Figure 13. Predicted and measured mean velocity profile for LEBU #2 configuration.

3. RESULTS AND DISCUSSION

The experiments with acoustic excitation of the LEBU were performed in order to:

i. Determine if proper acoustic excitation can enhance the effectiveness of a boundary layer plate manipulator.

ii. Investigate the properties of the resulting flow field downstream of the LEBU.

iii. Search for the optimum operating parameters of the experiment.

iv. Examine the effectiveness of the acoustic excitation with different experimental conditions.

3.1. BASIC RESULTS

3.1.1. SKIN FRICTION DRAG REDUCTION

The effect of the acoustic pulse upon the plain flow was first examined and the momentum thickness growth for the unexcited and the excited plain flows is compared on figure 14. The acoustic input caused no significant alterations in the flow and the average value of θ for the acoustically excited configuration was found to be higher than the unexcited configuration by only 0.5 percent. This slight increase in θ is due to an expected small increase in mixing near the acoustic source. Figure 14 shows that the acoustic input has no significant effect on the flow when the LEBU is

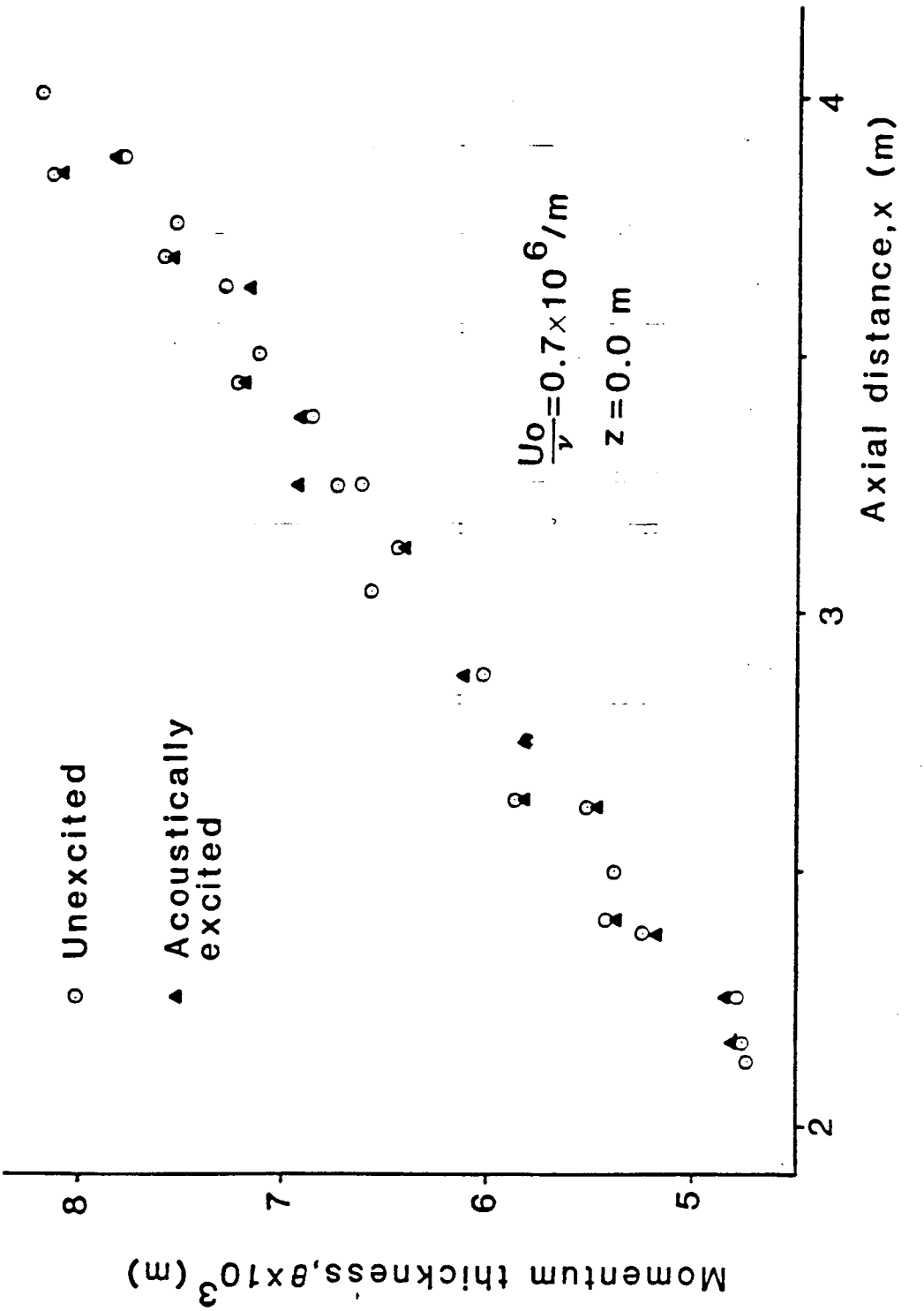

Figure 14. Momentum thickness, θ, versus axial distance, x, for the excited and unexcited plain flows.

not installed.

When the thin plate was installed turbulent boundary layer velocity profiles were obtained at midspan locations downstream of the LEBU manipulator. The momentum thickness, θ, was calculated as described in section 2.3 and plotted versus downstream distance, x, from the test surface leading edge. Figure 15 shows the axial variation of for the following configurations:

i. Plain flow with the upstream sensor installed

ii. The LEBU configuration with the upstream sensor installed but not operating.

iii. The LEBU configuration acoustically excited.

The momentum thickness of the manipulated flow is greater than the plain flow case near the LEBU because of momentum loss imposed by the embedded thin plate. The momentum thickness near the LEBU trailing edge (4 boundary layer thicknesses downstream) is within 5 percent of the sum of the momentum thickness of the plain flow case and the momentum thicknesses of the laminar boundary layers that develop on the upper and lower surfaces of the plate.

The acoustically excited case produces an even greater momentum loss at this location. If the acoustic input was merely tripping the laminar boundary layer, one might hope to repeat the above superposition using a calculation for turbulent boundary layers on the LEBU plate. The measured increase in θ with the acoustic input is, however,

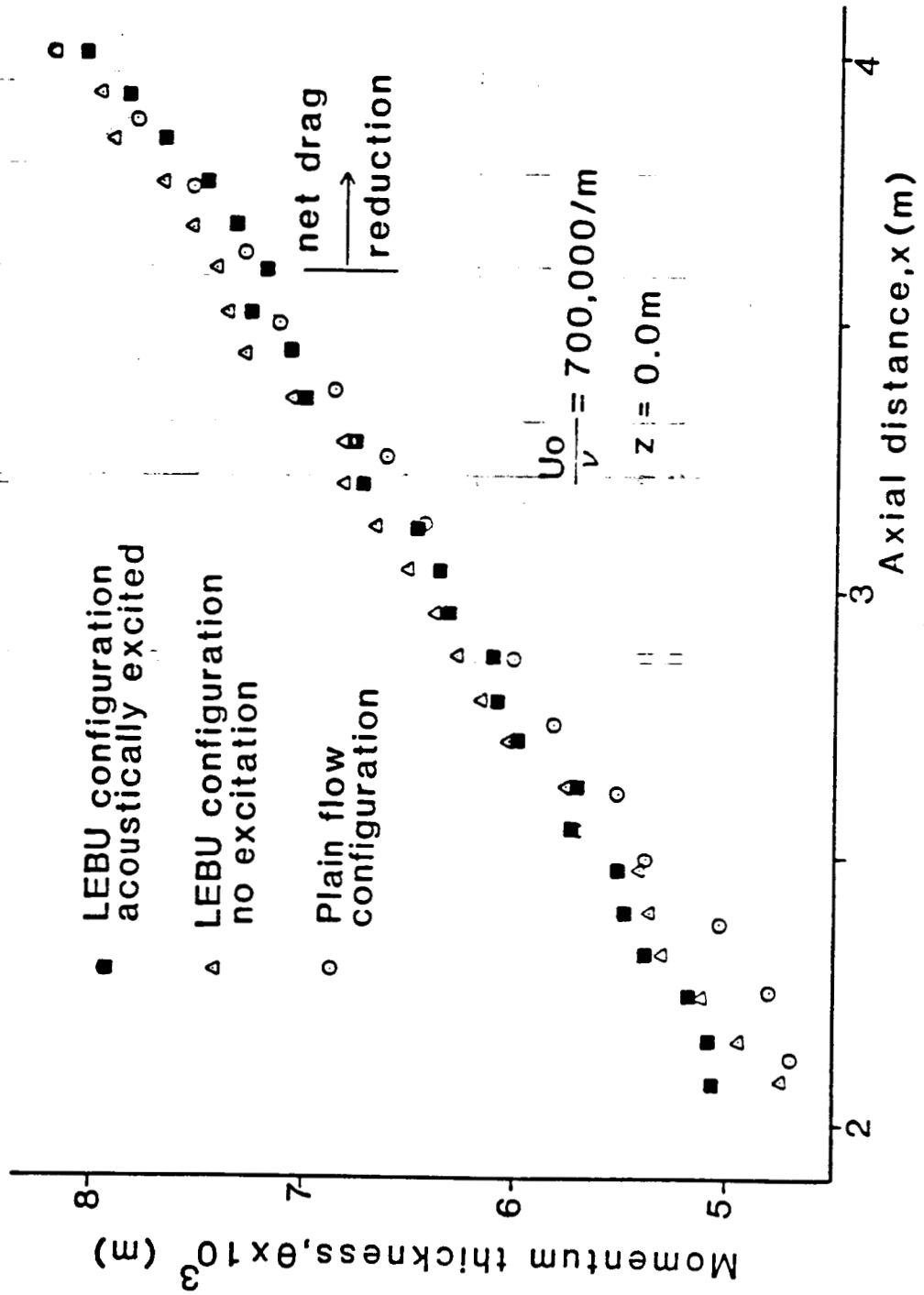

Figure 15. Momentum thickness, θ, versus axial distance ,X, for various flow configurations.

approximately ten times the expected increase that could be attributed to turbulent boundary layers. These results suggest that an additional mechanism may be active during the acoustic excitation; a mechanism which alters the trailing edge flow from the blade in a manner other than merely tripping a laminar layer to a turbulent boundary layer.

Further downstream at x=2.6 m (15δ from the LEBU) the momentum thickness of the acoustically excited configuration relaxes to that of the unexcited LEBU but grows at a slower rate. The same trend is noted at x=3.8 m where the momentum thickness of the acoustically excited flow becomes less than the plain flow configuration. This a clear indication of reduced skin friction coefficient and net drag reduction.

The approximate variation of the skin friction coefficient, c_f, with the axial distance from the test surface leading edge is shown in figure 16. All measurements were obtained at the test surface mid span. This location was aligned with the upstream sensor and the acoustic wave port. The numerical values of the skin friction coefficient were calculated according to the procedure described in section 2.3. All least square curve fits had a correlation coefficient above 0.99. The LEBU configuration and the acoustically excited flow were compared to the plain flow (hot film sensor installed). According to the numerical values of the skin friction coefficient, acoustic excitation can enhance the LEBU's effect by reducing c_f between

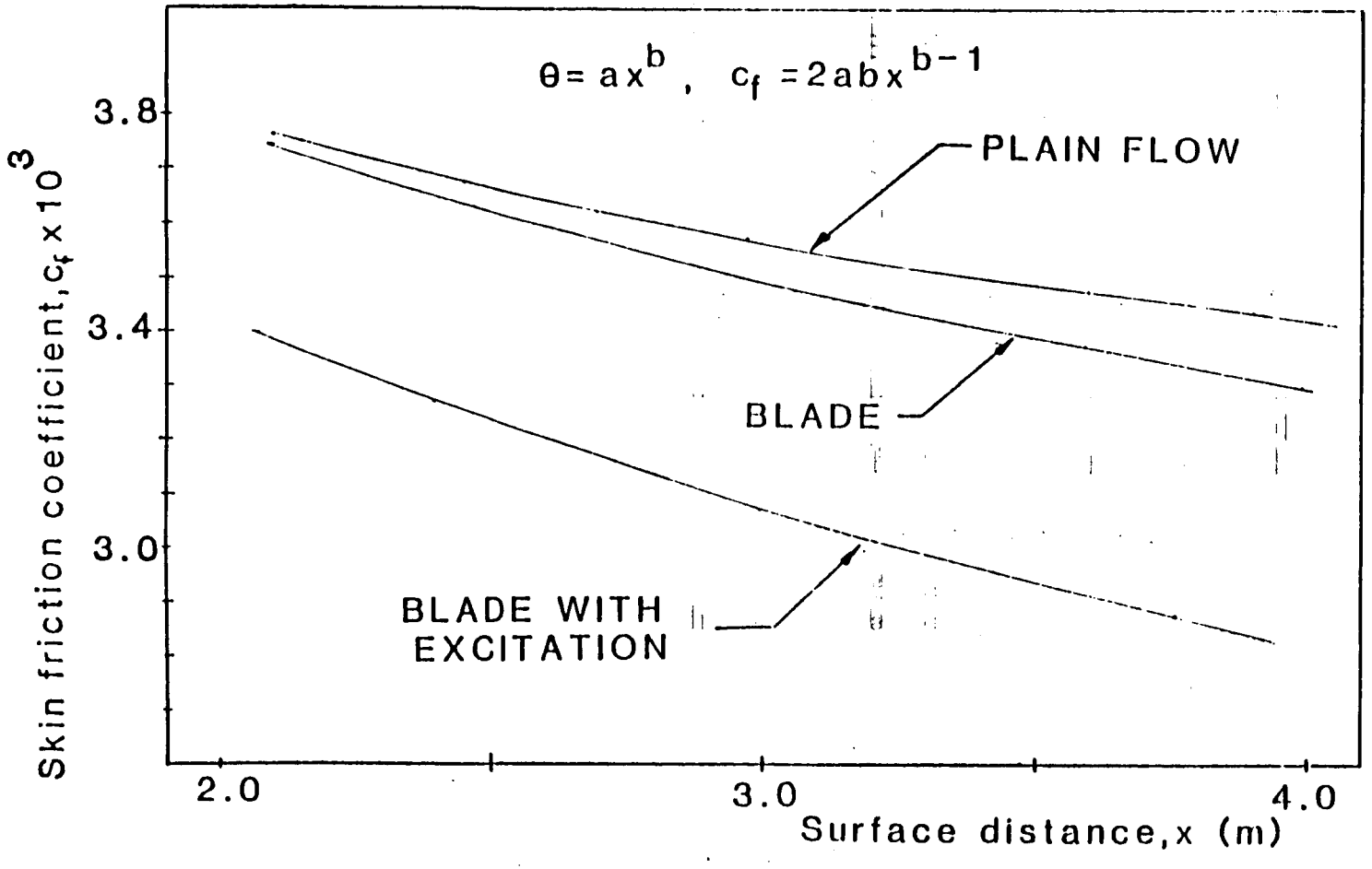

Figure 16. Variation of the skin friction coefficient ,c_f, for each configuration.

approximately 7 and 13 percent with respect to the unexcited LEBU configuration. Comparison with the plain flow shows a reduction of the wall shear stress between 9 and 15 percent.

3.1.2. SKIN FRICTION DRAG REDUCTION MECHANISM

Space-time cross correlation functions (CCF) were obtained using the hot film eddy detector probe upstream of the LEBU plate as a fixed reference location and another probe at various downstream locations as indicated in figure 17. A dual channel anemometer was utilized and the hot film probe signals were processed with a NICOLET 660B FFT analyzer. Figure 18 shows peak values of the space-time cross correlation functions versus probe separation distance, ξ, at various boundary layer heights. Far away from the LEBU, in the downstream direction, the residual acoustic far field produces higher cross correlation peaks when the acoustic excitation is applied. When the moving probe is located near the LEBU's leading edge the excitation causes significant increases in the cross correlation functions because the probes are exposed to both, the large scale eddies and the acoustic field. At the trailing edge of the plate in the outer region of the boundary layer the flow without excitation maintains a maximum CCF approximately equal to that of the leading edge. The wake of the LEBU in this case is clearly correlated to the incident flow. When acoustic excitation is applied the downstream flow is correlated to

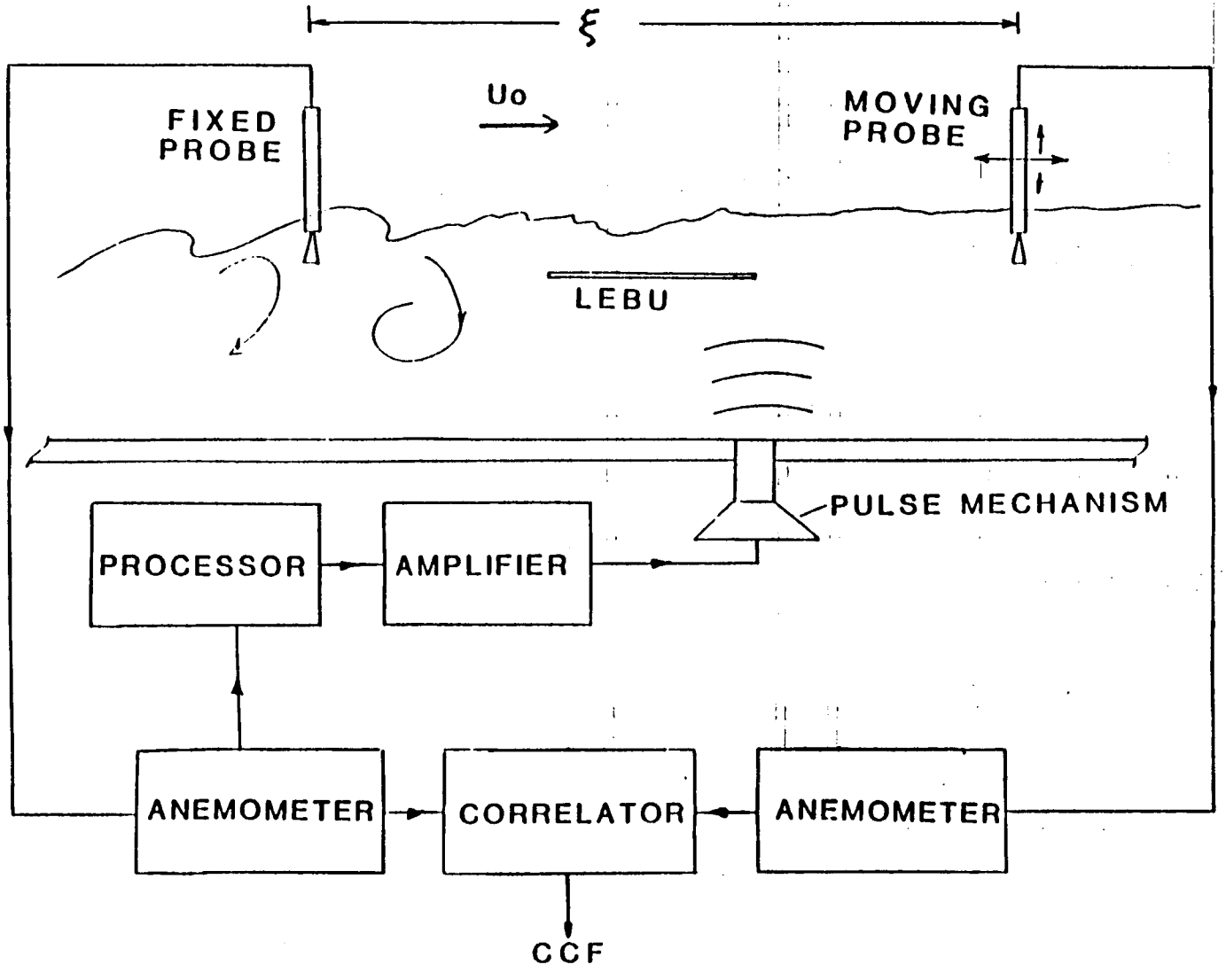

Figure 17. Schematic for velocity cross correlation measurements across the LEBU.

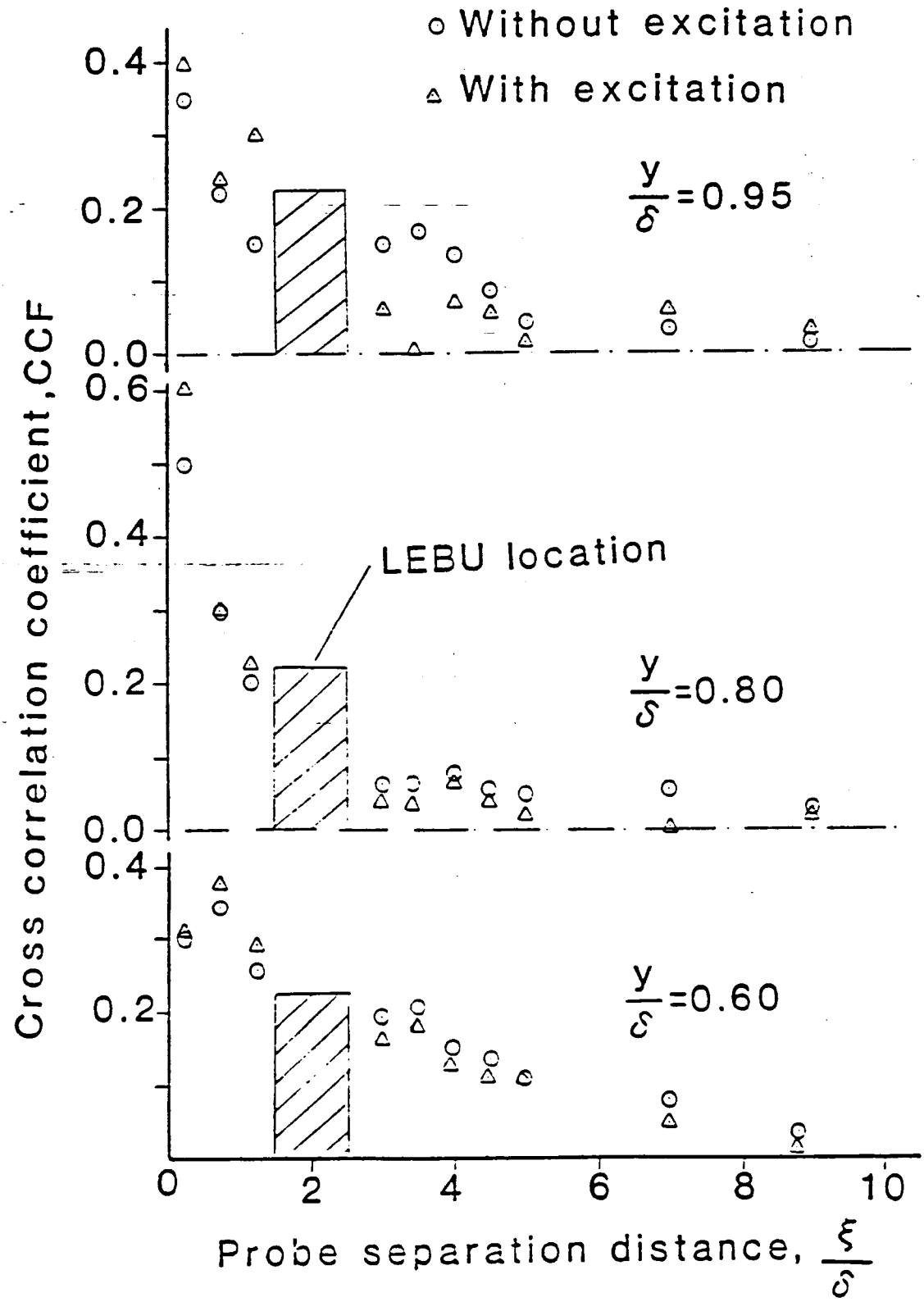

Figure 13. Maximum space-time velocity cross correlation in the boundary layer.

the upstream point significantly less. The reduction is more obvious at the outer region of the boundary layer ($\frac{y}{\delta}$=0.95) where the large eddies dominate. This indicates that acoustic excitation enhances the destruction of the large eddies which are sensed at the upstream location. It is assumed that the impinging sound wave at the LEBU trailing edge sheds a vortex of opposing rotation to the oncoming large eddies resulting in enhanced large eddy cancellation.

At downstream locations deeper inside the boundary layer ($\frac{y}{\delta}$=0.80, $\frac{y}{\delta}$=0.60) the reduction of the CCF, when acoustics are applied, is moderate because large eddies appear mainly in the outer part of the boundary layer. The reduction of the CCF when the moving probe is at the LEBU's height signifies that the acoustic pulses assist the manipulator in canceling large eddies. All time delay values associated with the cross correlation function peaks correspond to expected large eddy convection times and not to the acoustic wave propagation time.

The turbulence intensity of the low frequency part of the turbulence spectrum was examined downstream of the plate manipulator. A hot film probe was positioned slighty above (1.5 mm) the LEBU's height and the turbulence spectrum from 0 to 2,000 Hz was measured. Figure 19 compares the variation of the root mean square (RMS) of the fluctuating axial velocity component u' for the acoustically excited flow to the unexcited LEBU configuration at various downstream locations.

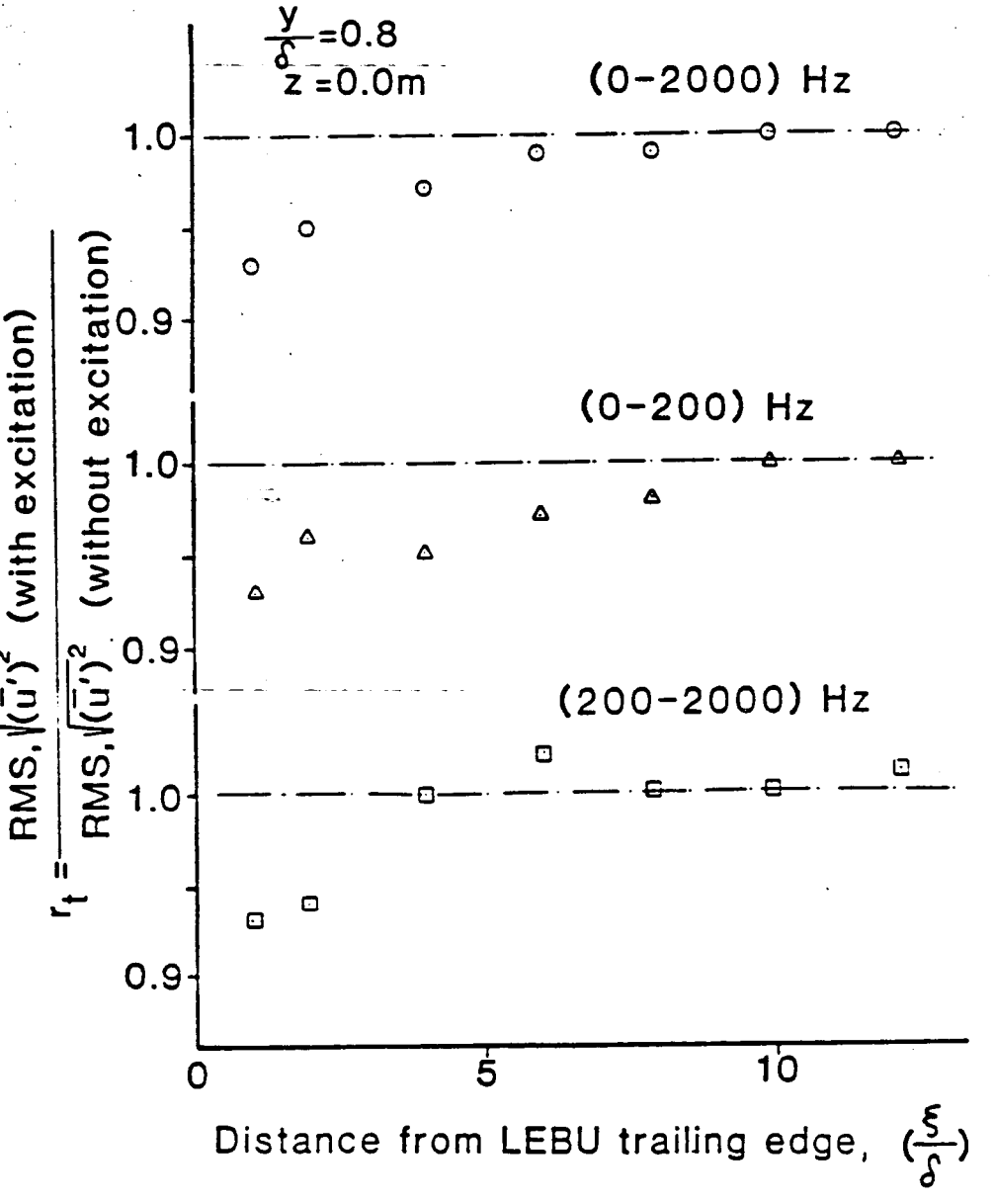

Figure 19. Relative variation of the low frequency RMS turbulence close to the LEBU trailing edge.

The turbulence level over 2 KHz is considerably reduced when acoustics are applied and the effect persists for a distance of 8δ downstream of the LEBU. When the low frequency (0 to 200 Hz) part of the signal is examined the level of the turbulence intensity appears further reduced. This range of frequencies approximately corresponds to the large eddy passing frequency which is estimated to occur near 110 Hertz and dominate the low frequency spectrum. The relatively higher frequency (200 to 2,000 Hz) part of the turbulence spectrum remains largely unaffected by the acoustic pulses. This indicates that only the large wavelength motions of the turbulent boundary layer are affected when the flow is acoustically excited. The measurements of the RMS velocity fluctuation, as for the previous CCF data, were limited to a distance of about 10δ downstream the LEBU.

To better understand the influence of the acoustic excitation on the flow manipulator, a pulsed smoke wire was used to obtain flow visualization photographs. The smoke wire was mounted downstream of the manipulator at the midspan of the tunnel. The fine wires ran vertically from the wind tunnel floor through the boundary layer. Figure 20 shows typical results for the three cases of concern. The large eddy break-up device reduces the large scale structure in the boundary layer and acoustic excitation of the device causes further reduction in coherent motion. The results were obtained at approximately 35δ downstream of the manipulator.

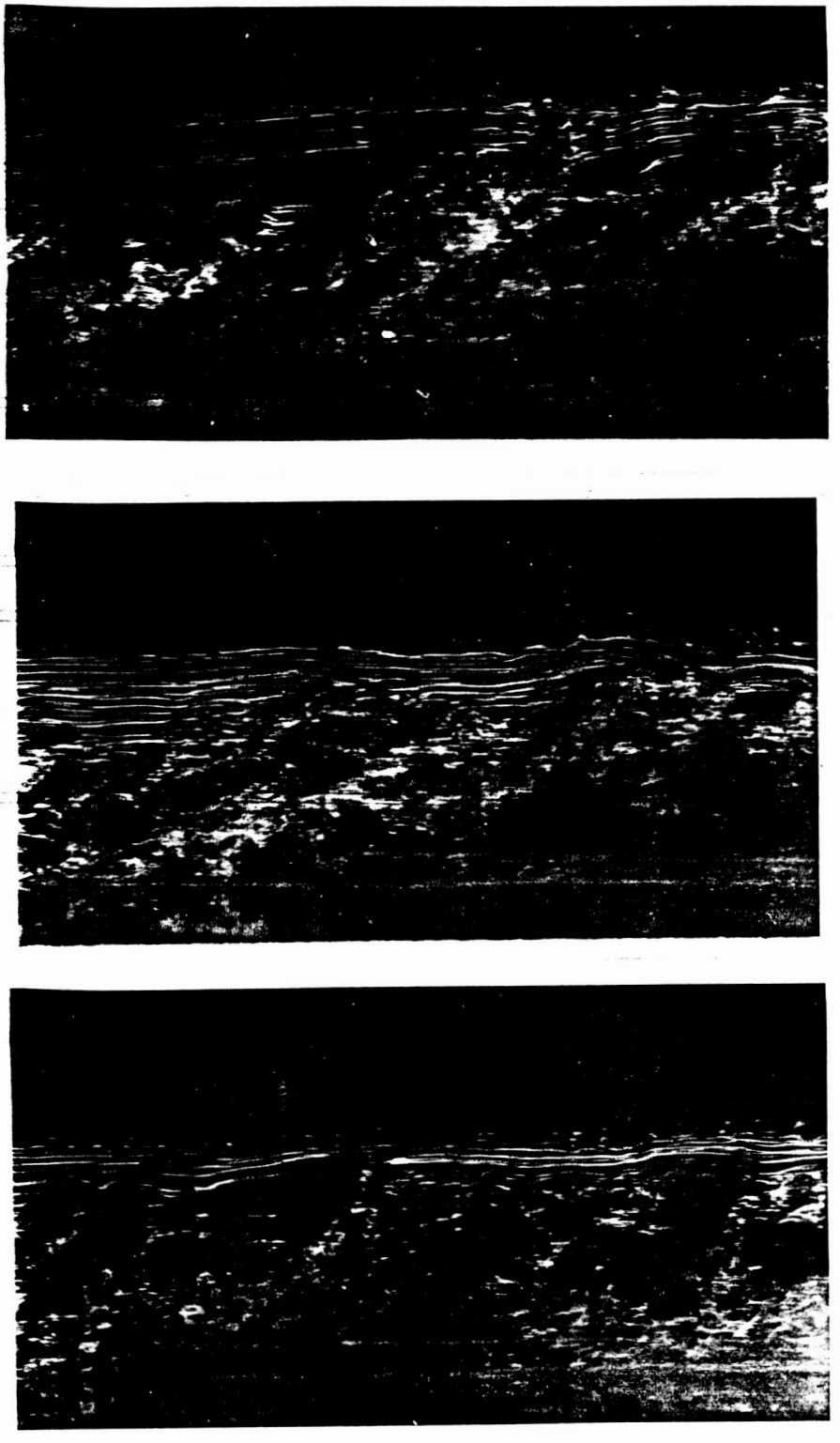

Figure 20. Boundary layer flow visualization for the (A) plain case (B) LEBU manipulated and (C) acoustically excited LEBU configuration.

The sound waves at the LEBU trailing edge apparently shed vorticity which helps cancel the oncoming large eddies.

The possibility of vertical oscillation of the thin ribbon when "hit" by acoustic waves was examined. The goal of this study is to control the large eddy break-up process without moving the LEBU. Motion of the device could generate more disturbances and alter the boundary layer on the device, thus altering the momentum thickness downstream. A small accelerometer was mounted on the LEBU above the acoustic wave port. Vertical displacement measurements were obtained with no flow; the pressure pulse device was excited with a previously recorded anemometer signal from the turbulent boundary layer. The measured vertical displacement when acoustics were applied could not be distinguished from the background electronic noise. The reduced correlation of the flow across the LEBU and reduction of RMS velocity fluctuations with acoustics, can be only attributed to the interaction of the acoustic input and the fixed LEBU, not the motion of the manipulator device. This is evident because the acoustic pulses had no effect upon the the plain flow; also they cause no vertical motion of the plate at zero flow conditions.

According to these results an acoustic pulse of the proper sound pressure level and phase locked to the convected large scale structures can enhance the effectiveness of a plate manipulator. Large scale eddies contribute

approximately 50 percent of the turbulent energy and 80 percent of the Reynolds stress when the outer part of the boundary layer is considered [9]. Turbulent "bursting" in the sublayer accounts for most of the turbulence and Reynolds stress close to the wall [26,27]. If the passage of the large eddies is related to the triggering of "bursting" events in the sublayer, then their enhanced destruction can lead to further reduction of skin friction drag downstream of the LEBU. Energy exchange between the mean flow and turbulence is governed by the dynamics of the large eddies [28] which extract kinetic energy from the mean flow. The break-up of the energy cascade from the very large eddies to the small energy dissipating structures can lead to reduced momentum transfer to the wall and reduced skin friction drag.

3.2. SPREADING EFFECT

It is clear from figure 15 that increased drag reduction due to acoustic excitation persists downstream for a considerable distance. Measurements of θ across the span of the test section indicated that the beneficial effects of excitation spread slowly in the spanwise direction as the flow convected downstream.

3.2.1. SPANWISE MAPPING DOWNSTREAM OF THE LEBU

The spreading of the acoustic excitation effect downstream of the LEBU was mapped indirectly. It has been

observed (section 3.1.2) that the output signals of two hot film probes across the LEBU at midspan of the test surface are less correlated when acoustic excitation is applied. The cross correlation function (CCF) between the upstream fixed sensor and another positioned at various spanwise locations downstream of the blade was measured. The ratio $r_c = \frac{CCF(LA)}{CCF(L)}$ was calculated; LA signifies the acoustically excited LEBU configuration and L signifies the LEBU configuration without excitation. Figure 21 shows a schematic top view of the test surface downstream of the LEBU with expanded z coordinates. The solid symbols indicate points on the test surface where the ratio r_c is smaller than unity because the acoustic waves enhance the large eddy destruction. The open symbols indicate points where the ratio r_c is greater than unity because the acoustic pulses make the probe signals more correlated. These measurements could not be extended further downstream because the large eddies have a limited life span and decay after traveling a distance of approximately 10δ. A slight spreading of the acoustic excitation effect at a half angle of about 2 degrees can be seen in figure 21. This spreading is verified by spanwise measurements of momentum thickness.

Figure 22 shows the variation of the ratio $r_\Theta = \frac{\Theta(LA)}{\Theta(L)}$ with the spanwise distance, z, from the test surface centerline for various axial locations. The variation of momentum thickness, Θ, (section 3.1.1) measured at the test surface centerline needs to be reconsidered. According to

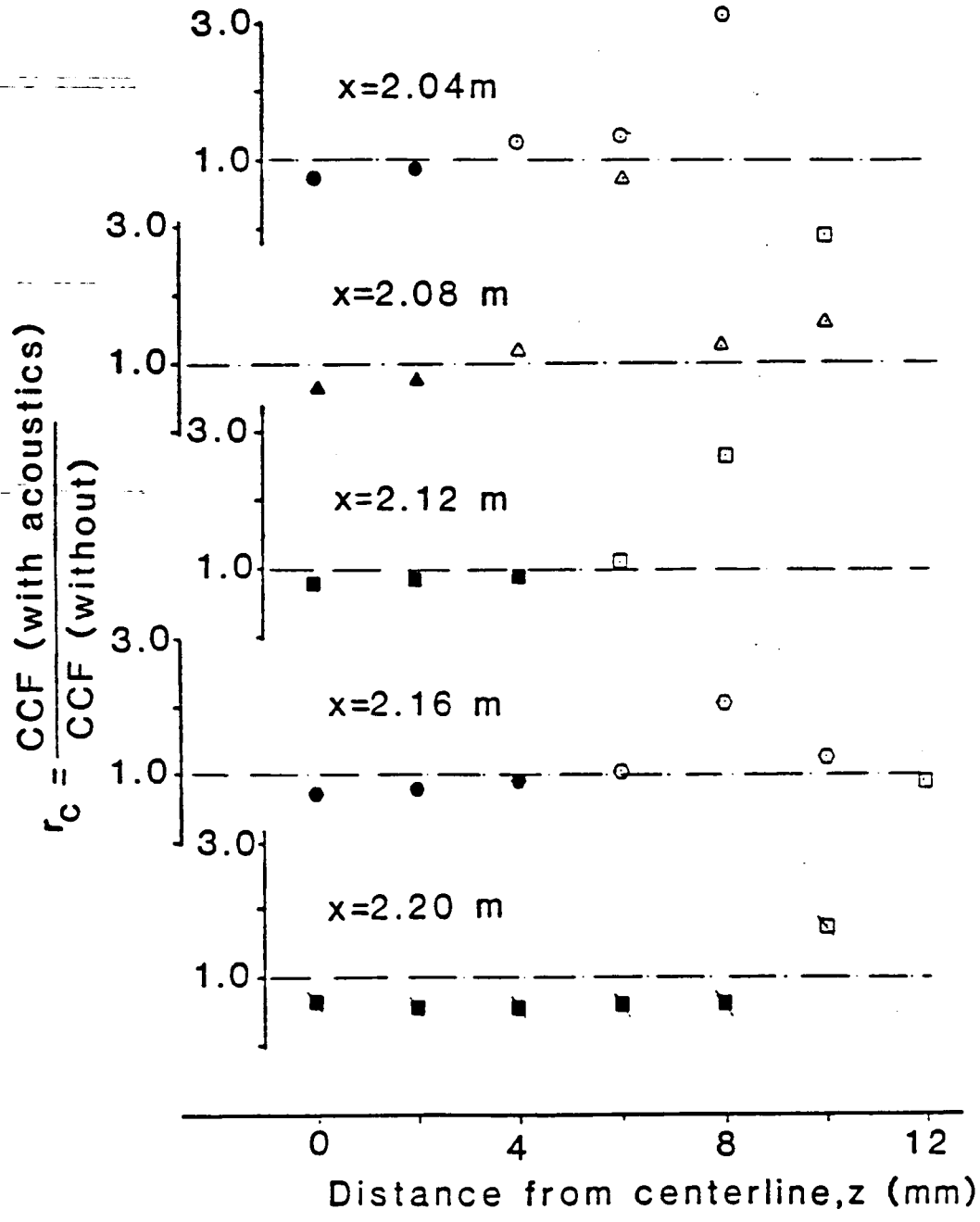

Figure 21. Spanwise mapping of the peak cross correlation downstream of the LEBU (solid symbols indicate less than 1.0).

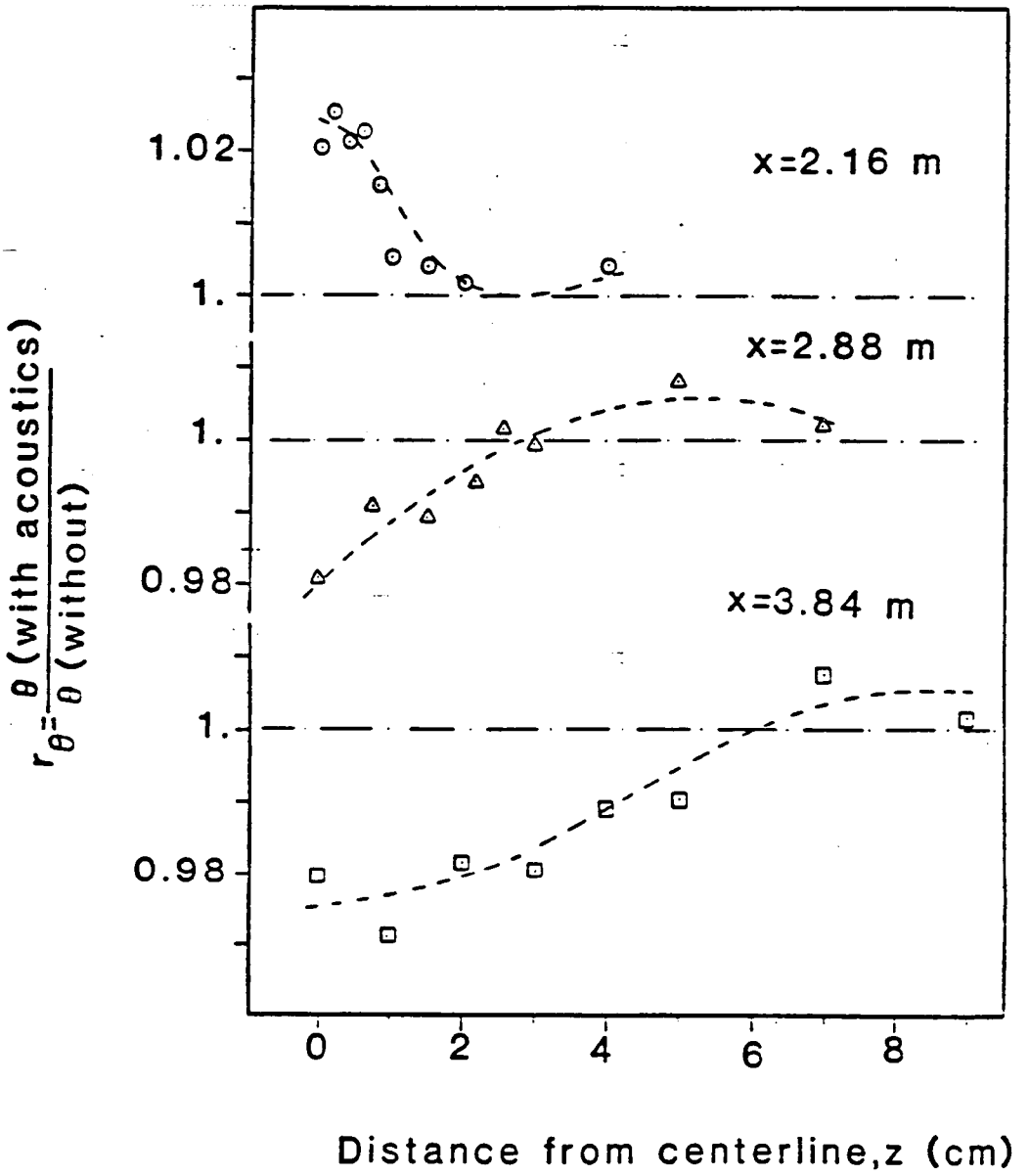

Figure 22. Spanwise variation of momentum thickness ,θ, for the excited and unexcited LEBU at three axial locations.

these data the ratio r_θ is greater than unity at axial locations close to the LEBU trailing edge. Further downstream at a distance of 6δ to 8δ from the LEBU trailing edge the ratio r_θ becomes smaller than unity, remaining as such for the rest of the test section. Returning to figure 22, at x=2.16 m, the spanwise measurements of θ indicate a narrow region where r_θ is greater than unity. Further downstream, at axial distances of 22δ and 47δ from the plate manipulator, the ratio r_θ was found to be smaller than unity over a broader extent in the z direction. These data show a tendency for the drag reduction phenomena to spread spanwise at a half angle of about 2 degrees. The experiment was limited to a distance of 50 boundary layer thicknesses from the LEBU because most of the previous investigations indicated that a manipulated turbulent boundary layer relaxes to the undisturbed flow after 50 to 100δ. Furthermore, the length of the test section did not allow good measurements beyond this point. The small value of the spreading angle is attributed to the mixing process of the surrounding turbulent boundary layer. This angle also agrees with the results observed for the spanwise spreading of the reduction in the space-time cross correlation near the LEBU.

The turbulence intensity,T, of the axial flow velocity component, with and without excitation was measured throughout the boundary layer at three axial locations. Figure 23 shows the variation of the parameter $r_T = \frac{T(LA)}{T(L)}$,

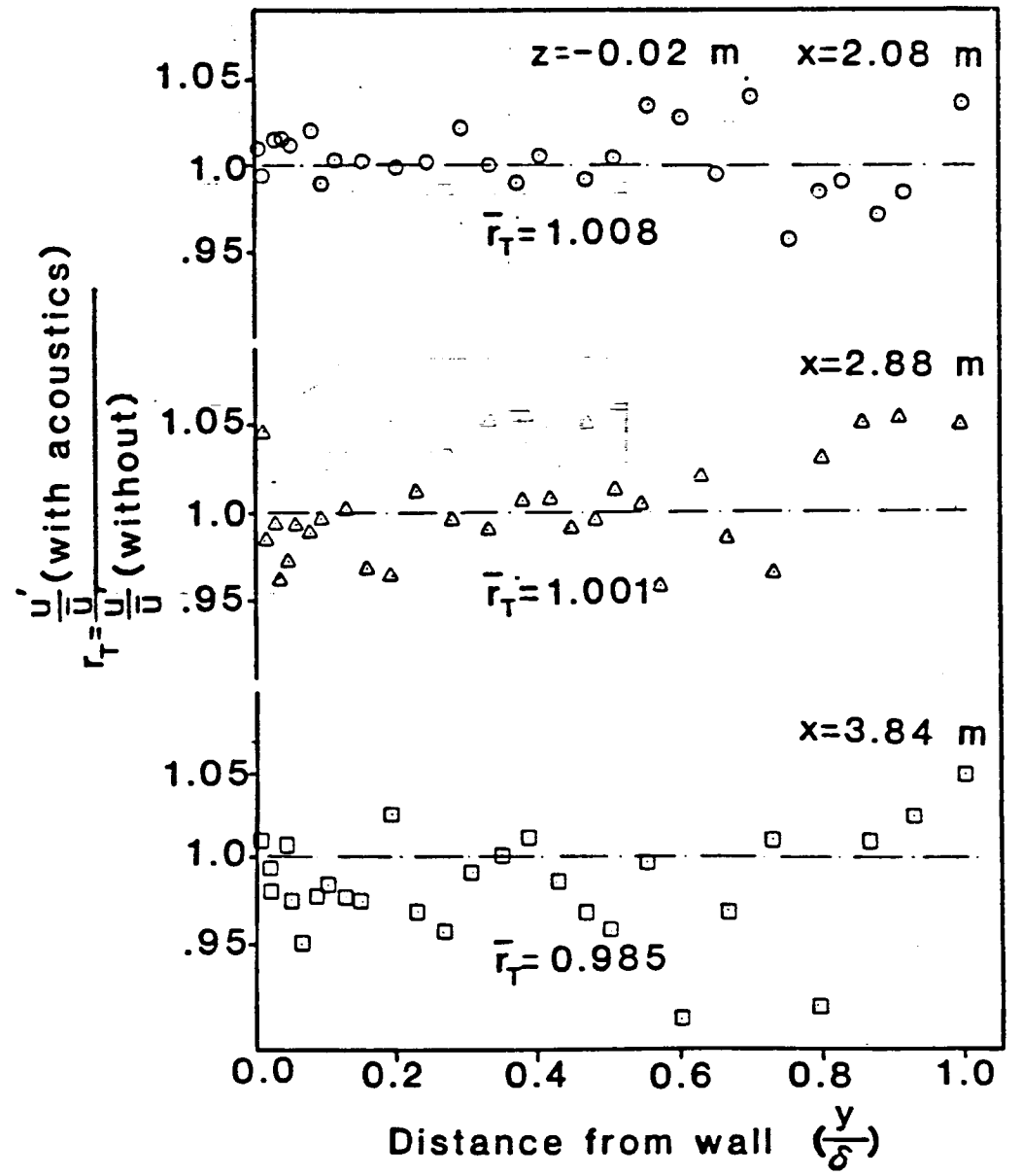

Figure 23. Relative turbulence intensity of the excited boundary layer across the "wedge" of acoustic influence.

where $T=\frac{\sqrt{u'^2}}{\bar{u}}$, versus the boundary layer height $\frac{y}{\delta}$ at a spanwise location 2cm off the test surface centerline, z=+2.0 cm.

At x=2.08 m, outside of the narrow "wedge" of acoustic influence, the average value of the parameter r_T is 1.008. Acoustic waves in this case make the excited flow more perturbed. At x=2.88 m, where this point is starting to be affected by the acoustic influence, the average ratio is 1.001. Well inside the cone of acoustic influence, at an axial distance of 47δ from the LEBU, the average value of the parameter r_T is smaller than unity. It should be noticed that the turbulence intensity level includes all frequencies, not just the lower frequency range which is primarily influenced by the acoustic input. The differences in turbulence intensity are small when acoustics is applied leading to a random oscillation of r_T around unity. The reduction of turbulence intensity seems to exist however, inside the narrow "wedge" of acoustic influence.

3.2.2. EXPLANATION OF THE SPREADING EFFECT

A recently proposed model of turbulent boundary layer coherent motion [29] was examined and a qualitative explanation of the spreading acoustic influence was based upon it. According to this model, large scale motions are initiated by the instability of the main flow and rotate in the direction of the mean flow shear. The sublayer bursting

events are caused by the interaction of the semi-periodic large scale motions with the wall. The burst is bound by a pair of counter rotating vortices which are inclined forward and the resulting ejection and sweep are flows induced by these vortices. A schematic representation of the suggested model is shown on figure 24a.

Using reference [30] applied to the particular experimental set-up, an approximate sketch of the resulting flow field from a single pressure pulse can be made as shown in figure 24b. This schematic is a side view of the flow field induced by an acoustic pulse impinging upon the LEBU as seen from a downstream location. The acoustic pulse is spread through the air with the vortex ring moving away from the acoustic input port. The resulting jet flow has a spanwise velocity component w' which is also augmented by the stagnation of the pulsating air upon the LEBU. The moving media causes a diverging motion of the generated vortices through the downstream boundary layer.

A top view of the flow across the flat plate manipulator is shown on figure 25. Upstream of the LEBU the large scale structures appear according to the model at a random rate and spacing. Only the eddies that are convected on the centerline are detected and canceled with acoustic waves. These acoustic waves partially stagnate upon the flat plate and induce a vortex "street" which is spread into the boundary layer downstream. These vortices interact out of phase with some of

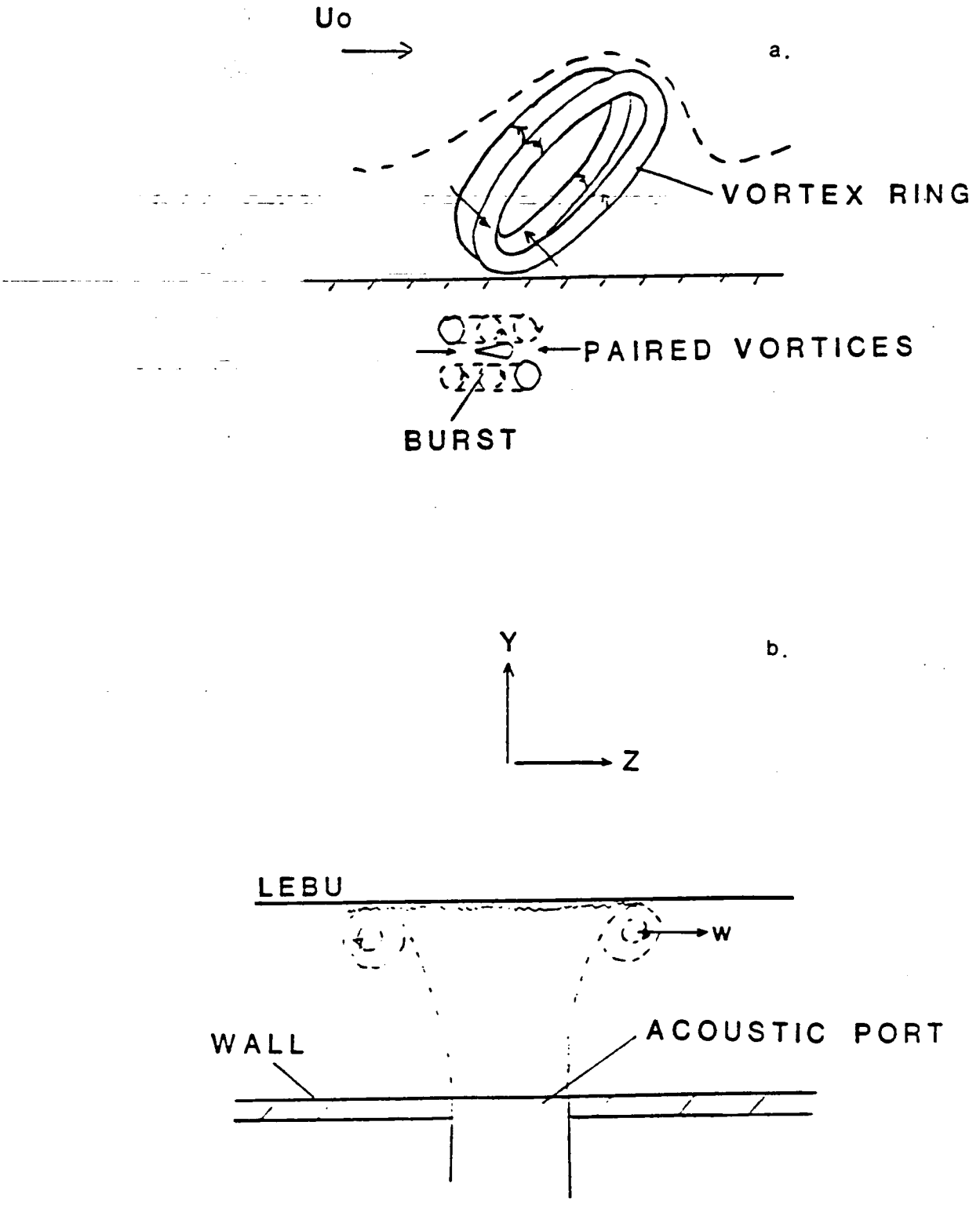

Figure 24. Model of (a) coherent structures and (b) acoustic pulse flow field.

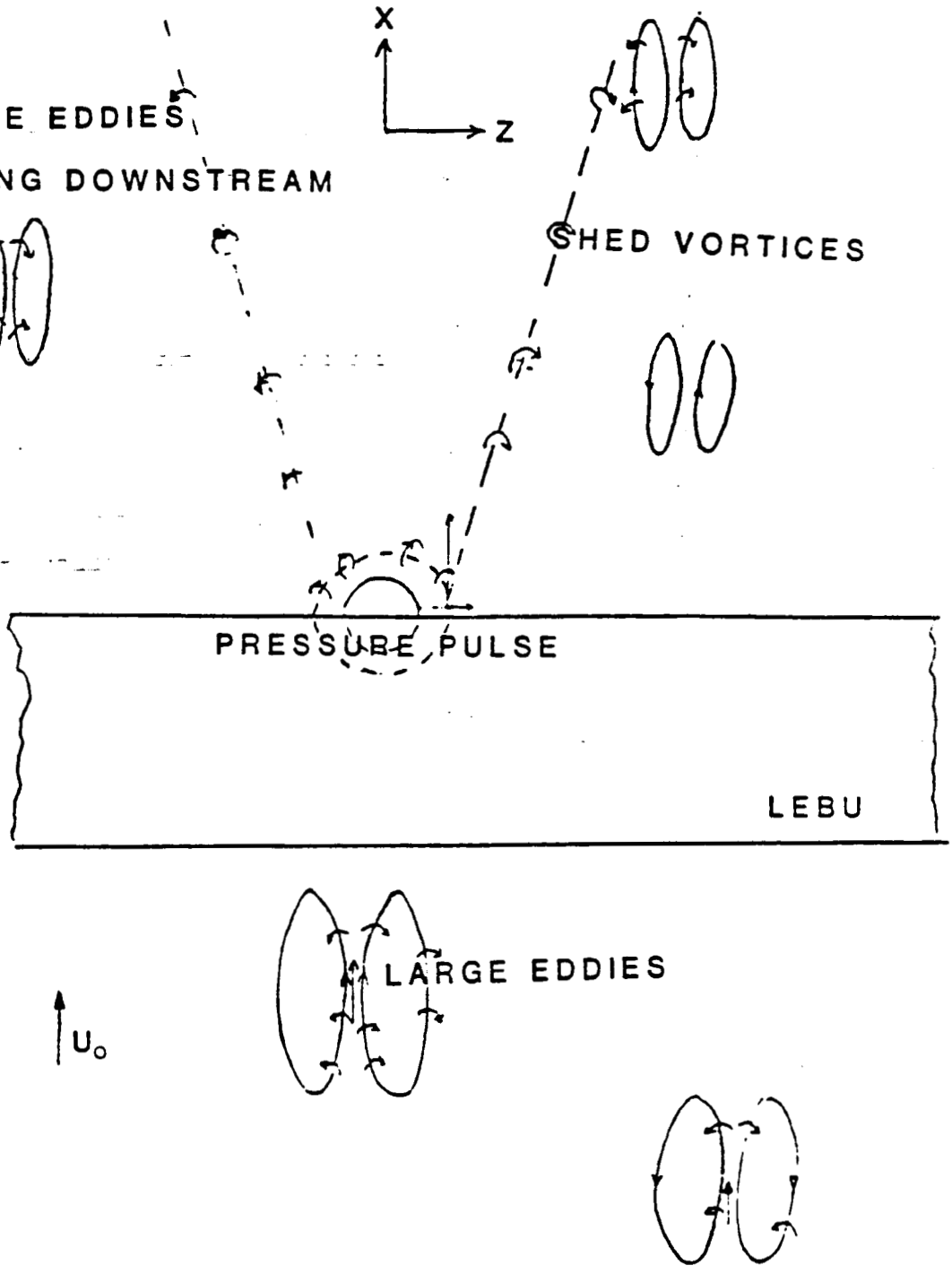

Figure 25. Top view of suggested acoustic spreading mechanism.

the large eddies which were not detected by the hot film probe but were partially canceled by the manipulator. This cancellation proceeds downstream within a narrow angle because the spanwise velocity component w' of the induced secondary flow is assumed far smaller than the axial velocity component u. Some of these vortices eventually decay because of strong mixing in the turbulent boundary layer. It should be noted that the angle of acoustic influence was reduced at higher free stream velocities which supports this proposed explanation of how the spanwise spreading of the phenomenon may occur.

An alternative explanation can be provided based upon the assumption that the large eddies and the sublayer phenomena of "burst" and "sweep" are closely interrelated and preserve each other. It is assumed that a burst of fluid is counteracted by large scale motion in order to preserve continuity at a point of the flow field. Also, the convected large eddies, being limited spanwise, trigger bursting events at other nearby locations in the z direction. These events account for most of the skin friction production. Consequently, the break-up of large eddies will spread spanwise interrupting the chain of events that might link the coherent motion to the sublayer bursting and sweeping of fluid.

3.3. OPTIMIZATION OF THE EXISTING CONFIGURATION

Since acoustic excitation reduces the correlation between two points across the LEBU, this was utilized to optimize the various parameters which control the function of the analog time delay processor. These parameters are the voltage reference, V_r, the time delay, t, and the pressure level of the acoustic pulse.

The downstream hot film sensor was positioned at a distance of 7cm (1.7δ) from the LEBU trailing edge, and at a height of 3.4 cm above the wall on the centerline of the test surface. The upstream hot film sensor was positioned at the usual distance of 2.5δ from the LEBU trailing edge. The ratio $r_c = \frac{CCF(LA)}{CCF(L)}$ is plotted versus the relative processor reference voltage, $\frac{V_r}{V_a}$ where V_r is the set reference voltage and V_a is the upstream anemometer voltage output. The values of r_c (open symbols) displayed in figure 26 indicate a minimum at $\frac{V_r}{V_a} = 0.970$. The turbulence intensity level at the upstream sensor's height was 2 to 3 per cent. The optimum range of the reference voltage is very narrow (10 millivolts) and it was repeatedly noticed during the experiments that V_r should be set just below the AC RMS level of the detector probe output, V_a.

The closed symbols of figure 26 represent the averaged number of processor pulses per second for different values of the ratio $\frac{V_r}{V_a}$. The average processor response frequency was determined by counting the number of output pulses from

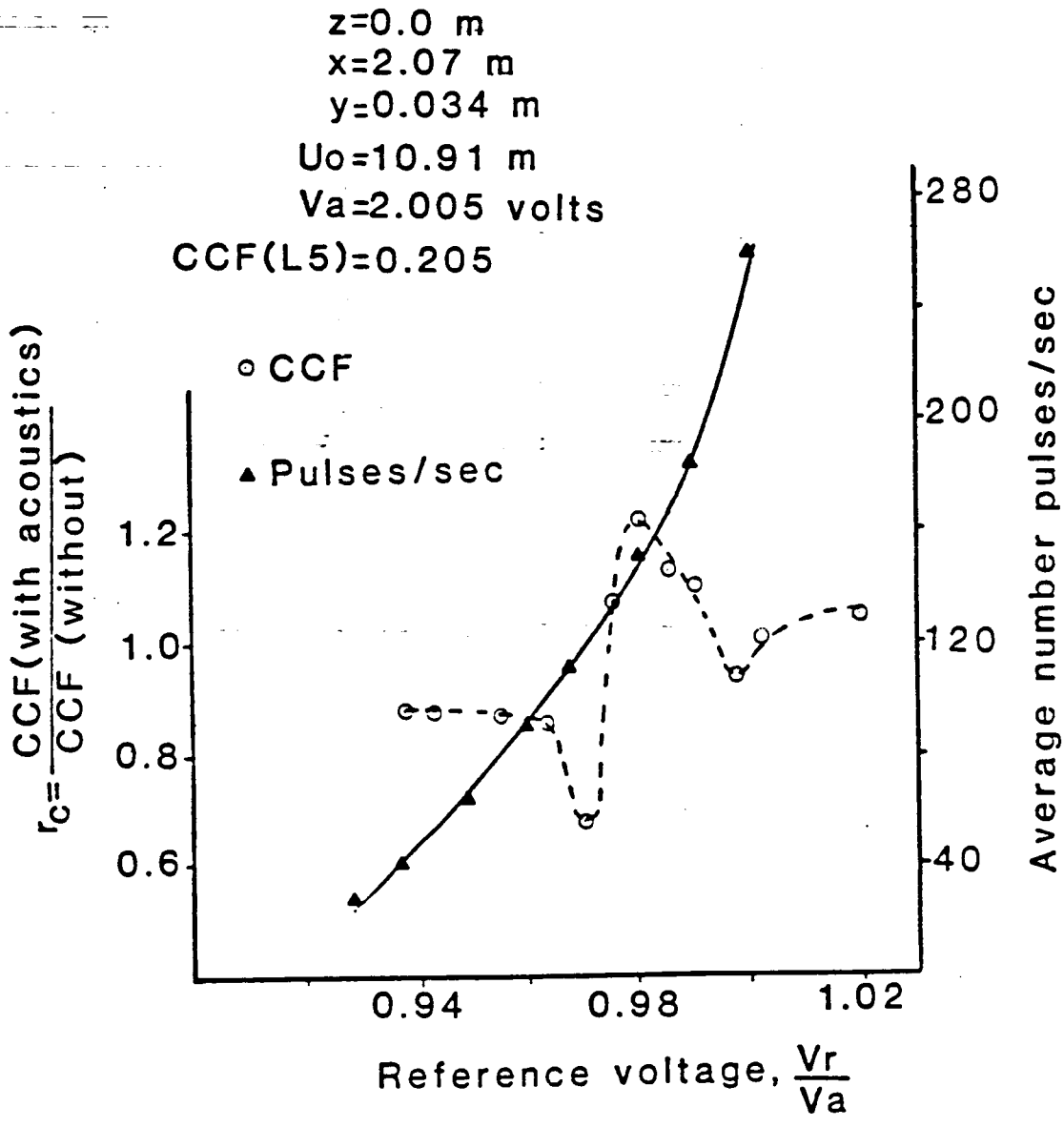

Figure 25. Relative peak correlation, r_c, and number of acoustic pulses per second, versus reference voltage $\frac{V_r}{V_a}$.

the processor over an interval of 200 sec. For the local boundary layer thickness of about 4 cm and free stream velocity of about 10.9 m/sec, a value of approximately 110 Hertz is predicted [8] for the large eddy passing frequency. This frequency is very close to that measured when V_r is set to its optimum value. Thus optimization of V_r is again associated with the large scale structure in the boundary layer.

The acoustic excitation remained effective when the reference voltage was set below the optimum value. In this case only very large eddies were recognized and the number of acoustic pulses per second was reduced. When the relative voltage $\frac{V_r}{V_a}$ was set at 0.91 the processor was unable to trigger the pulse mechanism. On the other hand, the acoustic excitation becomes less effective when the reference voltage is increased above the optimum range. In this case the acoustic excitation is triggered by additional smaller eddies. The number of acoustic pulses per second was increased to almost double the predicted number of large eddies per second. Increased correlation measured between the two points across the LEBU is then caused by acoustic waves. The optimum value of the reference voltage, V_r, depends upon the anemometer voltage output, V_a, which varies with the tunnel free stream velocity. Continuous monitoring and periodic adjustment was necessary to compensate for temperature variations of the flow.

The processor time delay, t, required to allow for a detected large eddy to be convected to the LEBU trailing edge was also optimized based upon the reduction of peak correlation across the LEBU when acoustics is applied. On figure 27 the ratio $r_c = \frac{CCF(LA)}{CCF(L)}$ is plotted versus the processor time delay t. The downstream probe remained at the same position and the reference voltage was set to the optimum value. According to the data, a minimum value of the ratio r_c can be distinguished corresponding to a time delay of 10 msec. For the particular tunnel velocity setting of 10.5 m/sec, the time delay, $t = \frac{s}{0.93U_o}$, was found to be 10 msec. This reinforces the concept of assisting the large eddy cancellation process with an acoustic pulse which arrives simultaneously at the trailing edge of the plate manipulator.

Finally, the time averaged sound pressure level of the acoustic waves impinging upon the thin plate was optimized using the same phenomenon of minimized CCF when acoustic excitation is applied. Measurements of the time averaged pressure level of the acoustic wave were obtained at "simulated" experimental conditions. The acoustic pulse mechanism was mounted upon a wooden baffle plate that had an acoustic port identical to that of the test section. The pressure pulse mechanism was triggered by a prerecorded output signal from the upstream sensor at real flow conditions. Sound pressure level measurements were obtained at the LEBU's height above the pressure port in a hard wall

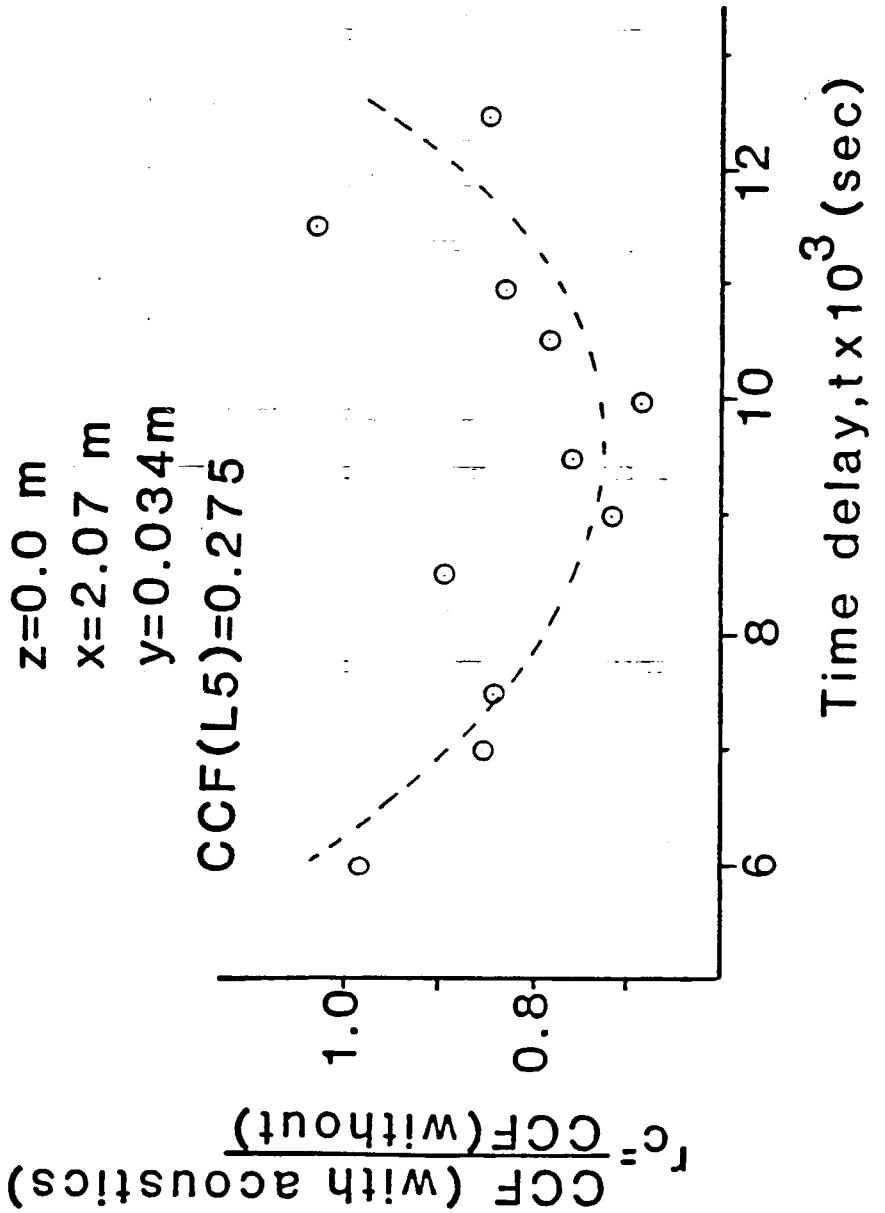

Figure 27. Variation of the relative peak correlation, r_c, with time delay, t.

room with no flow. The microphone was positioned at grazing incidence and the reference voltage, V_r, and time delay, t, were set at their optimum value. In this manner the sound pressure level at the LEBU was determined for various power amplifier settings. Measurements of the CCF were then taken inside the tunnel with real flow conditions. A hot film probe was positioned at midspan of the test section at a distance of 1.7δ from the LEBU trailing edge and at a height of 0.82δ from the wall. CCF measurements were obtained comparing the LEBU and the acoustically excited flow configurations for different settings of the acoustic wave pressure level. The ratio $r_c = \frac{CCF(LA)}{CCF(L)}$ versus the measured narrow band SPL at the LEBU's height is plotted on figure 28. Once more a minimum value can be observed, which indicates that an acoustic pulse with a SPL of about 102 decibels is most effective for canceling the large eddies.

The cross correlation across the LEBU remained reduced for a range of 2 dB around the optimum value but for values of the sound pressure level above 105 dB the acoustic wave field increases the correlation across the plate. The value of the sound pressure level required for optimum large eddy manipulation is of the same order of magnitude as the predicted and previously applied pressure pulse of 100 dB. In the beginning of the study it was assumed that a pressure pulse of the same order of magnitude as the pressure perturbations at the near wake of the thin plate (Appendix 1)

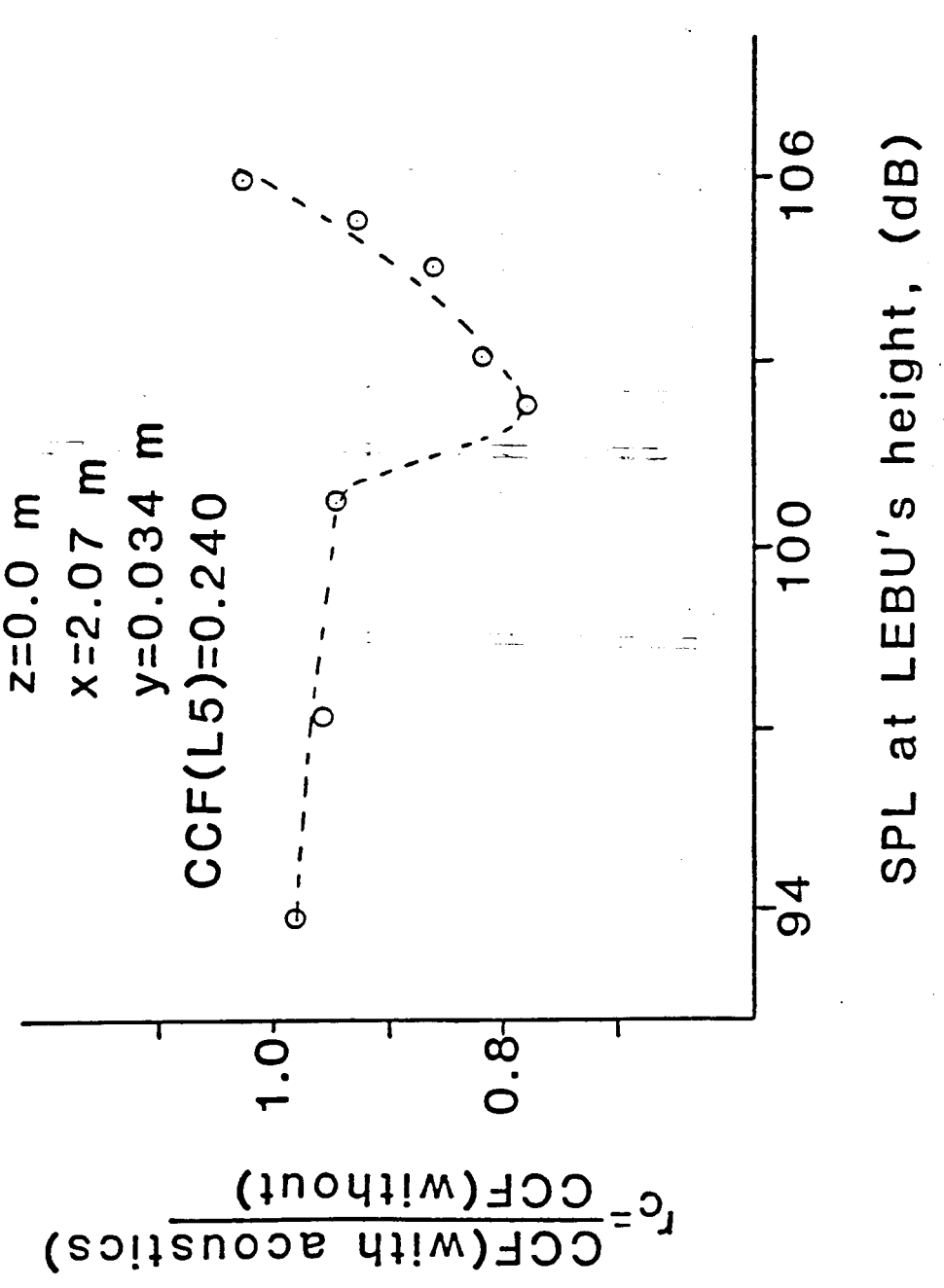

Figure 29. Variation of the relative peak correlation, r_c, with time averaged SPL of pressure pulse at LEBU's height.

might benefit the large eddy break-up process.

The observed phenomenon of reduced correlation at two points across the LEBU device when the flow is acoustically excited can be utilized to optimize the operating parameters of the acoustic input. The cancellation of the large eddies is maximized when the reference voltage is set to produce approximately the same number of acoustic pulses per unit time approximately as the number of predicted large eddies per unit time. The flow is least correlated (enhanced large eddy cancellation) when the time delay is set equal to the large eddy convection time from the detector probe to the LEBU trailing edge. The initial approximation of the pressure perturbation required to influence the flow downstream of the LEBU was found close enough to the optimum value for enhanced large eddy cancellation (it deviated by 2 dB). The optimum values of the experimental parameters were very close to those initially projected with the concept of acoustic excitation of a boundary layer plate manipulator. Thus, for further verification, boundary layer velocity profiles were measured downstream of the LEBU when the processor operating parameters were set at their optimum values.

3.4. MEASUREMENTS WITH AN OPTIMIZED CONFIGURATION

The operating parameters of the processor and power amplifier were set to the previously established optimum. Detailed boundary layer velocity profiles were obtained

downstream of the plate manipulator along the midspan of the test surface. The momentum thickness was calculated and plotted in figure 29 as a function of downstream axial distance x. The three configurations compared were

i. The plain flow

ii. The acoustically excited LEBU, and

iii. The optimally excited LEBU.

The axial variation of momentum thickness exhibited a trend similar to the initial configurations. The momentum thickness close to the LEBU trailing edge for the optimally excited flow was again slightly higher than the plain flow's but lower than the simply excited configuration. The slope of the curve is also smaller and the resulting momentum thicknesses downstream are less with optimum acoustic excitation.

The values of θ were least square curve fitted to a power law of the form $\theta = ax^b$ and the skin friction coefficient was estimated using $c_f = 2abx^{b-1}$. Numerical values of the coefficients a and b for various flow configurations are shown in table 2. According to these values of the skin friction coefficient, optimized acoustic excitation can enhance the LEBU's effect by reducing c_f between 2 and 0 percent with respect to the initially excited configuration and by 10 to 17.3 percent when compared to the plain flow configuration. The improvement of about 2 percent additional c_f reduction over the unoptimized case was

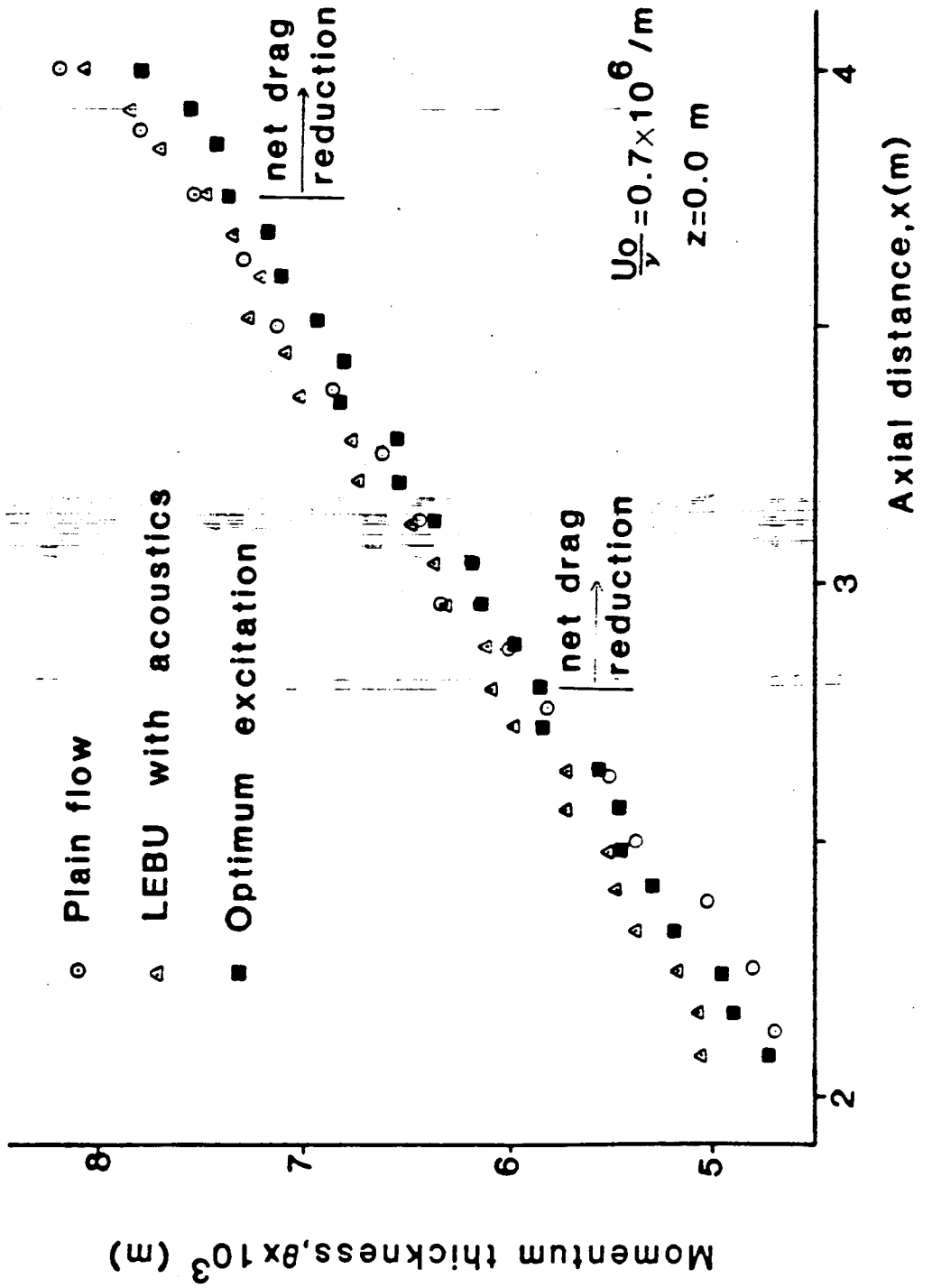

Figure 29. Momentum thickness, θ, versus axial distance, x, for various flow configurations (optimized acoustic excitation).

moderate. This is because the operating parameters of the initial configuration were set close to optimum and because the least square curve fitting procedure is itself an averaging process.

There may be some experimental error in the measurement of θ when the absolute numbers of figures 29, 14 and 15 are examined. It must be noticed that always during the data acquisition every point of the velocity profile was measured with and without acoustics. All the data indicate that excitation reduces drag and optimized excitation improves slightly the effectiveness of the pulse. Some of the data could be combined to show results superior to those given in figure 29, but the data shown are typical.

Table 2a. Curve fitting parameters for the acoustically optimized LEBU #5 configuration.

Configuration	a	b	r^2
plain	0.002442	0.85175	0.993
LEBU #5 (excited)	0.002912	0.717327	0.992
LEBU #5 (optimum acoustic excitation)	0.002776	0.731655	0.996

Table 2b. Axial variation of the skin friction coefficient, c_f, for the optimized configuration.

x[m]	$c_f(PL)$	$c_f(L5A)$	$\frac{c_f(PL)-c_f(L5A)}{c_f(PL)}$	$c_f(L5A_{op})$	$\frac{c_f(PL)-c_f(L5A_{op})}{c_f(PL)}$
2.0	0.003754	0.003425	0.087	0.003373	0.101
2.5	0.003632	0.003213	0.115	0.003177	0.125
3.0	0.003535	0.003049	0.137	0.003025	0.140
3.5	0.003455	0.002917	0.156	0.002902	0.160
4.0	0.003387	0.002808	0.171	0.002800	0.173

PL signifies the plain flow configuration

Table 2c. Axial variation of the total drag coefficient, c_D, for the optimized configuration.

x[m]	$c_D(PL)$	$c_D(L5A)$	$\frac{c_D(PL)-c_D(L5A)}{c_D(PL)}$	$c_D(L5A_{op})$	$\frac{c_D(PL)-c_D(L5A_{op})}{c_D(PL)}$
2.0	0.004407	0.004738	-0.086	0.004610	-0.046
2.5	0.004264	0.004495	-0.054	0.004342	-0.018
3.0	0.004150	0.004269	-0.029	0.004134	0.004
3.5	0.004056	0.004087	-0.008	0.003967	0.022
4.0	0.003977	0.003936	0.010	0.003827	0.037

3.5. NET DRAG REDUCTION

The momentum thickness, θ, at an axial distance x from the test surface leading edge can be used to calculate the total skin friction drag coefficient, c_D, at this point [2]. A momentum balance is applied considering a control volume bounded by the test surface and the undisturbed flow, and extending downstream from the test surface leading edge to an axial location x. Then the total drag coefficient is given by:

$$c_D(x) = 2.0 \frac{\theta(x)}{x} \qquad (3.1)$$

Figure 29 is reconsidered here observing that the momentum thickness corresponding to an acoustically excited flow is lower than for the other configurations. According to equation 3.1 and the data listed in table 2, a 4 per cent net drag reduction, with respect to the plain flow, can be obtained at a distance of 50δ downstream of the LEBU manipulator. The acoustic power input to the devices was not taken into account.

The actual results of optimization are, however, more beneficial than those revealed by table 2. Comparing figure 15, which is the unoptimized L5 case with figure 29, which is the optimized L5 case, two important differences can be noted. First, the momentum thickness near the trailing edge of the blade is larger with excitation in both cases, but the optimized case shows θ only slightly higher with excitation.

The more effective large eddy cancellation imparts less initial drag into the system when properly optimized. Secondly, for the optimized case, net drag reduction occurs earlier than the unoptimized case and over a significantly larger area. In the non optimized case of figure 15, net drag reduction is observed starting at approximately x=3.5 m. For the same flow and same configuration but with carefully optimized acoustic input, the region where net drag reduction begins has moved upstream to approximately x=2.8 m (figure 29). Measurements in the downstream direction beyond the range of 60δ were limited by the available length of the wind test section tunnel test section.

3.6. SKIN FRICTION MEASUREMENTS OF VARIOUS LEBU CONFIGURATIONS

Prior to the experimental set-up L5 (LEBU #5) various large eddy break-up devices were studied in a more preliminary manner to establish the effectiveness of a single plate and, the effect of an acoustic pulse upon the flow downstream of a large eddy manipulator. It is appropriate that some of this preliminary data should be presented here.

3.6.1. PRELIMINARY LARGE EDDY BREAK-UP DEVICES

All the boundary layer manipulators were mounted at a distance of 2.0m from the test section leading edge. The wind tunnel velocity was set for a unit Reynolds number of

700,000 m^{-1} and the pressure gradient throughout the flow was zero. The height of the boundary layer at the LEBU location was approximately 4 cm above the test surface. No upstream hot film sensor was installed and no acoustic excitation was applied. The geometry of these manipulators is given in table 3.

Table 3. Geometry of preliminary single LEBU's

configuration	height above floor [δ]	chord length [δ]	thickness [δ]
LEBU#1	1.00	1.25	0.0038
LEBU#2	0.83	1.215	0.0038
LEBU#3	0.50	0.96	0.0050

Boundary layer velocity profiles were measured downstream of the various LEBU plates along the centerline of the test surface. The measurements extended a distance of 63 boundary layer thicknesses from the LEBU, with a spacing for each axial station of 6δ. The values of the momentum thickness, θ, for the plain flow case and the various plate manipulators are shown in figure 30.

The values of θ for all the axial stations were least square curve fitted in a power law of the form $\theta = ax^b$ and the local skin friction coefficient was estimated following the method of section 2.3. Table 4 contains the numerical values of the curve fitting parameters a,b and r^2 for the

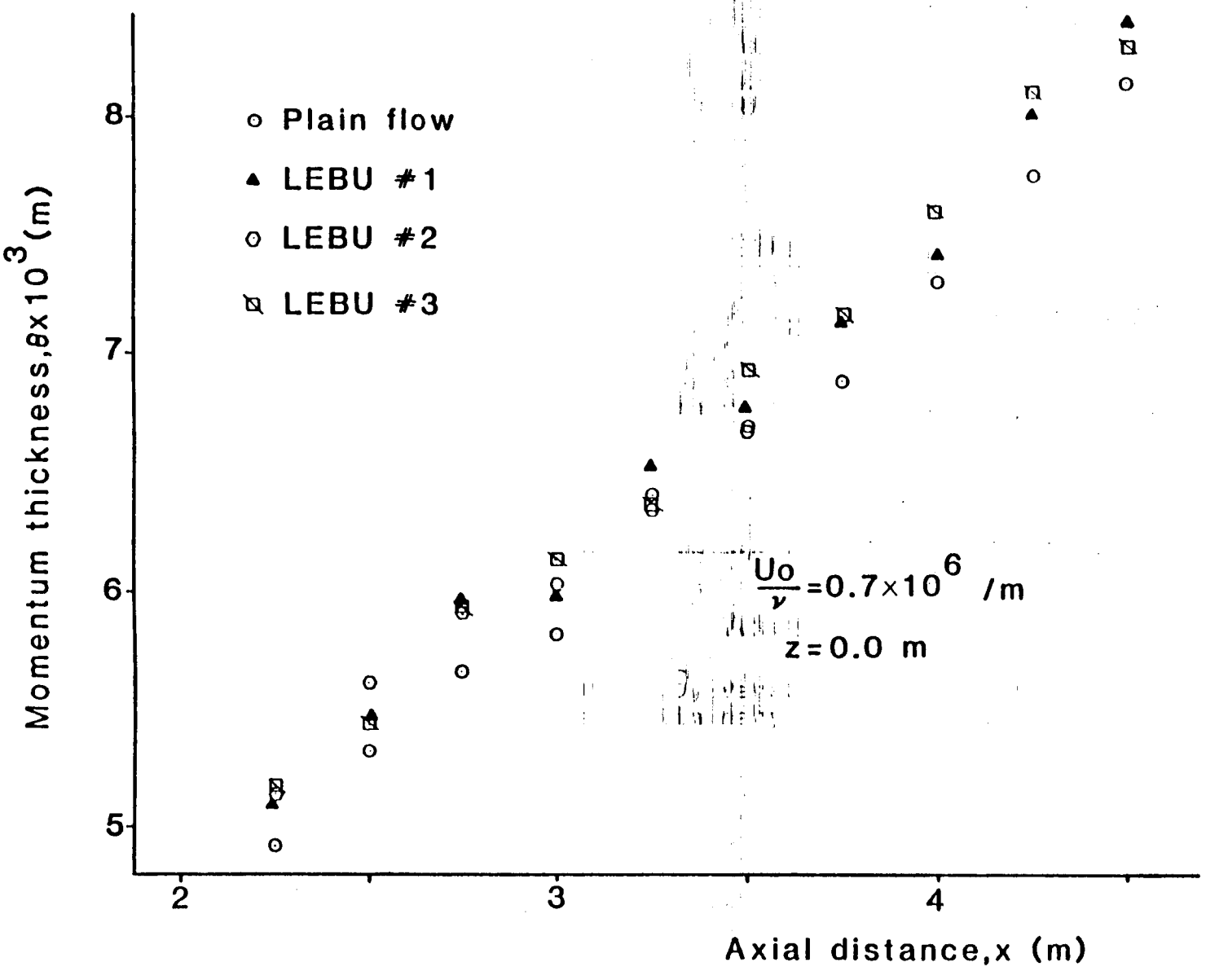

Figure 30. Momentum thickness, θ, versus axial distance, x, for various preliminary configurations.

skin friction drag reduction over a distance of 62δ from the LEBU.

Table 4. Curve fitting parameters for various flow configurations (was measured to a distance of 62δ from LEBU).

configuration	a	b	r^2	percent drag reduction at 62δ
PLAIN FLOW	0.002665	0.715993	0.994	-----
LEBU #1	0.003005	0.6596	0.991	-3.0
LEBU #2	0.003104	0.62774	0.963	2.7
LEBU #3	0.003094	0.62952	0.994	2.8

According to the data listed the achieved drag reduction was negative or moderate. These measurements were preliminary and mostly used to develop the experimental set-up and the data acquisition procedure. The configuration LEBU #3 was considered as reasonably effective device and it was decided to proceed with the acoustic excitation after achieving some moderate success with boundary layer manipulation.

3.6.2. PRELIMINARY ACOUSTIC EXCITATION

The acoustically excited thin plate configuration was designated as LEBU #4. The large eddy detector probe was installed upstream of the LEBU at a distance of 2.4δ from its trailing edge and at a height of 0.9δ above the wall. The time delay of the processor was set at 9.5 msec and the

pressure level of the acoustic wave at the LEBU's height was 100 dB. The geometry of LEBU #4 (chord,height,thickness) were identical to LEBU #3 as was the location of device and the wind tunnel operating unit Reynolds number.

Boundary layer velocity profiles for the following configurations were measured downstream of the LEBU at midspan axial locations over a downstream distance of 60δ.

i. Plain flow (hot film sensor was installed)

ii. LEBU #4 (hot film sensor installed but not operating)

iii. LEBU #4 acoustically excited.

The calculated values of momentum thickness are plotted on figure 31. No major changes between the configurations can be observed in the rate of momentum thickness growth and the local skin friction drag reduction was moderate. The values of θ were fitted to the power law and the local skin friction coefficient was calculated according to the method of section 2.3. The curve fitting parameters and the achieved drag reduction are shown on table 5.

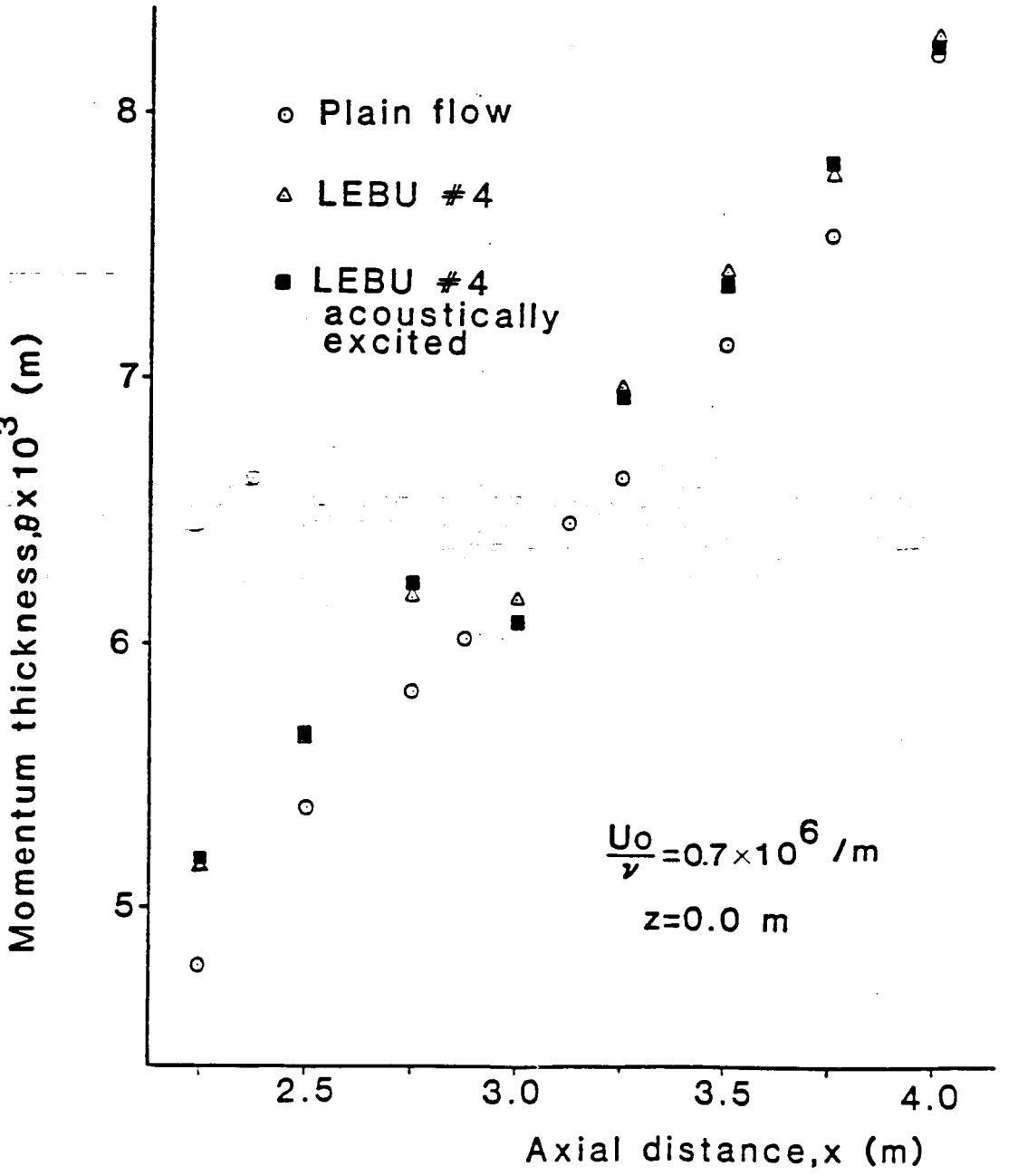

Figure 31. Momentum thickness,θ, versus axial distance, x, for preliminary acoustic excitation.

Table 5. Curve fitting parameter and per cent drag reduction for LEBU #4 configuration.

Configuration	a	b	r	percent drag reduction
plain flow	0.00246	0.84856	0.992	--------
LEBU #4	0.002576	0.81353	0.998	-1.7 to 0.6
LEBU #4 (acoust. excited)	0.002699	0.804223	0.995	0.0 to 2.2

No net drag reduction was achieved and it was decided, based upon flow visualization, to raise the LEBU to 0.8 in order to better intercept the incident large eddies. This configuration was LEBU #5 which is extensively described in the previous sections.

These preliminary data with little success are the result of much time and effort to obtain drag reduction with acoustic excitation. This method is not well understood and requires a considerable effort to find a configuration which works well. Because of inconsistencies with these early efforts, it was decided that another independent configuration must be tested to provide additional verification of the phenomenon.

3.7. ACOUSTIC EXCITATION AT UNIT REYNOLDS NUMBER OF $10^6 m^{-1}$

To further verify the generality of the large eddy cancellation process the wind tunnel velocity was set at a unit Reynolds number of $10^6 m^{-1}$ and LEBU #5 was replaced with a different manipulator. LEBU #6 was installed and tested in order to examine the effectiveness of the acoustic excitation at a higher speed. The detailed description of configuration LEBU #6 is given in table 6 and compared with the successful optimized LEBU #5.

Table 6: Experimental parameters for optimized LEBU #5 and LEBU #6 configurations.

EXPERIMENTAL PARAMETER	LEBU #5	LEBU #6
Unit Reynolds number	$0.7 \times 10^6 m^{-1}$	$10^6 m^{-1}$
Typical mean flow velocity	11 m/s	15.5 m/s
Boundary layer sandpaper trip length	21 cm	31 cm
Boundary layer trip location	3 to 24 cm	3 to 34 cm
LEBU trailing edge location	2. m	2. m
LEBU material	steel	steel
LEBU chord length	0.93δ	1.04δ
LEBU height above test surface	0.80δ	0.75δ
LEBU thickness	0.0050δ	0.0054δ
Boundary layer thickness at LEBU location	~4.1 cm	~3.7 cm
Acoustic input hole diameter (hole location at LEBU's trailing edge, midspan)	3/8 inches	3/8 inches
Upstream eddy detector distance from LEBU's trailing edge	2.45δ	2.5δ
Time delay between large eddy detection and acoustic pulse	10.5 msec	6.5 msec
Upstream eddy detector height	0.85δ	0.86δ
Momentum thickness Reynolds number at LEBU location	3,100	3,700
Expected large eddy passing frequency, Hz	110	165
Predicted pressure perturbation at LEBU's near wake	100 dB	104 dB
SPL of acoustic pulse at LEBU's height (2 dB higher than predicted pressure perturbation).	102 dB	106 dB

Turbulent boundary layer velocity profiles were measured at midspan locations downstream of the LEBU manipulator as usual. The momentum thickness, θ, was calculated as described in section 2.3 and plotted versus downstream distance, x, from the test surface leading edge. Figure 32 shows the axial variation of θ for the usual three configurations.

The momentum thickness of the manipulated flow is greater than the plain flow case because of momentum loss imposed by the embedded thin plate. The acoustically excited case produces a lower momentum loss at this location. This indicates that the acoustic pulse does not subtract kinetic energy from the flow and it improves the efficiency of the LEBU configuration in the wake region. From figure 32 it can be observed that the momentum thickness of the acoustically excited configuration again grows at a slower rate compared to the simply manipulated boundary layer. Further downstream at x=3.75 m (47δ from the LEBU) the momentum thickness of the acoustically excited configuration falls below that for the other configurations indicating net drag reduction.

The variation of the skin friction coefficient, c_f, with the axial distance from the test surface leading edge is shown in figure 33. All measurements were obtained at the test surface mid span aligned with the upstream sensor and the acoustic wave port. The numerical values of the skin friction coefficient were calculated according to the

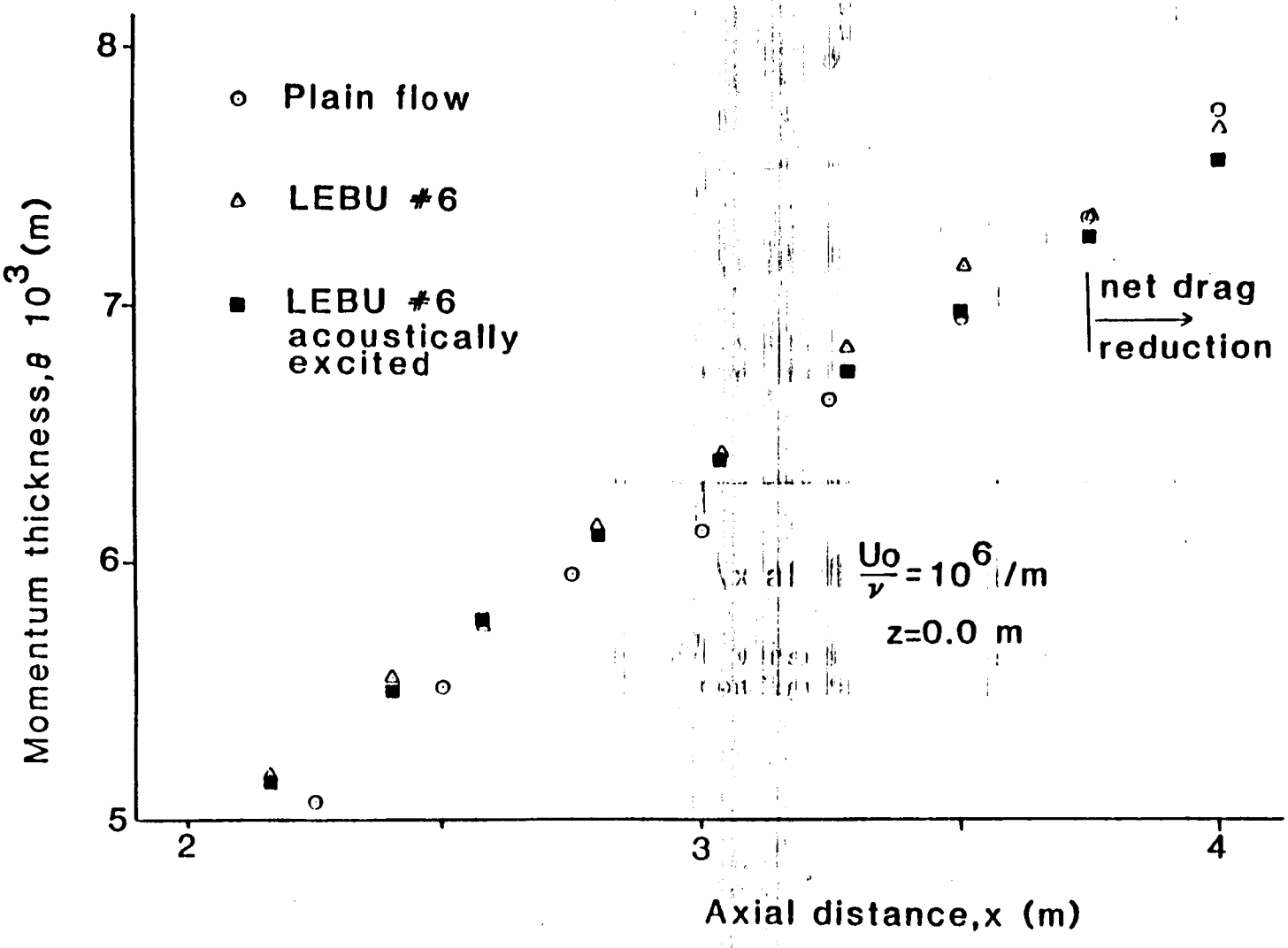

Figure 32. Momentum thickness, θ, versus axial distance, x, for various flow configurations at unit Re= $10^6 m^{-1}$.

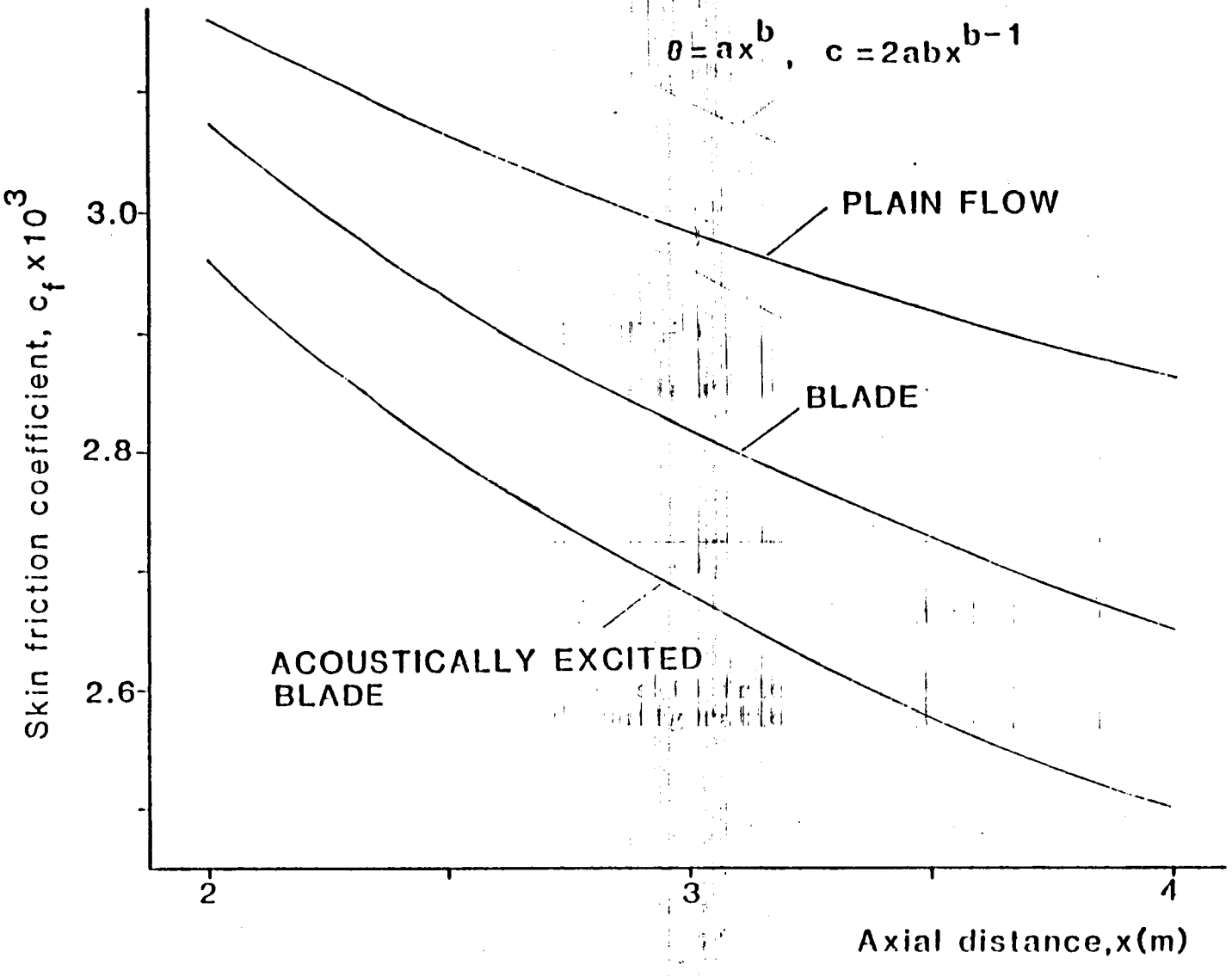

Figure 33. Variation of the skin friction coefficient, c_f, for each configuration at unit Re=10^6 m^{-1}.

procedure described in section 2.3. All least square curve fits again had a correlation coefficient above 0.99. The LEBU configuration and the acoustically excited flow were compared to the plain flow (hot film sensor installed). According to the numerical values of the skin friction coefficient, acoustic excitation can enhance the LEBU's effect by reducing c_f between 3.8 and 6.0 percent with respect to the LEBU configuration. Comparison to the plain flow shows a reduction of the wall shear stress between 6.5 and 13 per cent. In addition a 2 percent net drag reduction was measured at a distance of .54δ from the LEBU.

Although the data are not as impressive as the previous optimized configuration, they do suggest that the mechanism of enhanced large eddy cancellation is real. Anders [18], has shown that variations of the manipulator microgeometry exercises a strong influence upon the results so absolute numbers are not extremely meaningful. The trends of the data are, however, consistent with previous findings.

Space-time cross correlation functions (CCF) were obtained using the hot film eddy detector probe upstream of the LEBU plate as a fixed reference location and another probe at a distance of 4.0δ boundary layer thicknesses downstream (figure 17). The height of the downstream sensor was 0.9δ. Figure 34 shows representative space-time cross correlation functions for the plate manipulated and the acoustically excited boundary layers. When acoustic

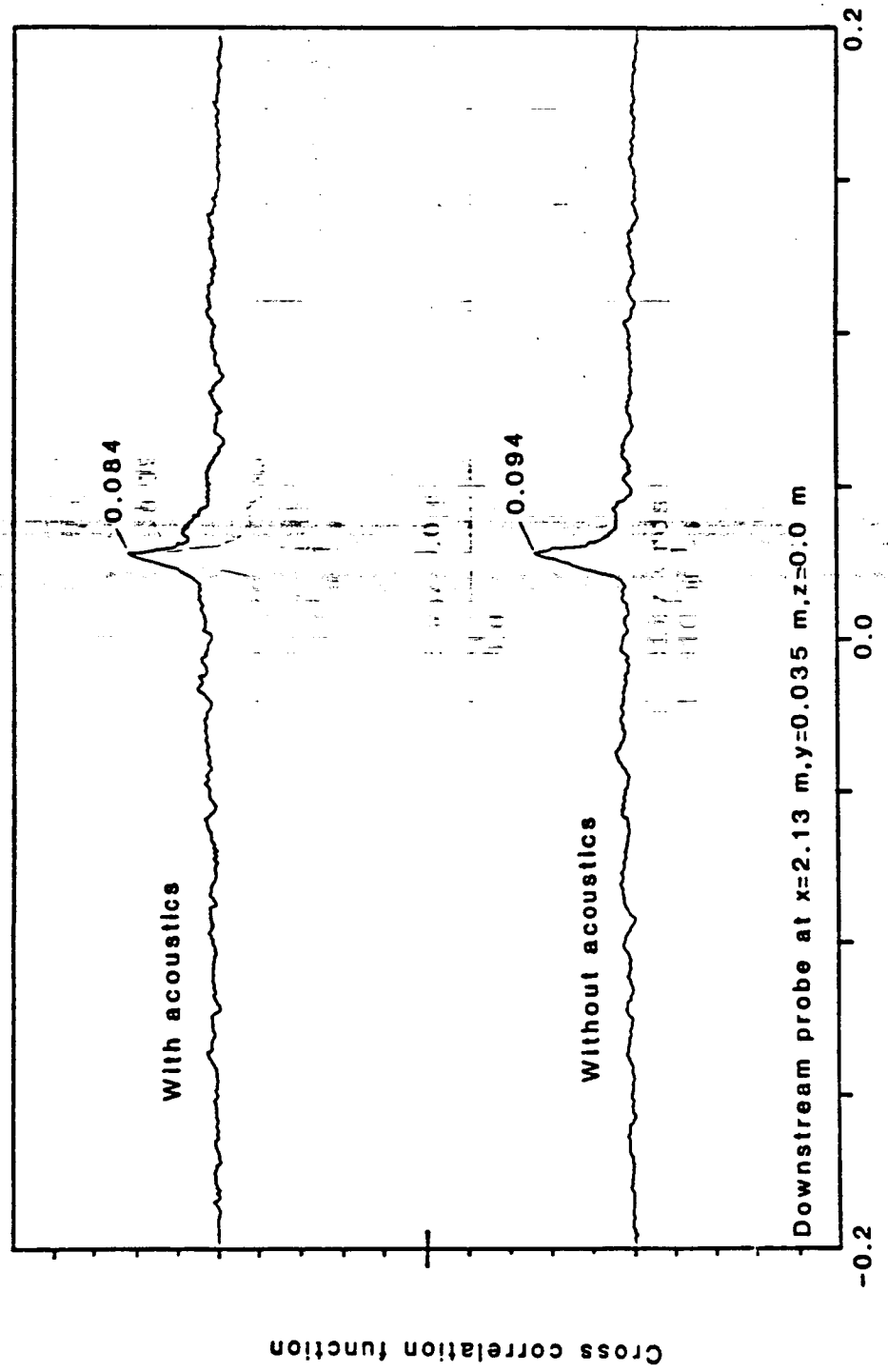

Figure 34. Time space velocity cross correlation across LEBU at unit Re=10^6 m^{-1}.

excitation is applied the downstream flow is again correlated to the upstream point significantly less. The peaks of the CCF correspond to eddy convection time from the upstream to the downstream sensor. This indicates that acoustic excitation enhances the destruction of the large eddies which are sensed at the upstream location. These measurements are in good agreement with similar results of configuration LEBU #5. In addition measurements of the low frequency turbulence spectrum, downstream of the plate manipulator showed that acoustic excitation can reduce the RMS value of the axial velocity fluctuation approximately 2 percent.

Figure 35 shows the variation of the ratio $r_\theta = \frac{\theta(LA)}{\theta(L)}$ with the spanwise distance from the test surface centerline, z, at a distance of x=1.76m from the LEBU. According to previous measurements of momentum thickness, θ, (figure 31) the ratio r_θ was found smaller than unity at this axial station. In this location it was found that the acoustic excitation persisted with a tendency to spread spanwise at a half angle of about 1.2 degrees. The reduction of the angle of acoustic influence when compared to LEBU #5 is attributed to the increased mixing process of the turbulent boundary layer due to higher free stream velocities in which LEBU #6 was tested.

Proper acoustic excitation of a thin flat plate operating in a higher unit Reynolds number flow was again found effective in enhancing the large eddy break-up process.

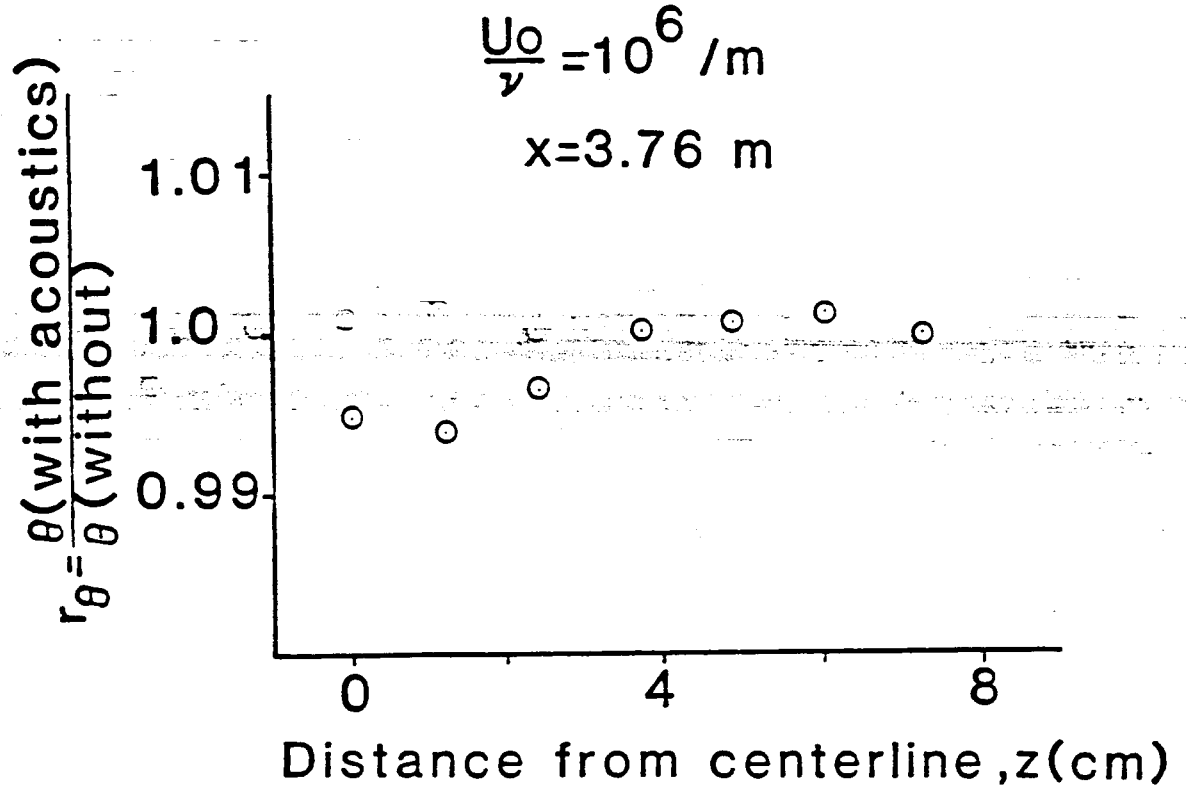

Figure 35. Spanwise variation of momentum thickness, θ, for the excited and unexcited LEBU at unit Re=10^6 m^{-1}.

The processor operating parameters were set according to higher free stream velocities. The achieved skin friction drag reduction, reduction of flow correlation across the LEBU, reduction of the low frequency turbulence and the moderate net drag reduction were consistent with the results obtained from LEBU#5. This reinforces the initial concept that proper acoustic excitation of a plate boundary layer manipulator can lead to enhanced large eddy destruction.

4. CONCLUSIONS AND RECOMMENDATIONS

4.1. CONCLUDING REMARKS

Large eddy structures in a turbulent boundary layer can be effectively manipulated by acoustic waves resulting in a net reduction in skin friction drag downstream of a manipulating plate. The vortex unwinding at the LEBU's trailing edge when the blade encounters a large eddy is assisted by acoustic waves. These acoustic pulses must be phase locked to the convected eddies (arrive at the LEBU trailing edge together) and must have an adequate sound pressure level in order to be effective. The coherent structure was assumed to be related to the Reynolds stress production and the sublayer bursting events. Thus, The additional elimination of the large scale structure caused by the acoustic waves improved the effectiveness of a single plate manipulator. Skin friction drag reduction was achieved for two different low Reynolds number LEBU configurations. The skin friction coefficient c_f was reduced as much as 18 percent at a distance of 50δ from the LEBU when the acoustically excited plate configuration is compared to the plain flow. In addition, a moderate net drag reduction was achieved at about the same distance from the manipulator.

The application of the proper acoustic input made the flow less correlated across the LEBU, and reduced the level of the low frequency part of the turbulence spectrum of the

manipulated boundary layer. In addition, flow visualization of the acoustically excited boundary layer showed the further reduction in coherent motion. The initial hypothesis, that a phase locked acoustic input to the flow can reduce the turbulence mixing and the wall skin friction was verified.

The effects of the acoustic excitation spread slowly in the spanwise direction as the flow convected downstream. This was verified by carefully measuring the momentum thickness, θ, in the spanwise direction downstream of the manipulator. The spreading was verified with velocity cross correlation and turbulence intensity measurements. The acoustic excitation effect spreads at a half angle of 2 degrees for the most effective configuration. The spreading angle was reduced as Re and turbulent mixing increased. It was assumed that secondary flow vortices induced by the acoustic pulse are convected into the turbulent boundary layer and cancel some of the "weakened" large eddies passing the plate manipulator. An alternative explanation for the spreading process can be based upon the assumption that the large scale structure and the sublayer bursting phenomena are interrelated and preserve each other. The passing of a large eddy causes sideways eruptions of fluid. These bursting and sweeping motions cause the generation of the large scale structure. The interruption of this chain of events by eliminating the large eddies at a spanwise position would yield has a spreading effect upon the reduction of bursting events and further generation of large

scales.

The operating parameters of the processor device which controls the acoustic input could be set to an optimum in order to account for the large eddy convection velocity, their particular frequency of appearance and the level of the velocity fluctuation they represent. The optimization of the processor operating parameter was based upon the observed phenomenon of reduced correlation across the LEBU when acoustics is applied. For maximum large eddy cancellation the reference voltage must be set to produce approximately the same number of acoustic pulses per unit time as the number of predicted large eddies per unit time. The process of reduced correlation is very much dependent upon the setting of the reference voltage and must be set within 10 millivolts from the optimum value for best results. The flow is least correlated when the time delay is set equal to the large eddy convection time from the detector probe to the LEBU trailing edge. Also, the initial approximation of the pressure perturbation required to influence the flow downstream of the LEBU was found close enough to the optimum value to achieve enhanced large eddy cancellation. The optimum values of the experimental parameters were very close to those initially projected. These results verify the concept of increased drag reduction by acoustic excitation of a boundary layer plate manipulator.

4.2. RECOMMENDATIONS FOR FURTHER INVESTIGATION

Acoustic excitation was proven effective in improving the plate manipulator effect upon a turbulent boundary layer. The basic concept of the large eddy cancellation by acoustic waves should be studied in the case of a manipulator plate in inviscid flow. A LEBU device should be positioned in undisturbed flow so that it may encounter vortices artificially generated upstream. Acoustic pulses must be made to arrive at the blade trailing edge together with these vortices [31]. The effect of acoustic waves upon the resulting flow field could be examined to further establish the basic mechanism developed in this study.

Further measurements, beyond the range of 50δ, are recommended in order to establish the extent of the persistence of the acoustic effect downstream of the LEBU. Extensive measurements of the axial and longitundinal velocity fluctuating components u' and v' should be taken to determine changes in the turbulence energy production. The production of skin friction drag is closely related to the Reynolds stress component $-\rho u'v'$; this quantity should be also examined comparing an acoustically excited LEBU configuration to single and tandem plate manipulated turbulent boundary layers.

Further investigation of the spreading tendency of the acoustic effect upon the flow regime downstream of the LEBU should be pursued. Two hot film "scout" probes can be

installed upstream of the plate and the acoustic pulses can be input from two different ports, located relatively close to each other. Boundary layer traverses will show if both zones of acoustic influence merger downstream of the LEBU.

A LEBU with two plates in tandem exposed to acoustic waves may be also examined because this configuration has been found most promising without excitation. The boundary layer upon a LEBU plate is laminar. Possible separation of the LEBU boundary layer can be prevented by forcing it turbulent with a trip wire at the thin plate leading edge or by roughening its surface. Such a LEBU configuration is also worth studying when exposed to acoustic pulses.

Most of the previous experiments with plate manipulators were carried out at a slightly higher speed than the present investigation. An experimental setting at higher velocities will require an acoustic pulse of higher frequency and sound pressure level. Improvements and redesign of the pressure pulse mechanism must be undertaken. Such a configuration, closer to real flow conditions, in conjunction with a variable pressure gradient and airfoil type LEBUs should also be studied.

5. LIST OF REFERENCES

1. White, F.M., Viscous Fluid Flow, pp. 426-432, pp. 518, pp. 448, pp. 503, pp. 480, pp. 481, pp. 518 McGraw-Hill Book Company, 1974.

2. Schlighting,H., Boundary Layer Theory, 7th edition, pp. 378-382, pp. 175-179, pp. 739-743, McGraw-Hill Book Company, New York 1979.

3. Hefner,J.N. and Bushnell, D.M. "An Overview of Concepts For Aircraft Drag Reduction," AGARD-R-654, pp. 1.1-1.30,1977.

4. Falco,R.E.,"Coherent Motions in the Outer Region of Turbulent Boundary Layer," The Physics of Fluids, Vol. 20, No. 10, Pt 11, October 1977, pp. S 124-S 132.

5. Falco, R.E., "The Production of Turbulence Near a Wall," AIAA paper 1980-1356.

6. Kline,S.J., Reynolds, W.C., Schraub ,F.A., Runstadler, P.N., "The Structure of Turbulent Boundary Layer ," Journal of Fluid Mechanics (1967), Vol 30,Pt 4, pp. 741-773.

7. Kovasznay, L.S.G., Kibens, V., Blackwelder, R.F., "Large-Scale Motion in the Intermittent Region of a Turbulent Boundary Layer ," Journal of Fluid Mechanics (1970), Vol. 41, pp. 283-325.

8. Corrsin,S., Kistler,A.L., "Free Stream Boundaries of Turbulent Flows," NACA TR 1244 (1955).

9. Blackwelder, R.F., Kovasznay,L.S.G., "Time Scales and Correlations in a Turbulent Boundary Layer ," The Physics of Fluids, Vol. 15, Number 9, Sept. 1972, pp. 1545-1554.

10. Yajnik,K.S., Acharya,M., "Non-Equilibrium Effects in a Turbulent Boundary Layer Due to the Destruction of Large Eddies," National Aeronautical Laboratory, Bangalore,NAL-BL-7, Aug. 1977.

11. Hefner,J.N.,Weinstein,L.M.,and Bushnell ,D.M., Large-Eddy Break-up Scheme for Turbulent Viscous Drag Reduction,Symposium on Viscous Drag Reduction, Dallas, Texas, Nov. 7-8,1979.

12. Corke,T.C.,Guezennec,Y.,Nagib, H.M.,"Modification in Large Scale Structures," Symposium on Viscous Drag Reduction, Dallas, Texas, Nov. 7-8,1979.

13. Corke,T.C.,Nagib, H.M., Guezzenec,Y.," A New View on Origin, Role, and Manipulation of Large Scales in Turbulent Boundary Layers," NASA CR-165861, Feb. 1982.

14. Bertelrud,A., Truong,T.V., Avellan,F., "Drag Reduction in Turbulent Boundary Layers using Ribbons, AIAA paper 82-1370.

15. Hefner,J.N., Anders, J.B., Bushnell D.M., "Alteration of Outer Flow Structures for Turbulent Drag Reduction ," AIAA paper 83-0293.

16. Plesniak, M.W.,Nagib, H.M., "Net Drag Reduction in Turbulent Boundary Layers Resulting from Optimized Manipulation," AIAA paper 85-0518.

17. Anders,J.B., Watson,R.D., "Airfoil Large-Eddy Break-up Devices for Turbulent Drag Reduction," AIAA paper 85-0520.

18. Anders, J.B., "Low Reynolds Number LEBU Performance," Drag Reduction and Boundary Layer Control Symposium, National Academy of Sciences, October 1985.

19. Guezennec,Y.G., Nagib, H.M., "Documentation of Mechanisms Leading to Net Drag Reduction in Manipulated Turbulent Boundary Layers," AIAA paper 85-0519.

20. Liss, A.Y. and Usol'tsev, A.A.,"Influence of Vortex Wing Interaction on Reducing Vortex Induction," Izvestiya Vuz. Aviatsionnaya Technika, Vol. 16, No. 3, pp. 5-10,1973.

21. Nagel,R.T., and Alaverdizadeh,O. "The NCSU Low Speed Boundary Layer Wind Tunnel," SAE Paper 851897, 1985.

22. Goldstein,R., Fluid Mechanics Measurements, pp.557-564, Hemisphere Publishing Corporation, Washington 1983.

23. Cebecci,T. and Bradshaw,P., Momentum Transfer in Boundary Layer, pp. 192-197, Hemisphere Publishing Corporation, Washington 1977.

24. Bradshaw, P., "A Simple Method for Determining Skin Friction From Velocity Profiles," Journal of Aerospace Science, 26, pp. 841, 1959.

25. Mueller, T.J., "Smoke Visualization of Subsonic and Supersonic Flows (The Legacy of F.N.M. Brown)," University of Notre Dame Report UNDAS TN-3412-1, June 1978.

26. Kim,H.T., Kline,S.J., Reynolds,W.C., "The Production of Turbulence Near a Smooth Wall in a Turbulent Boundary Layer," Journal of Fluid Mechanics (1971), Vol. 50, Pt.1, pp. 133-166.

27. Lu,S.S., Willmarth,W.W., "Measurements of the Structure of the Reynolds Stress in a Turbulent Boundary Layer," Journal of Fluid Mechanics (1973), Vol. 60, Pt. 3, pp.481-511.

28. Tennekes,H. and Lumley,J.L., First Course in Turbulence, 7th edition, Ch. 3, The MIT Press, Cambridge, 1972.

29. Kobashi,Y. and Ichijo,M., "Wall pressure and Its Relation to Turbulent Structure of a Boundary Layer," Experiments in Fluids, Vol. 4, No. 1, pp. 49-55, 1986.

30. Sturtevart, B. and Kulgurny, V.A., Journal of Fluid Mechanics, Vol. 73, pp. 651-671, 1976.

31. Karamcheti, K., private communication, July 1986.

32. Melnik,R.E., Chow,R., "Asymptotic Theory of Two-Dimensional Trailing Edge Flows," NASA SP-347, pp.177-249, 1979.

33. Cebecci,T., Chang,K.C., "Calculation of Incompressible Rough-Wall Boundary Layer Flows,"AIAA Journal,Vol. 16, July 1978, pp.730-735.

34. Rotta,J.C., Fluid Mechanics of Internal Flows, Elsevier, Amsterdam 1967.

35. Chevray,R.,Kovasznay,L.S.G.,"Turbulence Measurements in the Wake of a Thin Flat Plate," AIAA Journal, Vol. 7, No. 8, 1969, pp. 1641-1643.

36. Yetka,C.,"The Effect of a Large Eddy Break-Up Device on the Logarithmic Region of a Turbulent Boundary Layer," Southeastern AIAA Student Conference, 1986.

6. APPENDICES

6.1. FLUCTUATING PRESSURE AT THE LEBU'S TRAILING EDGE

Based upon the procedure suggested in reference [32], a prediction of the fluctuating pressure at the LEBU's trailing edge was obtained. This permitted the time averaged sound pressure level from 0 to 2000 Hertz of the acoustic waves impinging upon the flat plate to be set at a value which could influence the flow. The study of reference 32 examines a flat plate in an inviscid flow. The resulting equations are based upon the solution of the complete Navier-Stokes Equations using the Theory of Asymptotic Expansions.

The nondimensional perturbation pressure gradient at the LEBU trailing edge was found as (fig. 7, reference 32):

$$P(TE)=-0.301 \qquad (6.1)$$

The above quantity is defined by:

$$P(TE)=\frac{DP}{e^2 \rho \varepsilon^5 U_o^2}, \qquad (6.2)$$

where, DP is the fluctuating pressure. The parameter e for laminar flow is equal to $Re_c^{-\frac{1}{8}}$, where, Re_c is the Reynolds number based upon the LEBU's chord length. The constant $\varepsilon=0.33206$ appears in the Blassius solution for a flat plate. The flow density, ρ, was given a typical value of 1.25 Kg/m and U_o is the free stream velocity. Considering LEBU #5 mounted at a height $h=0.8\delta$, U_o was approximated as 10.5 m/s, and the parameter $\frac{U_o}{\nu}$ was 670,000 m^{-1} at the LEBU's height.

The Reynolds number, Re_c was found to be ~25,000 and

the boundary layer upon the LEBU was assumed to be laminar. The transition Reynolds number Re_x, with a 3 per cent turbulence intensity (typical at LEBU's height) was approximately 75,000.

After substituting the given quantities into (5.2), DP was found equal to 99.95 decibels. Similar calculations for the LEBU #5 resulted in a pressure perturbation of 104.3 dB. A sound wave with such a low frequency (0 to 200 Hertz) time averaged pressure level was considered adequate to trigger the shedding of a vortex at the LEBU's trailing edge and influence large eddy cancellation.

6.2. PREDICTION OF TURBULENT BOUNDARY LAYER.

6.2.1. INPUT DATA FOR HEAD'S METHOD

Head's method [23] was utilized to predict the growth of characteristic lengths of a plain turbulent boundary layer. Head's method requires the following data as input:

1. The momentum thickness at the beginning of the predicted flow regime (end of sandpaper trip).
2. The initial shape parameter, H.
3. The free stream velocity, U_o as a function of x.
4. The flow kinematic viscosity, ν, assumed constant for this case.

According to equation (3.1) the total drag coefficient c_D at the end of the sandpaper trip is defined as:

$$c_D(x) = 2\frac{\theta(x)}{x} \qquad (6.3)$$

The drag coefficient at the end of the sandpaper trip was empirically predicted [1] by:

$$c_f(x) = \frac{0.554\, e^{0.4\lambda}}{Re_x}\left[1 + \frac{0.3\, Re_x(\frac{\kappa}{x})}{\lambda}\right](1 - \frac{5}{\lambda}) \qquad (6.4)$$

In the above relation Re_x is the Reynolds number based upon the sandpaper trip length x, κ is the average roughness height of the sandpaper and λ is a parameter defined as

$$\lambda = (\frac{2}{c_f(x)})^{0.5}$$

The skin friction coefficient c_f at the end of the sandpaper trip was predicted by the empirical formula from White [1].

$$c_f(x) = (1.4 + 3.7\frac{x}{\kappa})^{-0.2} \qquad (6.5)$$

The average sand-paper roughness height κ was about 0.001 m, the sandpaper trip length was 0.24m, and the wind tunnel flow velocity unit Reynolds number $\frac{U_o}{\nu}$ was 700,000 m^{-1}. Proper manipulation of the above formulas can provide a prediction of the momentum thickness at the end of the sandpaper trip. The initial or starting values of H in Head's method are relatively unimportant except for the first few points of the calculation. A shape parameter for a flat plate flow H=1.375 was assumed by averaging measured values of H along the flat plate. The free stream velocity was considered to be 11. m/s. The growth of the momentum thickness, θ, predicted by Head's method for a plain flow configuration is compared with measured θ's in figure 9.

6.2.2. VELOCITY PROFILE OF A TURBULENT BOUNDARY LAYER

The logarithmic and the outer region of a plain turbulent boundary layer were predicted using a modified Coles velocity profile [33]. The velocity u at a boundary layer height y is thus given by:

$$\frac{u}{u_t} = \frac{1}{k}\left[\ln\left(\frac{y u_t}{\nu}\right)+\left(\frac{y}{\delta}\right)^2\left(1.-\frac{y}{\delta}\right)+\Pi w_1\left(\frac{y}{\delta}\right)\right]+B, \qquad (6.6)$$

where, u_t is the wall skin friction velocity, Π is the wake parameter and $w_1(\frac{y}{\delta})$ is the well known wake function. The logarithmic velocity law constants k and B were assumed equal to 0.41 and 5.0 respectively. The wake function $w_1(\frac{y}{\delta})$ [34] is defined as:

$$w_1\left(\frac{y}{\delta}\right)=39\left(\frac{y}{\delta}\right)^3-125\left(\frac{y}{\delta}\right)^4+183\left(\frac{y}{\delta}\right)^5-133\left(\frac{y}{\delta}\right)^6+38\left(\frac{y}{\delta}\right)^7 \qquad (6.7)$$

which also can be approximated with the sine function proposed by Coles [1]:

$$w(\frac{y}{\delta})=2\sin^2(\frac{\pi y}{2\delta}). \qquad (6.8)$$

The more complicated relation (6.7) was used because it gave better agreement with the measurements.

At the wall the relation (6.7) yields w(0)=0.0,and at the edge of the boundary layer ($y=\delta$), w(1.0)=2.0. Relation (6.6) then yields:

$$\frac{U_o}{u_t}=\frac{1}{k}(\ln(\frac{\delta u_t}{\nu})+\Pi 2.)+B \qquad (6.9)$$

Subtracting equation (6.6) from (6.9) one can get:

$$\frac{U_o-u}{u_t}=\frac{1}{k}[\ln(\frac{y}{\delta})-(\frac{y}{\delta})^2(1.-\frac{y}{\delta})+\Pi(2.-w_1(\frac{y}{\delta}))] \qquad (6.10)$$

The wake parameter for an equilibrium boundary layer remains constant ; for a flat plate measurements suggest $\Pi=0.55$ [1]. The wall skin friction velocity u_t was determined from the definition rearranged as:

$$u_t=U_o(\frac{c_f}{2})^{0.5} \qquad (6.11)$$

The local skin friction coefficient was predicted by Coles formula [1]:

$$c_f=\frac{0.3\,e^{-1.33H}}{(\log Re_\theta)^{1.74+0.31H}} \qquad (6.12)$$

The boundary layer velocity profile predicted by using these relations in equation (6.10) is compared with a measured plain flow profile in figure 11.

6.2.3. BOUNDARY LAYER VELOCITY PROFILE FOR A LEBU CONFIGURATION

The velocity, u_{LE}, at a height y of the LEBU manipulated turbulent boundary layer was predicted as:

$$u_{LE}=u_{PL}-du_w \ , \qquad (6.13)$$

where, u_{PL} is the velocity predicted for a plain configuration and du_w is the velocity defect caused by the LEBU plate wake. For inviscid free stream flow and a two dimensional wake, du_w is estimated by the relation [2]:

$$du_w=du_{max}\left[1.-\left(\frac{y_1}{\beta}\right)^{1.5}\right]^2 \ , \qquad (6.14)$$

where, du_{max} is the maximum velocity defect at the wake's axis of symmetry, $\beta(x)$ is the wake semi-width and y_1 is the longitundinal distance from the wake's axis of symmetry. According to previous studies [35] for a similar two-dimensional wake the quantities β and du_{max}, at a distance x from the plate trailing edge, are defined as follows:

$$\frac{\beta(x)}{\theta(0)}=\left(\frac{x}{\theta(0)}\right)^{0.5} \qquad (6.15)$$

and

$$\frac{du_{max}}{U_0}=\left(\frac{x}{\theta(0)}\right)^{-0.5} \ , \qquad (6.16)$$

where U_0 is the boundary layer velocity at the LEBU height (free steam velocity) and $\theta(0)$ is the momentum thickness at LEBU trailing edge. The quantity $\theta(0)$ was considered as being twice the momentum thickness of the laminar boundary layer grown upon the LEBU. The Blassius solution [2] for a flat plate with a laminar boundary layer suggests

$$\theta(c)=0.664\left(\frac{\nu c}{U_0}\right)^{0.5}. \qquad (6.17)$$

In the above relation c represents the LEBU chord length, and the parameter $\frac{U_o}{\nu}$ was 670,000 m^{-1} (at the LEBU's height). The logarithmic velocity law constant k was assumed to retain the value of 0.41 [36], and the wall skin friction velocity was calculated from (6.10). The skin friction coefficient resulted from previous measurements (section 2.3). A theoretically predicted velocity profile for LEBU #2 is compared with a measured profile on figure 13.

6.2.4. DETERMINATION OF C_f FROM VELOCITY PROFILE

The following method of calculating c_f is a variation of the procedure suggested by Bradshaw [24]. In the logarithmic region of a boundary layer, the velocity u at a distance y from the wall is given by:

$$\frac{u}{u_t} = \frac{1}{k} \ln\left(\frac{y\,u_t}{\nu}\right) + B; \qquad (6.18)$$

where u_t is the wall friction velocity, ν is the kinematic viscosity and k and B are constants equal to 0.41 and 5.0 respectively. For a flat plate the logarithmic region extends approximately over $35 < \frac{y\,u_t}{\nu} < 350$. So, for

$$\frac{y\,u_t}{\nu} = 200 \qquad (6.19)$$

relation (6.18) is valid and yields

$$\frac{u}{u_t} = 17.923. \qquad (6.20)$$

The skin friction coefficient is given by:

$$\frac{c_f}{2} = \left(\frac{u_t}{U_o}\right)^2, \qquad (6.21)$$

where U_o is the free stream velocity. Only one point (y,u) on the logarithmic region of a measured boundary layer satisfies

all the above relations. Determining this point can provide a value for c_f at a certain axial location. After traversing across a boundary layer various values of u are substituted into relation (6.20). The resulting u and corresponding y are used to determine the point on the logarithmic region which gives $\frac{yu_t}{\nu}$ closest to 200. This requires a local least square fitting of the form

$$u=ay^b \qquad (6.22)$$

which is applied for measured values of u and y in the vicinity of this point. Thus, although the precise point where $y^+=200$ may not have been measured, the corresponding u and y for $\frac{yu_t}{\nu}=200$ can be approximated very accurately. Manipulation of these formulas yields:

$$y=\left(\frac{3584.6\,\nu}{a}\right)^{\frac{1}{1+b}} \qquad (6.23)$$

The resulting value of y and u satisfies the relation (6.20) and can be used to determine c_f from (6.21).

Example calculation:

Measured quantities at x=2.75 m, z=0.0 m.

$\frac{U_o}{\nu}=700{,}805\ m^{-1}$, $\nu=1.514\ 10^{-5}$, $U_o=11.311$ m/s

y[m]	u[m/s]	u_t[m/s]	$\frac{yu_t}{\nu}$
0.005	7.528	0.420	130.1
0.006	7.700	0.430	159.708
0.008	8.033	0.448	222.376

Least square curve fitting of the measured values of u at a distance 0.004 to 0.016 m from the wall results in $u=0.007256y^{0.1556}$ with correlation coefficient equal to

0.998. Then substituting into the proper relations one can get: y=0.007266 m, u=7.961056m/s, u_t=0.4442m/s, and c_f=0.003084. The value of c_f is the desired result.

6.3 Pressure Pulse Controling Device

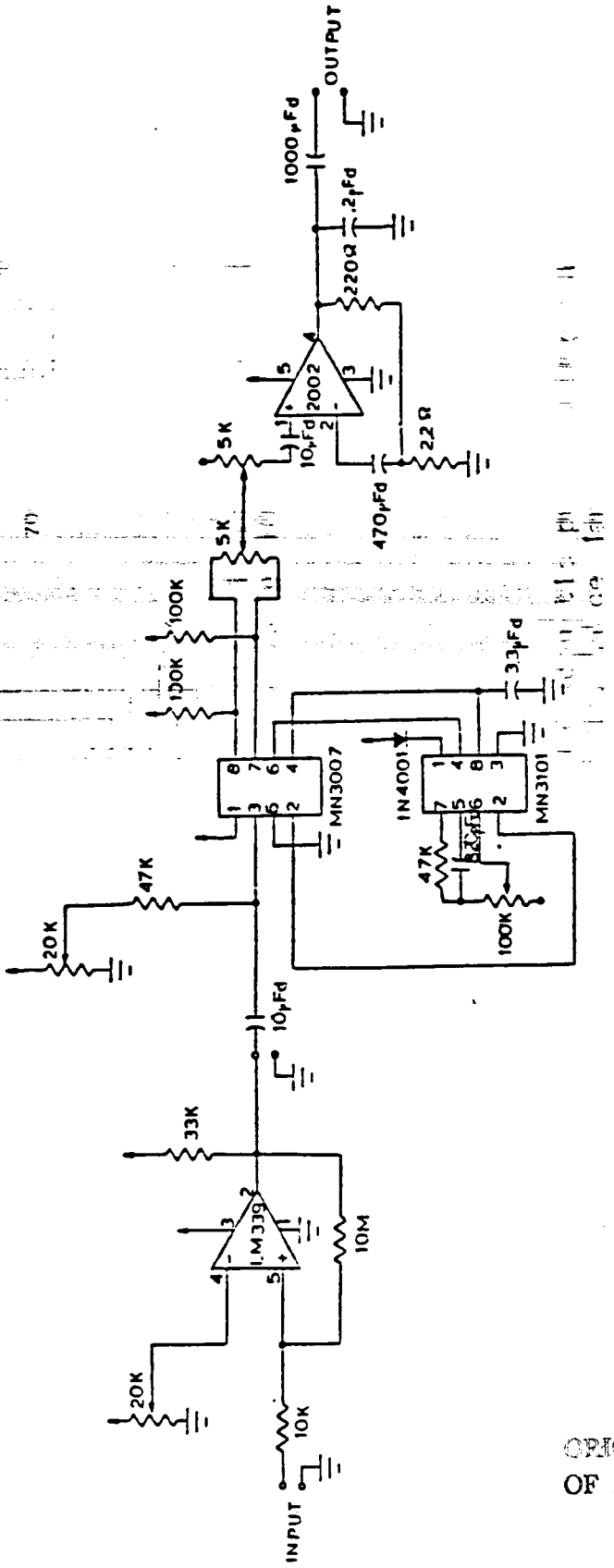

Figure 36. Electronic diagram of acoustic pulse triggering device (Courtesy of Mr. Lance Mangum).